ROYAUME DU MAROC
Université Mohammed V - RABAT -
جامعة محمد الخامس – الرباط –
Faculté des sciences
كلية العلوم
CENTRE D'ETUDES DOCTORALES - SCIENCES ET TECHNOLOGIES

N° d'ordre : 3444

THESE

En vue de l'obtention du : **DOCTORAT**

Centre de Recherche : Centre de Recherche en Energie
Structure de Recherche : Laboratoire de Mécanique et des Matériaux
Discipline : Physique
Spécialité : Mécanique et science des matériaux

Présentée et soutenue le : 13/03/2021 par :

SEMLALI AOURAGH HASSANI Fatima Zahra

Implementation, characterization and modeling of composite materials based on natural fibers: prediction of mechanical properties before design.

JURY

Mohamed BOUKALOUCH	PES, Faculté des Sciences, Université Mohammed V, Rabat	Président
Omar OUSSOUADDI	PES, Faculté des Sciences, Université Moulay Ismaïl, Meknes	Rapporteur/ Examinateur
Ahmed MZERD	PES, Faculté des Sciences, Université Mohammed V, Rabat	Rapporteur/ Examinateur
Kamal GUERRAOUI	PES, Faculté des Sciences, Université Mohammed V, Rabat	Rapporteur/ Examinateur
Abou El Kacem QAISS	Dr, Directeur du centre composite et nanocomposite, Fondation MAScIR, Rabat	Invité
Rachid BOUHFID	Dr, Chercheur senior, Fondation MAScIR, Rabat	Invité
Mohammed Ouadi BENSALAH	PES, Faculté des Sciences, Université Mohammed V, Rabat	Directeur de thèse

Année Universitaire : 2020-2021

"With time and patience, the mulberry leaf becomes a silk gown"

- Old Chinese quote -

Preface

Firstly, I would like to thank **GOD** for his generous blessing and undying strength bestowed upon me during the course of this research.

This work was carried out in Morocco (Rabat) as part of a joint thesis between the Mechanics and Materials Laboratory of the faculty of Science, Mohammed V University and composite and nanocomposite Center of the Moroccan Foundation for Advanced Science, Innovation and Research (MAScIR). If it was born, it is because several people have made their contribution. I want to thank them ...

First of all, I would like to thank **Pr. Mohammed Ouadi Bensalah**, my thesis director for having supported and supervised me for four years. Swimming in the materials science pool without drowning in it was not easy but, thanks to his precious advice scientists, his encouragement and the freedom of work he left me I was able to progress.

I wish also to express my gratitude to **all the members of the jury** who have honored me and accepted to judge my work.

I would like to start by thanking **Pr. Mohamed Boukalouch,** Professor at the Faculty of Sciences, Mohammed V University of Rabat, for honoring me and accepting to be the president of the jury members despite all its commitments.

My sincere thanks also go to **Pr. Omar Oussouaddi,** Professor at the Faculty of Sciences, Moulay Ismail University of Meknes, and Vice-president in charge of academic affairs and university development, for honoring me and accepting the task of rapporteur and examiner of my thesis despite the distance that separates him from Rabat.

My deep thanks also go to **Pr. Ahmed Mzerd,** Professor at the Faculty of Sciences, Mohammed V University of Rabat, and head of Energy Research Center, who brought me a lot during my university studies, especially on the human level. His presence, encouragement, invaluable suggestions, constructive advices and his pedagogy have served me well. Today I want more than that, to express my deep gratitude to him for honoring me and accepting to report and examine my thesis.

Also find my huge thanks **Pr. Kamal Guerraoui**, Professor at the Faculty of Sciences, Mohammed V University of Rabat, for all the time he devoted to reading, reporting and reviewing my thesis.

My deep thanks also go to **Pr. Abou El Kacem Qaiss** the current director of the composites/nanocomposites center of the MAScIR foundation, for entrusting me with this research work, as well as for his help and his precious advice during this thesis period. His excellent supervision and dedication allowed me to complete this thesis work without delay. I thank him for his patience and his humor always present even during the various adventures encountered during our trips to attend conferences. Finally, I owe him the scientific culture that I was able to acquire during this thesis work. I also thank him for his confidence in me, for his infectious enthusiasm and for the philosophical-scientific discussions.

I would then like to thank my professor, **Pr. Rachid Bouhfid**. His advice and help at key moments in my thesis, allowed me to unlock situations where the progress of my work has stagnated somewhat.

I would also like to thank **Pr. Mourad Belkacemi**, Professor at the Faculty of Sciences, Mohammed V University of Rabat, who has brought me a lot through his presence, both on a human and scientific level. His humor, kindness and many tips were very helpful to me. His immense knowledge and rigorous attitude have inspired me to pursue high-quality research. Thank you for trusting me, I will never thank you enough.

The thesis would not have ended without the help and collaboration of all the members of **the composites/nancomposites center** of the MAScIR foundation. Thank you for all these great moments that we spent together ... I will never forget you!

Many thanks to **Pr. Nadia Zari**, senior researcher in the composites/nanocomposites center, for her availability, her many advices, her encouragement and her warm welcome.

I would also like to thank **Pr. Hamid Essabir**, Professor at ENSA Agadir who followed my work more closely during the first years of my thesis, and who, through his instructive advices and encouragements, was able to help me move forward.

The completion of this work would not have been possible without the technical support of **Mr. Mehdi Ait Dahi**, I thank him very much for having shared with me his expertise on polymer materials.

Also finds here the expression of my deep gratitude, **Pr. El Mostapha Boudi**, Professor at the Mohammadia School of Engineers, for his guidance, his professionalism, his advice. I would also like to underline his pedagogical talent and his human qualities.

The start of the thesis like all the beginnings was quite hard, but the presence of my best friend, **Khadija El Bourakadi**, made the start pleasant. Her daily support, starting with the morning hello and the encouragement throughout the day, kept me going, especially during the first months of my integration. At the same time, I would especially like to thank her for her boundless kindness, flawless availability, sincerity, sensitivity, scientific advices and encouragement which undoubtedly allowed me to evolve. I also thank her for her confidence in me, for her always efficient help and more particularly for sharing with me her knowledge on organic chemistry.

In my thanks, find a special place my best friend and little sister, **Oumayma M'ghari** who distinguished herself from other colleagues mainly by her laughter and her open-mindedness. I thank her for the time spent together, for our coffee/tea breaks, for our discussions of everything and anything, and above all for her sincere friendship.

The most important part of my life is my family. Family is so important that it should never be forgotten or left behind. No matter if we are now building our own family, our grandparents, parents, siblings, and spouse will always be present in our lives. It would be time to thank them even with just a few words for everything they have done for me.

Firstly, I would like to thank **my grandfather "ABI"**, **Pr. Abdelmajid Semlali Aouragh Hassani,** Professor at the Faculty of law and member of the Supreme Scientific Council of the Kingdom of Morocco, my greatest example in life, for all his love, warm welcome, his availability, the many advices, and encouragements he gave me. He has always been able to transmit his passion for research and studies in general to me and I hope to one day can accomplish even a quarter of his exploits. I love you, admire you and respect you more than you can imagine.

I am also indebted to my parents **"Moulay Ahmed** and **Ikbal"**. As far back as I can remember, my memories by their side have always been happy, joyful, full of laughter, full of tenderness and full of emotion. This comforting, reassuring family atmosphere has punctuated my life. Their benevolent gaze helped me to push straight, to grow properly, and be firmly rooted in the ground with my head high, full of dreams to fulfill. So I wanted to tell them through these few words, thank you from the bottom of my heart. Thank you for these roots, these values, and this unconditional love. Thank you for the financial and emotional support throughout this stage of my life. Thanks to you I am today Dr. Fatima Zahra Semlali Aouragh Hassani. And thanks to you, I in turn know which parent I would like to be. It's not difficult. My example in life is you! Thanks to my brother **"Sidi Mohammed"** and sisters **"Ibtihaj and Majdouline"** who have always been there to support and encourage me. I couldn't have gotten through the tough times without their encouragement and would never have been able to accomplish any of my goals without their love and supports. I love you all more than anything.

I cannot forget to thanks my husband, **Anas Saoudi**, my source of inspiration, for his growing support and love. I will never be able to express all my gratitude. How can I thank him for his presence, kindness and love? Can the word "Thank You" be enough? Will my "I love you" be enough? Today I am telling him and writing, thank you for everything you did for me and for us. Thank you for all your helps, sacrifices and unconditional love.

At the same time, I address my thanks to my husband's family**,** in particular my second parents **''Abdelkrim Saoudi and Hakima Bennani''**, as well as my husband's brother and his wife **''Oussama Saoudi** and **Imane El Gouzi''** for their availability, their many advices, their support, their encouragement, their warm welcome and above all for their unconditional love. I love you all so much.

Finally, my thanks to every other individual who had made this research work possible but not mentioned personally here.

Dedication

To my grandfather, my parents and husband,

Without whom none of my success would be possible

Table of content

Chapter II. Mechanical properties prediction of polypropylene/Short coir fibers composites using a self-consistent approach

Chapter III. Injection molding of short coir fiber polypropylene bio-composites: Prediction of the mold filling phase

Chapter IV. Injection molding of short fiber thermoplastic bio-composites: Prediction of the fiber orientation

List of figures

Symbol glossary

$(C_3H_6)_n$	Polypropylene formula
$(C_2H_4)_n$	Polyethylene formula
E_V	Voigt elastic modulus
E_R	Reuss elastic modulus
E_f	Fiber elastic modulus
E_m	Matrix elastic modulus
V_f	Fiber volume fraction
E_{mROM}	Modified Rule of Mixture elastic modulus
η_e	Efficiency factor
η_o	Efficiency factor of orientation
η_l	Efficiency factor of length
B’	Coefficient of stress concentration rate at the ends of the fibers
r	Mean radius of fiber
α_o	limit angle
$E_{H-T/L}$	Halpin-Tsai Longitudinal elastic modulus
$E_{H-T/T}$	Halpin-Tsai Transversal elastic modulus
ξ	Adjustable parameter for the fiber morphology
L	Length of the fiber
T	Thickness of the fiber
D	Diameter of the fiber
K	Consistency of the fluid
n	Flow behavior index
$\dot{\gamma}$	Velocity gradient
η_0	Zero shear viscosity
η_∞	Infinite shear viscosity
Λ	Time constant
M	Constant
α	Transition between the low shear behavior and the power law
Σ	Applied stress
σc	Characteristic stress
P	Slope of the curve at the point of inflection
X	Parameter that depends on the volume fraction
Vx, Vy and Vz	Velocities in x, y and z directions
P	Pressure
G	Acceleration of gravity
A	Thermal diffusivity
H	Enthalpy
P	Density
N	Kinematic viscosity
Q	Flow rate

$E_{m\text{-}H\text{-}T/L}$	Modified Halpin-Tsai longitudinal elastic modulus
ϕ_{max}	Volume apparent occupied by filler
$E_{H\text{-}S/L}$	Hui-Shia longitudinal elastic modulus
$E_{H\text{-}S/T}$	Hui-Shia transversal elastic modulus
β	Aspect ratio of the fiber
$E_{Ha\text{-}S}$	Hashin and Shtrikman young modulus
K_L	Longitudinal bulk modulus
K_T	Transversal bulk modulus
G_L	Longitudinal shear modulus
G_T	Transversal shear modulus
K_f	Fiber bulk modulus
K_m	Matrix bulk modulus
G_f	Fiber shear modulus
G_m	Matrix shear modulus
$E_{T\text{-}P}$	Tsai-pagano elastic modulus
E_H	Hirsch elastic modulus
x	Empirical Hirsch parameter
τ	Shear stress
η	Dynamic viscosity
γ	Shear rate

S0	Section
T	Period
B	Aspect ratio
D	Fiber diameter
Ci	interaction coefficient
$\Psi(P,t)$	Orientation distribution function
$\overline{\overline{a_2}}$	Orientation tensor
f_x	Hermans factor
$\varepsilon(V)ij$	Volume averaged vorticity
$\Omega(V)ij$	Strain rate tensors
D_r	Brownian diffusion coefficient
G*	Torsion modulus
G'	Storage modulus
G''	Loss modulus
$\tan\delta$	Loss factor
E_h	Modified Hirsch elastic modulus
α	Orientation factor
θ	Fiber orientation angle
Ω	Vorticity tensor
Φ	Predicted fiber orientation angle

Terms

PP	Polypropylene
PE	Polyethylene
LDPE	Low density polyethylene
HDPE	High density polyethylene
LLDPE	Linear low density polyethylene
PC	Polycarbonate
C_o	Coir fiber
C_a	Cactus fiber

Abstract

The aim of this thesis project is to develop methods and techniques to accurately predict the whole material mechanical properties before design. This will enable to improve parts quality as well as reducing production cost and time, thus leading to reduce/eliminate lengthy experimental testing.

Firstly, a self-consistent approach was developed based on a modified version of Hirsch model to predict the composite mechanical properties while considering the effect of reinforcement content and orientation. Considering that, the fiber orientation depends closely on the flow field, a three-dimensional model for the non-isothermal and non-Newtonian mold filling prediction model was developed to study the flow behavior. Indeed, the incompressible Navier–Stokes equations are simplified into a single Poisson equation, and then solved to estimate the flow velocity, which under a constant flow rate allows the flow front shape and position prediction for the composites. Finally, a quantitative model allowing the flow induced fiber orientation prediction for different flow cases encountered is presented. The resulted equation relates the fiber orientation angle to the flow field, the fiber aspect ratio and the mold shape.

To conclude, by combining the three developed models, it is feasible to begin predicting the materials mechanical properties before design, independently of the used materials, the ultimate goal of this thesis.

Key words: Injection molding – Thermoplastics – Natural fibers – Composites – Modeling – Mechanical performance – Flow front – Fiber orientation.

Résumé

Le but de ce projet de thèse est de développer des méthodes et des techniques pour prédire avec précision les propriétés mécaniques d'un matériau composite avant sa conception. Cela permettra d'améliorer la qualité des pièces ainsi que de réduire les coûts et le temps de production, conduisant ainsi à réduire / éliminer les longs essais expérimentaux.

Tout d'abord, une approche auto-cohérente a été développée sur la base d'une version modifiée du modèle de Hirsch pour prédire les propriétés mécaniques du composite tout en tenant compte de l'effet de la concentration et de l'orientation des fibres. Considérant que l'orientation des fibres dépend étroitement du champ d'écoulement, un modèle tridimensionnel pour la prédiction du remplissage de moule non isotherme et non newtonien a été développé pour étudier le comportement de l'écoulement. En effet, les équations incompressibles de Navier – Stokes sont simplifiées en une seule équation de Poisson, puis résolues afin d'estimer la vitesse d'écoulement, ce qui sous un débit constant permet la prédiction de la forme et de la position du front d'écoulement des composites. Enfin, un modèle quantitatif permettant la prédiction de l'orientation des fibres induites par l'écoulement pour différents cas d'écoulement rencontrés est présenté. L'équation résultante relie l'angle d'orientation de la fibre au champ d'écoulement, le facteur de forme de la fibre et la forme du moule.

Pour conclure, en combinant les trois modèles développés, il est possible de commencer à prédire les propriétés mécaniques des matériaux avant la conception, indépendamment des matériaux utilisés, objectif ultime de cette thèse.

Mots clés: Moulage par injection - Thermoplastiques - Fibres naturelles - Composites - Modélisation - Performances mécaniques - Front d'écoulement - Orientation des fibres.

Résumé Détaillé

Le moulage par injection est l'une des méthodes de traitement des polymères la plus largement utilisées. En effet, il a été démontré que les thermoplastiques renforcés de fibres naturelles courtes amélioraient considérablement leurs performances mécaniques sans compromettre leur capacité de traitement. Mais une conception réussie nécessite une bonne estimation des performances du produit avant la production. L'objectif de ce projet de thèse est donc de développer des méthodes et des techniques pour prédire avec précision les propriétés mécaniques du matériau composite avant sa conception. Cela permettra d'améliorer la qualité des pièces ainsi que de réduire les coûts et le temps de production, conduisant ainsi à réduire/éliminer les longs essais expérimentaux.

Tout d'abord, une approche auto-cohérente a été développée sur la base d'une version modifiée du modèle de Hirsch pour prédire les propriétés mécaniques du composite tout en tenant compte de l'effet de la concentration et de l'orientation des fibres. Ensuite, les résultats ont été comparés à d'autres modèles (Hirsch et Tsai-Pagano) et validés avec des données expérimentales. Dans l'ensemble, notre approche a permis de mieux prédire les résultats mécaniques en termes de module de Young, de résistance à la traction et de module de torsion. Cependant, les valeurs d'orientation des fibres ont été mesurées expérimentalement via le logiciel ImageJ, et bien évidemment une détermination précise des propriétés mécaniques du composite avant la conception nécessite la caractérisation de l'écoulement à l'intérieur de la cavité du moule et la prédiction de l'orientation des fibres mise en place lors du processus d'injection.

Considérant que l'orientation des fibres dépend étroitement du champ d'écoulement, un modèle tridimensionnel pour la prédiction du remplissage de moule non isotherme et non newtonien a été développé afin d’étudier le comportement d'écoulement. En effet, les équations incompressibles de Navier–Stokes sont simplifiées en une seule équation de Poisson, puis résolues pour estimer la vitesse d'écoulement, ce qui sous un débit constant permet la prédiction de la forme et de la position du front d'écoulement des composites. Il a été constaté que le modèle proposé est en bon accord avec les résultats expérimentaux pour la gamme de conditions étudiées. Enfin, un modèle quantitatif permettant la prédiction de l'orientation des fibres induites par l'écoulement pour différents cas d'écoulement rencontrés est présenté. L'équation résultante relie l'angle d'orientation de la fibre au champ d'écoulement, le facteur de forme de la fibre et la forme du

moule. En évaluant l'efficacité de notre approche développée en testant différentes matrices, fibres et formes de moules, une prédiction très qualitative de l'orientation des fibres a été obtenue. A la fin de cette partie, un modèle combinant les trois équations développées est abordé et validé avec les résultats expérimentaux.

Pour conclure, en combinant les trois modèles développés, il est possible de commencer à prédire les propriétés mécaniques des matériaux avant la conception, indépendamment des matériaux utilisés, objectif ultime de cette thèse.

Mots clés: Moulage par injection - Thermoplastiques - Fibres naturelles - Composites - Modélisation - Performances mécaniques - Front d'écoulement - Orientation des fibres.

GENERAL INTRODUCTION

Increasing environmental awareness throughout the world has prompted design of materials that are compatible with the environment [1]. Indeed, short natural fibers addition in thermoplastics matrix was shown to dramatically improve their mechanical performance without compromising their process ability due to their weight-resistance ratios and high specific properties [2], [3]. As the objective is to increase both the productivity and the mechanical quality of parts, the composite materials are obtained using the injection molding process. This method makes it possible to obtain parts of various geometric sizes and complexities. It also remains an economical process well suited to large series, offering dimensional tolerances generally sufficient to overcome machining operations. These composite materials thus have the advantage of being able to be shaped by the same processes as the uncharged thermoplastics and this without much modification of the tools [4]–[6].

Many researchers have focused on improving the performance of these composites to extend their use to applications where constraints are critical. The final performances will thus depend on the choice of the matrix, the reinforcements, the shaping and especially the process parameters since the latter condition the distribution and orientation of fibers inside the matrix. In order to assess the properties of the final product, it is very important to understand the phenomena acting on the distribution of fibers and to know how they orient themselves during the flow [2], [5], [7].

The problem of fiber orientation is therefore complex. During the mold filling phase, each fiber is transported by the flow and its orientation evolves according to the constraints imposed by the matrix, the other particles, and the mold walls. This result in a complex orientation distribution, which varies considerably in the part, and thus affect the thermomechanical properties [2], [8]. So, to predict the mechanical properties of a part, the flow front advancement and fibers orientation must be clearly described. This enables to improve parts quality as well as reducing production cost and time, thus leading to reduce/eliminate lengthy experimental testing [5].

Consequently, the aim of this thesis is to develop mathematical models for a complete injection molding study to anticipate the material structural performance by coupling the flow behavior with fiber orientation, and thus optimizing the mold design and processing variables.

Thus, this work is based on an experimental approach to characterize the thermomechanical behavior of a thermoplastic matrix (PP) reinforced with short coir fibers. The different samples

necessary for this study were obtained by a compounding-injection process. The main objective is to understand and visualize the main physical mechanisms (fibers orientation and distribution, flow front advancement, material rheological properties, etc.) to consider in order to propose a modeling strategy making it possible to predict the behavior of these composites and optimize their future performance. The conclusions of this study prompted to propose three mathematical models allowing the composites mechanical properties prediction before production. This manuscript thesis is presented as article chapters and is subdivided into four chapters; the first one is about the literature review, while the last three chapters were devoted to the results as follows:

- **The first chapter** is devoted to a complete bibliographic study of the injection molding process. After a brief presentation of composites based on polymeric matrices and their implementation process, some macroscopic models encountered in the literature allowing the material mechanical properties prediction have been described. While the influence of the flow front behavior on the fibers orientation during injection process and the essential mathematical tools to describe this orientation are discussed at the end of this chapter.
- **The second chapter** presents a developed self-consistent approach to predict the composite properties in terms of Young's modulus, tensile strength and torsion modulus while considering the effect of reinforcement content and orientation. The obtained results are compared with other models (Hirsch and Tsai-Pagano) and validated with experimental data. However, the used fibers orientation values were measured experimentally via the ImageJ software, and since a precise determination of the composite mechanical properties before designing requires the characterization of the flow inside the mold cavity and the prediction of fiber orientation set up during the injection process, other models are developed and presented in the following chapters.
- **The third chapter** is a first step to respond to the second chapter by a developed three-dimensional model for the non-isothermal and non-Newtonian materials mold filling prediction. Also, it describes the effect of fiber concentration on the flow front progression of polypropylene melts and then explains in detail the effect of temperature, viscosity, and shear rate on the flow front shape and position. The obtained theoretical results are compared with experimental data to confirm that the model can provide good prediction. Finally, the Moldflow software is used to further understand the effect of

processing conditions such as pressure, as well as melt and mold temperature on the flow front behavior. This chapter allows an explicit description of the flow front as spline according to the materials rheological and thermal properties, as well as the mold shape. The obtained results have been used in the next chapter to describe the fiber orientation during the processing techniques.

- **The fourth chapter** is the second and last step to respond to the second chapter. It presents a quantitative model to determine the flow induced fiber orientation for different flow cases by considering the effect of fiber aspect ratio and mold geometry. To validate the numerical model, experimental data were taken with different matrices (polypropylene and high-density polyethylene), fibers (coir and cactus) and mold geometries (rectangular and rounded rectangle mold). To test the efficiency of the three developed model, the models developed for the flow induced fiber orientation prediction is introduced in the self-consistent approach and then the obtained results are compared with the experimental ones.

The manuscript is completed with a general conclusion and perspectives.

Chapter I. State of the art – short natural fiber based thermoplastic bio-composites

I.1. Introduction

The use of composite materials in the construction of structures offers designers new possibilities compared to traditional materials. They provide many functional advantages: lightness, mechanical and chemical resistance, reduced maintenance, ease of implementation. Thus, the needs of industry in these sectors have become more and more advanced and have made necessary the knowledge and mastery of composite materials. Composite materials such as thermoplastics reinforced with short natural fibers combine both the mechanical properties of natural fibers and those of the matrix in which they are immersed. These properties are clearly better than those of the matrix, particularly the stiffness and the tensile strength.

However, during the mold filling phase, each fiber is transported by the flow and its orientation evolves according to the stresses imposed by the matrix, the other particles and the mold walls. This result in a complex orientation distribution, which varies considerably in the part, and thus affect the thermomechanical properties [2], [8]. To conclude that the composite mechanical properties are mainly related to the injection process itself, the material rheological properties, the fibers orientation distribution and the mold cavity shape [2].

When a short-fiber reinforced polymer is injection molded, the flow during mold filling creates patterns of preferential fiber orientation in the part. This leads to considerable point-to-point variation and anisotropy in the mechanical properties of the produced materials [9]. Thus, the rheology of fiber-filled polymers is quite complex due to fiber–fiber and wall–fiber interactions, fiber breakage and migration. These add considerable complexities to the already complex rheology of the polymer matrix. Hence, the study of the rheological properties of concentrated suspensions in polymer melts remains most challenging. The flow of fiber filled thermoplastics in the molten state is modified by the presence of fibers and reciprocally the fiber motion and rotation is affected by the flow [10]. These complex interactions between all the parameters must be related to the mold geometry and the melt flow properties. So, to predict the mechanical properties of a part, all those factors must be considered. This enables to improve parts quality as well as reducing production cost and time, thus leading to reduce/eliminate lengthy experimental testing [5].

This chapter constitutes a bibliographical synthesis. Recalling on one hand, a brief presentation of thermoplastic composites and their implementation process, and on the other hand, the main factors influencing naturally-reinforced composites mechanical properties such as flow front behavior and fibers orientation.

I.2. Thermoplastic bio-composites

Bio-composites are composite materials comprising one or more phase(s) derived from a biological origin. In terms of the reinforcement, this could include plant fibers such as cotton, flax, hemp and similar, or fibers from recycled wood or waste paper, or even by-products from food crops [11]. Regenerated cellulose fibers (viscose/rayon) are also included in this definition, since ultimately they too come from a renewable resource, as are natural 'nano fibrils' of cellulose and chitin [11]. Matrices may be polymers, ideally derived from renewable resources such as vegetable oils or starches [11]. Alternatively, and more commonly at the present time, synthetic, fossil-derived polymers preponderate and may be either 'virgin' or recycled thermoplastics such as polyethylene, polypropylene, polystyrene and polyvinyl chloride, or virgin thermosets such as unsaturated polyesters, phenol formaldehyde, isocyanates and epoxies [11]. Nowadays, thermoplastics can be found in a wide range of applications and fields due to their relatively low cost and easy processing, especially by injection molding. But most commodity polymers, such as polypropylene (PP), have relatively low mechanical properties limiting their use to non-structural applications. Nevertheless, the addition of short natural fibers in these matrices was shown to substantially improve their mechanical performance without compromising their process ability. This is related to natural fibers advantages such as good specific mechanical properties, low densities, low production costs, non-toxicity, high specific properties, and easy recycling [2].

I.2.1. Thermoplastic material

I.2.1.1. Definition

Thermoplastics are defined as polymers that can be melted and recast almost indefinitely. They are molten when heated and harden upon cooling. When frozen, however, a thermoplastic becomes glass-like and subject to fracture. These characteristics, which lend the material its

name, are reversible, so the material can be reheated, reshaped, and frozen repeatedly [12]. As a result, thermoplastics are mechanically recyclable. Some of the most common types of thermoplastic are polypropylene, polyethylene, polyvinylchloride, polystyrene, polyethylenetheraphthalate and polycarbonate. It's very important to note that the repeat heated of the polymer affect the polymeric chain length, which, is directly correlated to rheological behavior of materials [12].

I.2.1.2. Polypropylene (PP)

Polypropylene (PP) is a linear polyolefin, of formula $(C_3H_6)_n$ (Figure I.2-1a), obtained by Ziegler-Natta polymerization or by polymerization by catalysis with a metallocene. There are a wide variety of properties and behavior of PP depending on its chemical nature, its formulation and the formatting conditions. The positioning of methyl group (CH_3) characterizes the kind of the PP in terms of Isotactic, Syndiotactic and Atactic classification [12].

I.2.1.3. Polyethylene (PE)

Polyethylene (PE) is a thermoplastic polymer produced from the monomer ethylene, of formula $(C_2H_4)_n$ (Figure I.2-1b),. It is sometimes called "alkathene" or "polythene". With a high strength-to-density ratio, PE is used in the production of plastic bottles, corrosion-resistant piping, geomembranes and plastic lumber. PE is commonly recycled, and has the number "2" as its resin identification code. Several kinds of PE according to polymeric chain conformation can be cited as Low density polyethylene (LDPE), High density polyethylene (HDPE) and Linear low density polyethylene (LLDPE) [12].

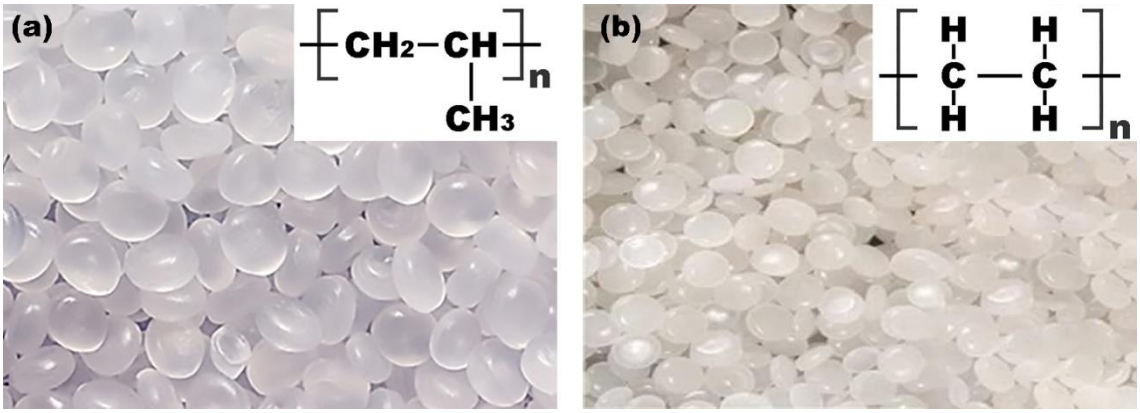

Figure I.2-1: Chemical formula and granules of: (a) polypropylene and (b) Polyethylene.

I.2.2. Natural fibers

I.2.2.1. Definition

Vegetable fibers are biological structures mainly composed of cellulose, hemicelluloses and lignin. In a much smaller proportion they also contain extractable, proteins and certain inorganic compounds. Each fiber is in the form of a multifibrill composite in which the lignin plays the role of a matrix coating a very rigid structuring element which is cellulose (Figure I.2-2) [13].

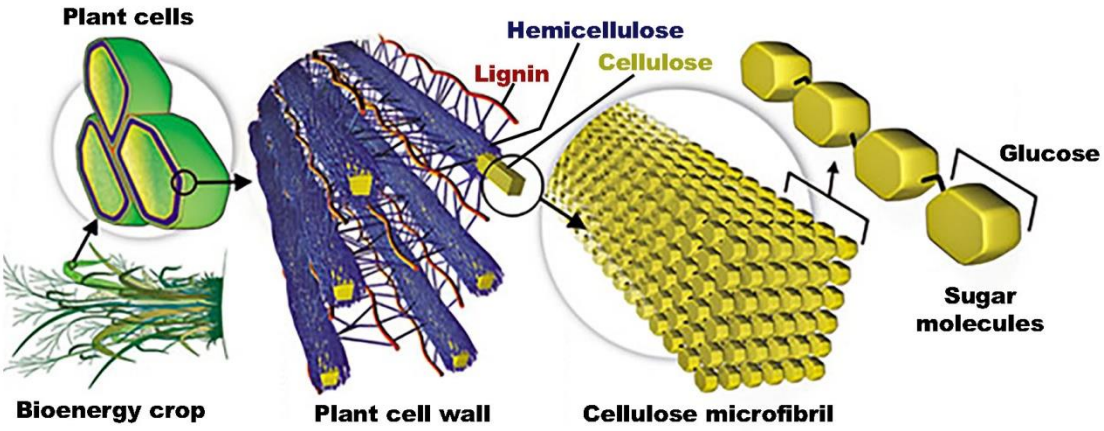

Figure I.2-2: Structure of a vegetable fiber.

I.2.2.2. Classification and structure

There are several criteria for differentiating fibers:

– **The plant organ**

Vegetable fibers can be subdivided into 5 groups according to their origin (Figure I.2-3) [14]. Fibers from seminal seed hairs (cotton, kapok …), Liberian fibers extracted from plant liber (flax, hemp, jute, ramie …), fibers extracted from leaves (sisal, abaca …), from fruit husks (nuts coconut …) or hard fibers extracted from plant stems (bamboo, alfa …) [14]. The cited origin materials in figure I.2-3 are for indication and not for limitation.

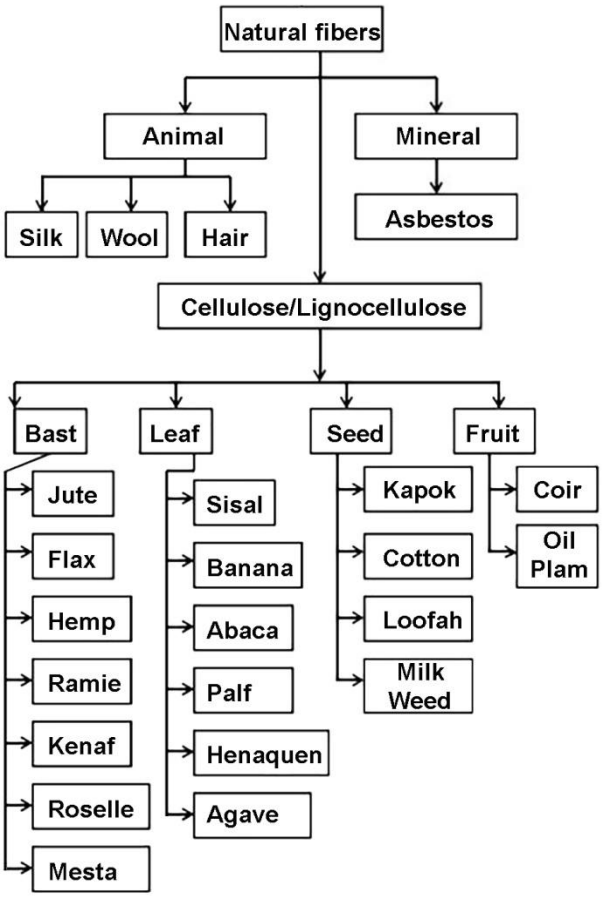

Figure I.2-3: Classification of vegetable fibers by origin.

– **Cellulose, hemicellulose and lignin content**

We can distinguish woody fibers (hard and rigid) from woody materials such as lumber, residues from the wood industry and non-woody fibers (soft, flexible), from non-woody plants often relatively annual less rich in lignin such as kenaf, hemp, sisal, jute and flax [14].

– **Length**

Plant fibers can be grouped into two categories: long fibers, so-called liberians, from the stems and bark of the stems of annual plants. They are soft, while the long fibers from leaves or tree trunks are harder and more rigid because of their high lignin content. Short fibers or tows which are associated with long fibers.

I.2.2.3. Use of vegetable fibers as reinforcements for polymers

The environmental and economic context pushes researchers and industrialists to use renewable resources for the development of new materials. Indeed, the depletion of fossil resources and the increasing global constraints on the control of polluting gas emissions accelerate the use of so-called renewable resources which have the capacity to be inexhaustible and have a carbon neutral balance thanks to photosynthesis. One of the avenues of study is the partial replacement of synthetic fibers (glass fibers, ...) by fibers from biomass, some works take stock and argue this potential from a mechanical and environmental point of view and point out their advantages and inconvenient. Thus, their specific properties are interesting for the development of thermoplastic matrix composites, which suggests that these naturally charged composites may be intended for applications in which the mechanical and thermal stresses are not very great [15]–[17]. For example, Bodros et al. [15] argue that it is possible to replace a polyester/glass fiber laminate with a polylactic acid-L(PLA)/flax fiber composite if the structure essentially supports tensile stresses.

Obtaining a composite with plant reinforcements requires perfect mastery of the shaping process (obtaining and production), and as synthetic fibers, chemical or physical preparation of plant fibers is necessary in order to ensure fiber/matrix adhesion. Indeed, without prior adequate preparation the use of these fibers as reinforcements risks creating a composite whose mechanical characteristics are less than expected with poor dimensional and geometrical stability. The development of a polymer matrix composite reinforced with vegetable fibers is complex and many constraints must be taken into consideration [18], [19]:

- The hydrophilic nature of the hydroxide groups (OH) of lignocellulose fibers makes them incompatible with most thermoplastics, generating an aggregation phenomenon reducing the effectiveness of the reinforcement.
- The choice of matrix is limited. In fact, the processing temperature must not exceed 200°C, the natural fibers quickly degrade at high temperatures. Tests have been carried out to improve the temperature resistance by depositing a layer of monomers on the fibers.

I.2.2.4. Presentation of some vegetable fibers used as reinforcement in bio-composite materials

- **Alfa fibers**

The term "Alfa" is an Arabic designation formerly designating all steppe grasses with resistant leaves and rushes in times of drought. The word of Latin origin "spartum", which gave "sparto" or "esparto", is the name used by the Spanish. Currently, only one plant is called alfa, it is "Stipa tenacissima L" [20]. The alfa is an endemic wild plant which grows in the form of tufts in the arid regions of the Mediterranean rim (Algeria, Morocco, Tunisia, Libya) (Figure I.2-4a). Nevertheless, its territorial distribution in Morocco remains the highest with a value of 3,186,000 ha. The roots of esparto trap soil particles and thus fight against erosion and desertification. The aerial part is made up of stems carrying nested sheaths one inside the other, the ears protruding its leaves which can reach 120 cm in length. The structure of the alfa fibers is heterogeneous. The tiny, microscopic fibers stuck to the leaves are called cellulosic filaments or fibrils. They have a length which varies from 1 to 5 mm and a diameter which varies from 5 to 10 µm. These fibrils are linked together by hemicellulose and thus form fibers [20].

- **Doum fibers**

The Chamaerops humilis (doum) is located in Southern Europe (Italy, Sardinia, and Spain), Algeria, and North Africa (Morocco). It has a short aerial part in the wild, hence its name (Figure I.2-4b). In cultivation, the ornamental palm can reach 8m high with several stems inclined, and the beauty of old specimens is absolutely stunning. In cultivation, the ornamental palm can reach 8m high with several stems inclined, and the beauty of old specimens is absolutely stunning. The Chamaerops is now one of the most cultivated palms. It is very hardy to cold, drought and, highly resistant to salt spray on the Atlantic coast. It can survive temperatures of −12°C, where the leaves can be reached but rarely the heart. The plant normally outs a new palm crown after such cold, and although the central part of the plant is destroyed, it releases normally and appears in the following spring [21]. The trunk is covered with several layers of brown fibers interlaced and bases of old petioles that persist several years after the leaves fall before breaking down and reveals a ringed stripe, relatively late, brown gray. Thirty to fifty palmate leaves are very variable

in width depending on the variety (from 40 cm in Chamaerops var. cerifera to 70 cm in the variety broadleaf), light green on top, and often wooly below (whitish fibers) [21].

– **Coir fibers**

Coir comes from coconut shell. It is grown mostly in western, central, and southern Africa, India, and on The Ivory Coast (Figure I.2-4c). The world production of coir fiber is estimated at 250,000 tones. The diameter of elementary fiber is 10–16 µm. Coir is used for brushes, mattresses, bags, and ropes. Combined with other materials, it is also applied for upholstery and in automotive industry [14].

– **Cactus fibers**

Cactus (Opuntia ficus indica) is a plant native to Mexico, which has naturalized in other continents, notably the Mediterranean basin and in South Africa and North Africa (Figure I.2-4d). It is a species of the Cactaceae family. It has been well adapted to extreme climatic conditions. The Opuntia family has about 1500 species of cactus and is primarily used for its fruit. Opuntia ficus indica is a plant that can reach 3 to 5 m high. It is organized in cladodes, known as modified rods. They have a flattened shape (30 to 40 cm long, 15 to 25 cm wide and 1.5 to 3 cm thick). This species is characterized by its rackets that contain spines. As a vegetable, an edible fruit is produced which can be used culinary or in the treatment of ulcer, wounds, liver conditions and fatigue. In North Africa, the cactus cultivation is also used to avoid the soil erosion, or as a forage substitute [22].

– **Jute fibers**

Jute fiber is extracted from the stem of an annual plant (Corchorus), belonging to Tiliaceae family, grown in Asia, Europe, and South America. Its technical fiber is long and soft with a lot of luster (Figure I.2-4e). The diameter of elementary fiber is about 15–35 µm. The cross section shows polygonal shape with the canal of different size. Jute is mostly used for sacks and all kinds of dressing materials. It is applied for packaging, conveyor belts, upholstery, and decorative fabrics [14].

– **Sisal fibers**

Sisal fiber is extracted from the leaves of Sisalana, a perennial plant originating in Mexico (Figure I.2-4f). Sisal plantations are located in South and Central America and Eastern Africa. The technical fiber in cross section is visible as a crescent or a horseshoe. Inside, polygonal elementary fibers with a round canal can be seen. The diameter of elementary fiber is about 15–30 µm. The fiber is mostly used for ropes, strings, bag fabrics, plaiting, mats, dart targets, and fishnet [14].

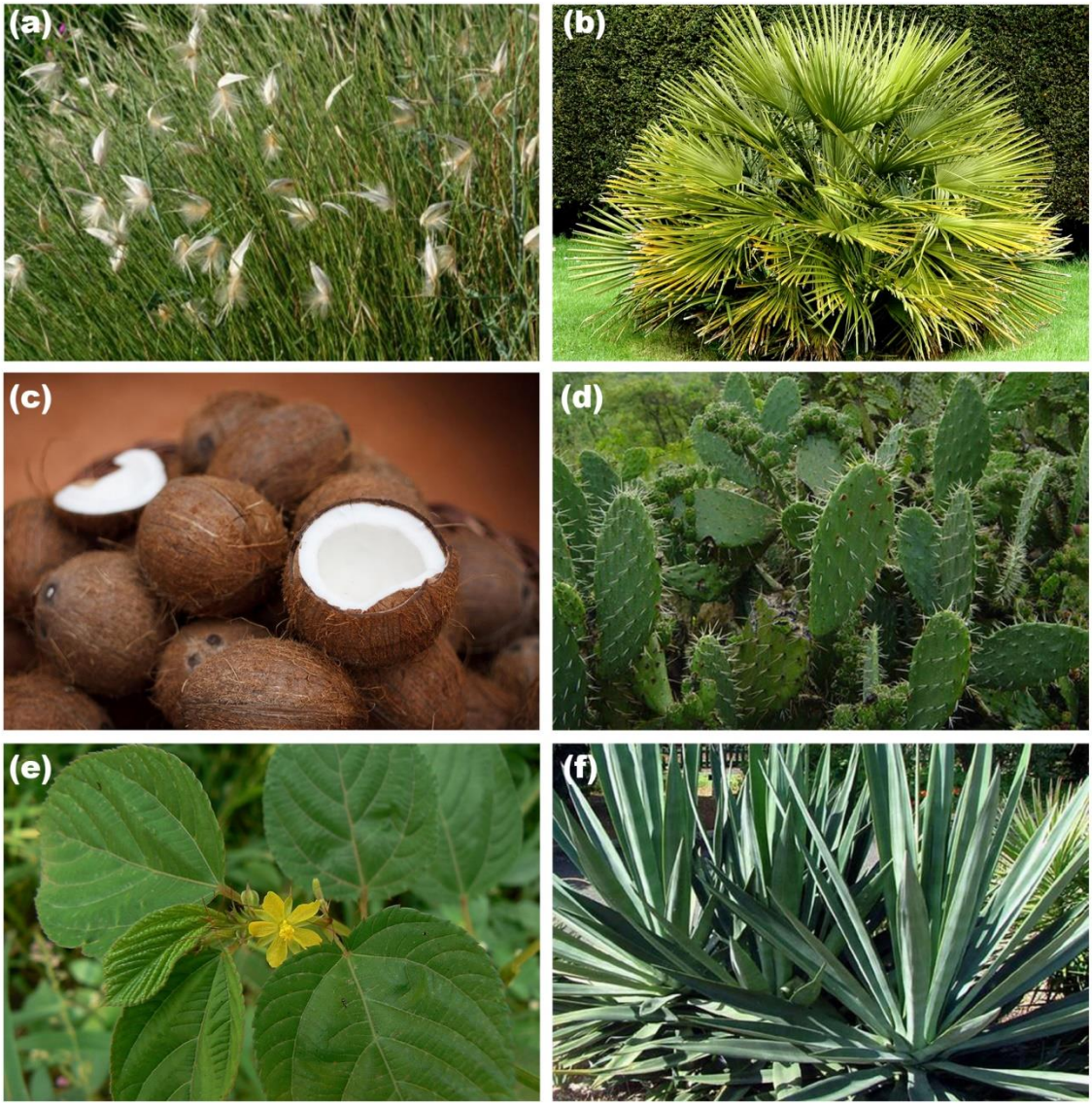

Figure I.2-4: Vegetable fibers: (a) Alfa fiber, (b) Doum fiber, (c) Coir fibers, (d) Cactus fibers, (e) Jute fibers and (f) Sisal fibers.

I.2.3. Processing of thermoplastic Bio-composites

One of the most commonly used forming methods for composite parts with a thermoplastic matrix reinforced with short fibers (<3mm) consists of a compounding step by extrusion/granulation, making it possible to obtain granules of mixture, subsequently shaped via an injection molding process. In addition, the compatibility between the fibers and the matrix is a decisive factor for the final behavior of the composite. This section will therefore be devoted to the presentation of the basic concepts of the shaping steps and to the description of the complexity of the use of coupling agent and its impact on the composites properties and behavior at melting state [23], [24].

I.2.3.1. Compounding

Compounding is a process allowing the melting of thermoplastic plastics and additives (reinforcing fillers, rubber and fibers), the final product is often in the form of granules. Various methods of compounding by extrusion/granulation exist but the principle is identical and is presented here through a separate dosage on a screw extruder (Figure I.2-5). The thermoplastic matrix is inserted at the start of the extruder and undergoes the first transformation, it's melting (Zone 1), the fibers cut to a length of the order of 3mm are then added to the molten matrix (Zone 2), and the last phase corresponds to the homogenization of the mixture and degassing (Zone 3). The latter is responsible for the decrease in the length of the fibers. At the outlet of the extruder, a composite rod is obtained, which is then cooled and then ground to obtain the granules of raw material necessary for the final shaping via injection molding [23].

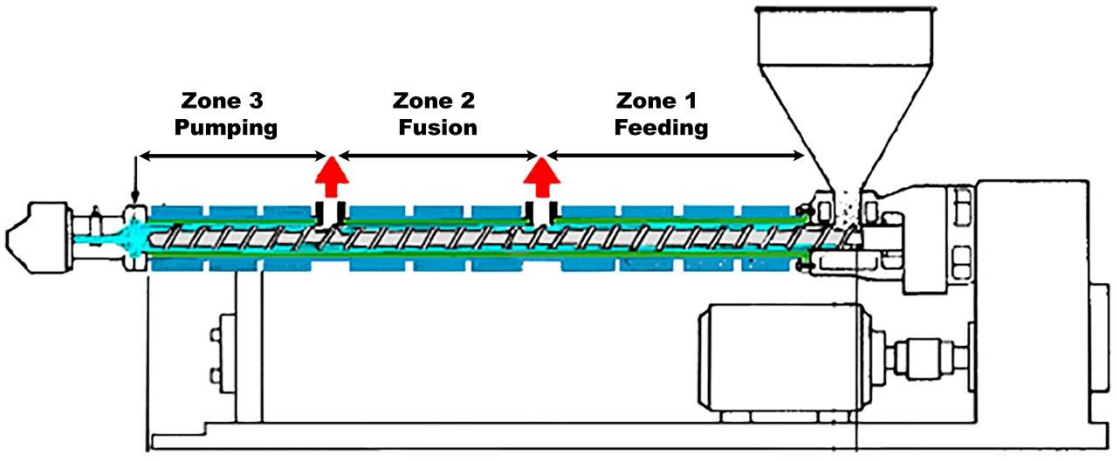

Figure I.2-5: Schematic representation of an extruder.

I.2.3.2. Injection molding

Injection molding represents one of the most important and popular molding technologies to manufacture plastic parts, especially those with complex geometry due to its low cost, high productivity and high precision [5], [25]. A typical injection molding cycle involves four distinct stages, namely clamping, injection, cooling and ejection stages (Figure I.2-6) [5], [25]. At first, the granules fed into the injection molding machine are gradually heated, melted and homogenized by the shear due to the rotation of the screw. The energy required for fusion comes from the combined action of mechanical dissipation and heat transfer from the heated sheath. This step is one of the origins of the decrease in the average length of the fibers, and will thus induce a non-homogeneous length distribution in the flow. At the chosen moment, the screw is pushed axially and plays the role of a piston by injecting at a controlled speed the molten polymer in the cavity of the mold. During filling, the fibers will be oriented in preferred directions according to the stresses involved. Once mold cavities have been filled, high pressure is maintained as far as possible until the material is frozen. An additional quantity of polymer is then introduced into the cavity, in order to limit the heat shrinkage and gradually standardize the pressure in the mold. Finally, the piece remains a few moments in the mold so that cooling can continue. Once the part is cooled, the mold opens and a mechanism to push the part out of the mold-Force is applied to eject the part because during cooling the part shrinks and adheres to the mold. During this time, the clamping phase starts again, so as to prepare the next cycle [5], [25].

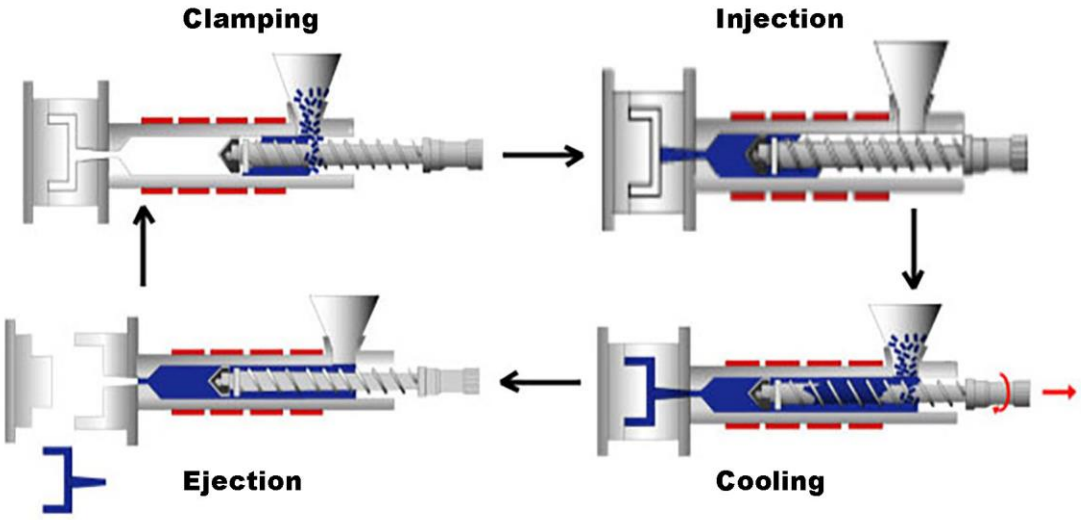

Figure I.2-6: Injection molding process cycle.

I.2.4. The impact of the injection molding process on the material final properties

The quality and final properties of the parts injected are strongly linked to the parameters of the process as well as the geometry of the part and the mold, since the latter, condition the distribution and orientation of fibers. In order to assess the properties of the solid-state part, it is important to understand the phenomena acting on the distribution of fibers and to know how they orient themselves during flow [2], [7].

During the filling phase of the charge in the mold, each fiber is transported by the flow and its orientation changes according to the constraints imposed by the matrix, the other particles as well as the walls of the mold. This results in a complex orientation distribution, varying considerably in the part, in particular depending on the thickness, thus affecting the mechanical properties [2], [7].

Consequently, in the next part of this chapter the description of the macroscopic models encountered in the literature for the prediction of the mechanical properties of bio-composites will be presented. While, the study of the flow front advancement as well as the flow induced fibers orientation will be detailed in the last two parts of this chapter.

I.3. Prediction of the thermoplastic bio-composite mechanical properties

Several mechanical models exist, and all focus on predicting the mechanical behavior of materials, being in relation with the microstructure of the inclusions (shape, orientation, volume fractions ... etc.). Among the models:

- **Voigt upper bound and Reuss lower bound (V-R model)**

The simplest way to predict the material mechanical properties, is to assume that the fibers and matrix are subjected to the same uniform strain in the fiber direction (Voigt) or that the fibers and matrix are aligned perpendicular to the direction of the externally applied stress (Reuss) Both models can be described respectively by equation I.3-1 and I.3-2 [2], [26]:

$$E_V = V_f E_f + (1 - V_f) E_m \quad \text{(I.3-1)}$$

$$E_R = \frac{E_f E_m}{V_f E_m + (1 - V_f) E_f} \quad \text{(I.3-2)}$$

Where E_V and E_R are respectively the Voigt and the Reuss elastic modulus, E_f and E_m represent the fiber and the matrix elastic modulus, respectively, and V_f is the fiber volume fraction.

– **Modified Rule of Mixture (mROM)**

The ROM has been modified by introducing an efficiency factor η_e which can be expressed as the product of the efficiency factor of orientation η_o and the efficiency factor of length η_l, being $\eta_e=\eta_o.\eta_l$. Its formulation for the Young's modulus is (Eq. I.3-3) [27], [28]:

$$E_{mROM} = \eta_e V_f E_f + (1 - V_f)E_m \quad \text{(I.3-3)}$$

According to Cox-Krenschel's model, the length efficiency factor η_l can be expressed following equation (I.3-4) [27], [28]:

$$\eta_l = 1 - \frac{\tanh(\beta'.l/2)}{(\beta'.l/2)} \text{ with } \beta' = \frac{1}{r}\sqrt{\frac{E_m}{E_f.(1-\nu).\ln.\sqrt{\pi/4.V_f}}} \quad \text{(I.3-4)}$$

Where, β' is the coefficient of stress concentration rate at the ends of the fibers, r is the mean radius of fiber, l is the fiber's length and ν is the Poison's ratio.

On the other hand, Fukuda and Kawata developed a methodology for calculating the efficiency factor of orientation η_o according to the fiber distribution in the matrix by using a limit angle (α_o) (Eq. I.3-5)[27], [28]:

Rectangular distribution:

$$\eta_o = \frac{\sin(\alpha_0)}{(\beta'.l/2)}.\left(\frac{3.\nu.\sin(\alpha_0)}{4.\alpha_0} + \frac{(1-\nu).\sin(3.\alpha_0)}{4.3.\alpha_0}\right) \quad \text{(I.3-5a)}$$

Sinusoidal distribution:

$$\eta_o = \frac{\pi^2}{16}.\left(\frac{1}{\frac{\pi}{2}+\alpha_0} + \frac{1}{\frac{\pi}{2}-\alpha_0}\right)\cos(\alpha_0).\left[\frac{3-\nu}{4}.\left(\frac{1}{\frac{\pi}{2}+\alpha_0} + \frac{1}{\frac{\pi}{2}-\alpha_0}\right)\cos(\alpha_0) + \frac{1+\nu}{4}.\left(\frac{1}{\frac{\pi}{2}+3\alpha_0} + \frac{1}{\frac{\pi}{2}-3\alpha_0}\right)\cos(3\alpha_0)\right] \quad \text{(I.3-5b)}$$

Triangular distribution:

$$\eta_o = 4.\frac{1-\cos(\alpha_0)}{\alpha_0^2}.\left(\frac{3-\nu}{4}.\frac{1-\cos(\alpha_0)}{\alpha_0^2} + \frac{1+\nu}{4}.\frac{1-\cos(3\alpha_0)}{9.\alpha_0^2}\right) \quad \text{(I.3-5c)}$$

– **Halpin-Tsai model**

It is used in the system of polymeric blends for unidirectional continuous and discontinuous phases. It also considered the fiber morphology by including an adjustable parameter noted ξ as expressed on Equation I.3-6. It is worth noting that for L→0 and ξ→0, the H-T model is reduced Reuss model. Contrariwise, For L→∞ and ξ→∞ it is reduced to Voigt model [27]–[30].

$$E_{H-T/L} = E_m\left(\frac{1+\xi.\eta_L.V_f}{1-\eta_L.V_f}\right) \text{ with } \eta_L = \frac{(E_f/E_m)-1}{(E_f/E_m)+\xi} \;;\; \xi = 2L/T \text{ or } \xi = 2L/D \quad \text{(I.3-6a)}$$

$$E_{H-T/T} = E_m\left(\frac{1+2.\eta_T.V_f}{1-\eta_T.V_f}\right) \text{ with } \eta_T = \frac{(E_f/E_m)-1}{\left(\frac{E_f}{E_m}\right)+2} \;;\; \xi = 2L/T \text{ or } \xi = 2L/D \quad \text{(I.3-6a)}$$

Where, $E_{H-T/L}$and $E_{H-T/T}$ denotes respectively the Halpin-Tsai longitudinal and transversal elastic modulus. L, T and D are the length, thickness and diameter of the fiber, respectively. ξ represents the measure of fiber geometry, fiber distribution and fiber loading conditions.

– **Modified Halpin-Tsai model**

Nielson modified the Halpin–Tsai equation by considering the particle packing fraction which is the true (apparent) volume occupied by filler noted ϕ_{max}. Theoretically, it can take a maximum value of 0.785, 0.907 and 0.82 for the arrangement of square, hexagonal and random fibers. According to this (Eq. I.3-7) [30]:

$$E_{m-H-T/L} = E_m\left(\frac{1+\xi.\eta_L.V_f}{1-\eta_L.\Psi.V_f}\right) \text{ with } \Psi = 1 + 1\left(-\frac{\phi_{max}}{\phi^2_{max}}\right)V_f \quad \text{(I.3-7)}$$

Where, $E_{m-H-T/L}$ is the modified Halpin-Tsai longitudinal elastic modulus.

– **Hui-Shia model**

It has been developed for longitudinal and transversal alignment fiber according to their aspect ratio β and expressed as following (Eq. I.3-8) [30], [31]:

$$E_{H-S/L} = E_m\left(1 - \frac{V_f}{\xi}\right)^{-1} \quad \text{(I.3-8a)}$$

$$E_{H-S/T} = E_m\left(1 - \frac{V_f}{4}\left(\frac{1}{\xi} + \frac{3}{\xi+J}\right)\right)^{-1} \quad \text{(I.3-8b)}$$

Where,

$$\xi = V_f + \frac{E_m}{E_f+E_m} + 3(1-V_f)\left[\frac{(1-g)\beta^2-\frac{g}{2}}{\beta^2-1}\right] \quad \text{(I.3-8c)}$$

$$g = 1 - \frac{\ln(2\beta)-1}{\beta^2} \text{ with } \beta \geq 1 \quad \text{(I.3-8d)}$$

$$J = (1-V_f)\left[\frac{3(\beta^2+0.25)g-2\beta^2}{\beta^2-1}\right] \quad \text{(I.3-8e)}$$

$E_{H\text{-}S/L}$ and $E_{H\text{-}S/T}$ are respectively the Hui-Shia longitudinal and transversal elastic modulus.

- **Hashin and Shtrikman model**

It considers the macroscopic isotropic orientation and the quasi-homogeneity of the composite where the shape of the filler is not a limiting factor, and estimated the Longitudinal and transverse Young's modulus by adjusting the bulk moduli K and shear moduli G of the composites as expressed on equation I.3-9 [31], [32].

$$E_{Ha-S} = \frac{9.K}{1+3.K/G} \quad \text{(I.3-9a)}$$

$$K_L = K_f + (1-V_f)\left[\frac{1}{K_m-K_f} + \frac{3.V_f}{3K_f-4G_f}\right]^{-1}; G_L = G_f + (1-V_f)\left[\frac{1}{G_m-G_f} + \frac{6.V_f(K_f+2.G_f)}{5.G_f(3K_f-4G_f)}\right]^{-1} \quad \text{(I.3-9b)}$$

$$K_T = K_m + V_f\left[\frac{1}{K_f-K_m} + \frac{3.(1-V_f)}{3K_m-4G_m}\right]^{-1}; G_T = G_m + V_f\left[\frac{1}{G_f-G_m} + \frac{6.(1-V_f)(K_m+2.G_m)}{5.G_m(3K_m-4G_m)}\right]^{-1} \quad \text{(I.3-9c)}$$

$E_{Ha\text{-}S}$ is the Hashin and Shtrikman young modulus, K_L, K_T, G_L and G_T denote respectively the longitudinal and transversal bulk and shear modulus, and K_f, K_m, G_f and G_m represent respectively the fiber and the matrix bulk and shear modulus.

– **Tsai-Pagano model**

It assumes a random filler orientation in the matrix as well as good dispersion and perfect fiber-matrix interfacial adhesion. It also includes the reinforcing fibers length and diameter. According to equation I.3-10 he use as a values of 3/8 and 5/8 as a contribution of the longitudinal and transversal models, respectively [27], [28], [33].

$$E_{T-P} = \frac{3}{8}E_V + \frac{5}{8}E_R \quad \text{(I.3-10a)}$$

$$E_{T-P} = \frac{3}{8}E_{H-T/L} + \frac{5}{8}E_{H-T/T} \quad \text{(I.3-10b)}$$

Where, $E_{T\text{-}P}$, E_V, and E_R are the Tsai-Pagano, Voigt and Reuss elastic modulus, respectively.

– **Hirsch model**

It takes into account the effects of fiber orientation and stress concentration (fiber ends) by introducing into its equation (Eq. I.3-11) an empirical parameter ‘‘x’’ (0 <x < 1) which is also the combination of parallel and serial models. A value of x = 0.5 has been proposed for a random fiber orientation [28], [29], [34].

$$E_H = x\,E_V + (1 - x)E_R \quad \text{(I.3-11)}$$

Where, E_H is the Hirsch elastic modulus.

As a conclusion, an accurate determination of the composite mechanical properties before designing requires the prediction of the fiber orientation field during injection molding. So, the fiber motion and rotation is closely affected by the flow front behavior.

I.4. Study of the thermoplastic bio-composite flow front advancement

The bio-composite polymer during injection molding undergoes significant thermomechanical transformations, which condition the quality of the final product. However, the study of the molten material flow in the mold imprint brings together a lot of phenomena, namely the evolution of the rheological parameters.

I.4.1. Rheological behavior of the bio-composite material

Rheology is the deformation, thermal and material flow study. It is dedicated to the study of viscoelastic materials that include both liquid and solid properties; we talk about soft material. The rheological behavior of the reinforced polymers depends on many parameters, such as the nature of the fillers (size, shape), the concentration, the interactions between the fillers and between the polymer and the fillers. These parameters cause not only an increase in viscosity, but also particular phenomena such as, for example, the existence of a flow threshold, a thixotropic, shearing thinning or shearing thickening behavior. In the case of polymers, rheology therefore only studies the displacements, which are large relative to the size of the macromolecules. Intramolecular movements and the entanglement of chains are movements that rheology by nature cannot describe. On the other hand, these local movements are at the basis of the explanation of the molten polymers rheological behavior [35].

I.4.2. Viscoelasticity of the bio-composite material

The goal of rheology is not only to study the viscoelastic properties of fluids but also to model and classify certain families of materials with each other. The manner in which the material flows makes it possible to draw different characteristic curves of the material as shown in figure I.4-1. Thus the rheometer achieves discrete stress ramps and measures the shear rate or applies shear rates and measures the resulting shear stress. In both cases, the measurement makes it possible to measure the viscosity at different shear gradients or at different stresses [36].

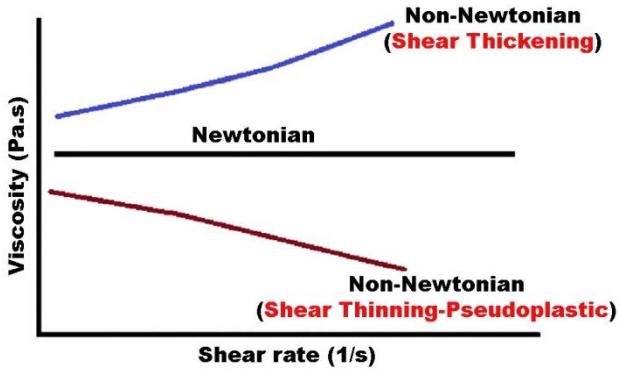

Figure I.4-1: Different characteristic curves of the material.

I.4.2.1. Newtonian fluids

The rheological behavior of solutions and suspensions depends largely on their concentration and the nature of the material that constitutes them. It can vary from Newtonian behavior to more complex behavior. A solution or suspension is said to be diluted if the particles are sufficiently distant from each other so that the interactions between them can be neglected.

By definition, a Newtonian fluid has a dynamic viscosity independent of the shear rate ("Newtonian curve (perfect viscous)" following the equation I.4-1. In this case, the viscometer alone is sufficient, giving directly a value of viscosity valid whatever the shear conditions [36].

$$\tau = \eta.\gamma \quad \text{and} \quad \eta = \frac{\tau}{\gamma} \tag{I.4-1}$$

Where, τ is the shear stress, η is the dynamic viscosity and γ the shear rate.

I.4.2.2. Non-Newtonian fluids

A non-Newtonian fluid is characterized by the non-linear relationship between shear stress and shear rate. This is due to the complex structure and deformation effects exhibited by the materials involved in such fluids. The non-Newtonian fluids are however diverse and can be characterized as pseudoplastic and dilatant fluids [37].

- **Pseudoplastic behavior (Shear thinning)**

The shearing thinning behavior is the most common; it corresponds to a decrease in viscosity when applying a growing shear rate. For polymer solutions, this behavior is due to the separation of entangled macromolecules and their alignment in the direction of flow as the shear rate increases. In suspensions the decrease in viscosity comes from the gradual disappearance of organized structures [38]. Numerous models have been developed to account for the shear flow of a fluid, giving as many phenomenological models for viscosity.

A much used empirical law for the variation of the viscosity with the velocity gradient is the power law, proposed by Ostwald in 1925 (Eq. I.4-2a) [38]:

$$\tau = k.\dot{\gamma}^{n} \quad \text{and} \quad \eta = k.\dot{\gamma}^{n-1} \tag{I.4-2a}$$

Where “k” is a coefficient (also called consistency of the fluid) and “n <1” an exponent which expresses the difference with the Newtonian behavior for which “n = 1” (or index of flow behavior). Although this model can solve a large number of flow problems, it should be borne in mind that it does not describe well the low and high shear rate behavior (as we will see later in the last chapter) and that parameters “k” and “n” do not have a clear physical interpretation. In reality, a shear thinning fluid is only for a certain range of shear rates. For low and high shears, Newtonian behavior is observed with the possible appearance of a viscosity region. An extension of the power law model is the model of Cross (Eq. I.4-2b) [39]:

$$\frac{\eta-\eta_\infty}{\eta_0-\eta_\infty}=\frac{1}{1+(\lambda.\dot{\gamma})^m} \qquad \text{(I.4-2b)}$$

Another more sophisticated model than the power law model taking into account zero and infinite shear viscosity trays is the Carreau-Yasuda model (Eq. I.4-2c):

$$\frac{\eta-\eta_\infty}{\eta_0-\eta_\infty}=\left[1+(\lambda\dot{\gamma})^\alpha\right]^{\frac{m-1}{\alpha}} \qquad \text{(I.4-2c)}$$

For these two models, η_0 and η_∞ are respectively the zero and infinite shear viscosity, λ is a time constant, m is a constant and has a parameter "α" which describes the transition between the low shear behavior and the power law.

Another approach is that of Quemada [40] which has the advantage of having a more physical sense than the previous ones. The Quemada model [40], [41] was developed to account for viscosity variations in materials containing aggregates rigid, spherical and non-interactive (concentrated particle suspensions). It is based on the principle of minimal dissipation of energy within the fluid and admits the relation (Eq. I.4-2d):

$$\eta=\eta_\infty\left[\frac{1+(\frac{\sigma}{\sigma_c})^p}{\chi+(\frac{\sigma}{\sigma_c})^p}\right]^2 \qquad \text{(I.4-2d)}$$

Where “σ” is the applied stress, “σ_c” is the characteristic stress, “p” is the slope of the curve at the point of inflection and “χ” is a parameter that depends on the volume fraction ($\chi=\frac{\eta_\infty}{\eta_0}^{1/2}$) [35].

– **Dilatant behavior (Shear thickening)**

These are fluids whose viscosity increases with the shear rate. Shear thickening is much more rarely observed than shear thinning. However, some concentrated suspensions (corn starch) and wet sand have a pseudoplastic behavior. A fluid can be dilatant for a certain range of shear rates, and pseudoplastic or even Newtonian for other ranges [42]. The shear thickening was first observed by the dilatation phenomenon evidenced by the Reynolds experiment in 1885. Then, various theories have been developed to explain the phenomenon of shear thickening [43]–[45]. Actually, it is believed that the shear thickening is due to the temporary formation of aggregates of particles under shear whose conditions of appearance may differ according to the type of suspensions [35].

I.4.3. Fluid flows

A fluid can be incompressible when its density does not depend on pressure or temperature (Figure I.4-2). Generally, in fluid statics, liquids are considered to be incompressible and gases are compressible. It is the flow nature, which makes it possible to distinguish the compressible flow from the incompressible flow and not the nature of the fluid [35].

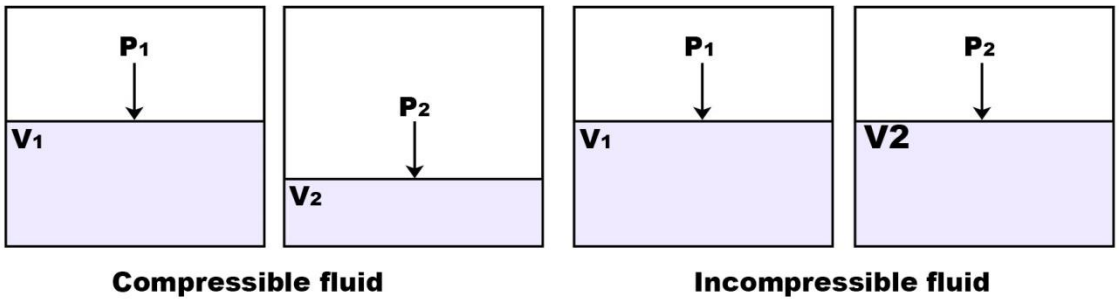

Figure I.4-2: Compressible and incompressible fluid.

Apart from the physical criterion which distinguishes compressible and incompressible flows, as well as viscous and non-viscous flows, there are other criteria which distinguish fluid flows:

– **The geometric criterion:**

- Internal flows: they take place inside a pipe. Examples: river, canal.
- External flows: they occur around solid bodies, for example a ship or an airplane.

– **The kinematic criterion:**

- Uniform flows: if its velocity components are independent of space coordinates.
- Permanent or stationary flows: if its velocity components are independent of the time variable.

A final distinction concerns laminar and turbulent flows (Figure I.4-3) [46]:

- **Laminar flow** or streamline flow in pipes (or tubes) occurs when a fluid flow in parallel layers, with no disruption between the layers. At low velocities, the fluid tends to flow without lateral mixing, and adjacent layers slide past one another like playing cards. There are no cross-currents perpendicular to the direction of flow, nor eddies or swirls of fluids. In laminar flow, the motion of the particles of the fluid is very orderly with all particles moving in straight lines parallel to the pipe walls. Any lateral mixing (mixing at right angles to the flow direction) occurs by the action of diffusion between layers of the liquid. Diffusion mixing can be slow however if the diameter of the pipe of tube is small then this diffusive mixing can be very significant. Laminar flow is also characterized by Reynolds numbers below 2000.
- **Turbulent flow** is a flow regime characterized by chaotic property changes. This includes rapid variation of pressure and flow velocity in space and time. In contrast to laminar flow the fluid no longer travels in layers and mixing across the tube is highly efficient. Flows at Reynolds numbers larger than 4000 are typically (but not necessarily) turbulent.

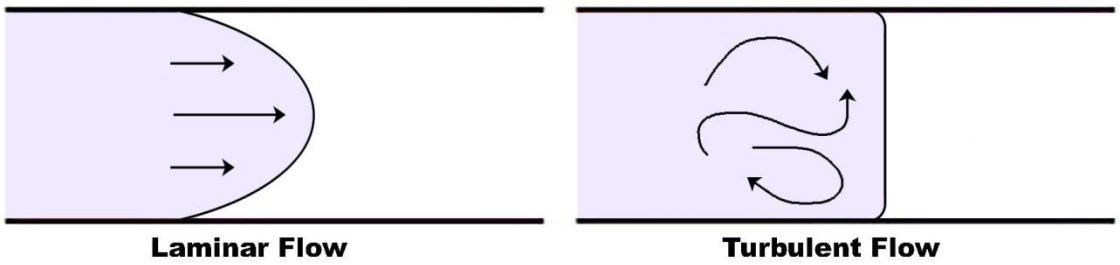

Figure I.4-3: Laminar and turbulent flow.

I.4.4. Internal flows-Laminar established flows between two parallel planes

Internal flows have the particular character of the absence of infinite boundary conditions, which is not the case for external flows. The influence of the walls is therefore manifested in all

directions, except possibly at the fluid inlet and outlet sections. The diversity of the possible geometries obviously leads to a great variety in the structure of the flows, but they are most often flows of the boundary layer type, as for example in the pipes.

I.4.4.1. Properties of established flows

The model for studying the filling phase of a mold during injection molding is based on three principles of the physics of continuous media. This will allow determining the mechanical parameters at all points of the part and at all times (Pressure, Speed, Shear rate, etc.) [5].

Mass conservation (continuity):

$$\frac{\partial \rho}{\partial t} + \text{div}\,(\rho V) = 0$$

$$\frac{\partial \rho}{\partial t} + \frac{\partial(\rho V_x)}{\partial x} + \frac{\partial(\rho V_y)}{\partial y} + \frac{\partial(\rho V_z)}{\partial z} = 0 \qquad \text{(I.4-3)}$$

Momentum conservation:

$$\rho\left(\frac{\partial V}{\partial t} + V\text{grad}V\right) = -\text{grad}\,P + \eta(\Delta V) + \rho g$$

$$\rho\left(\frac{\partial V_x}{\partial t} + V_x\frac{\partial V_x}{\partial x} + V_y\frac{\partial V_x}{\partial y} + V_z\frac{\partial V_x}{\partial z}\right) = -\frac{\partial P}{\partial x} + \eta\left(\frac{\partial^2 V_x}{\partial x^2} + \frac{\partial^2 V_x}{\partial y^2} + \frac{\partial^2 V_x}{\partial z^2}\right) + \rho g_x \qquad \text{(I.4-4a)}$$

$$\rho\left(\frac{\partial V_y}{\partial t} + V_x\frac{\partial V_y}{\partial x} + V_y\frac{\partial V_y}{\partial y} + V_z\frac{\partial V_y}{\partial z}\right) = -\frac{\partial P}{\partial y} + \eta\left(\frac{\partial^2 V_y}{\partial x^2} + \frac{\partial^2 V_y}{\partial y^2} + \frac{\partial^2 V_y}{\partial z^2}\right) + \rho g_y \qquad \text{(I.4-4b)}$$

$$\rho\left(\frac{\partial V_z}{\partial t} + V_x\frac{\partial V_z}{\partial x} + V_y\frac{\partial V_z}{\partial y} + V_z\frac{\partial V_z}{\partial z}\right) = -\frac{\partial P}{\partial z} + \eta\left(\frac{\partial^2 V_z}{\partial x^2} + \frac{\partial^2 V_z}{\partial y^2} + \frac{\partial^2 V_z}{\partial z^2}\right) + \rho g_z \qquad \text{(I.4-4c)}$$

Energy conservation:

$$\frac{dH}{dt} = \left(\frac{\partial H}{\partial t} + V.\overrightarrow{grad H}\right) = \alpha\,\Delta H + \eta\dot{\gamma}^2 \qquad \text{(I.4-5a)}$$

$$\left(\frac{\partial H}{\partial t} + V_x\frac{\partial H}{\partial x} + V_y\frac{\partial H}{\partial y} + V_z\frac{\partial H}{\partial z}\right) = \alpha\left(\frac{\partial^2 H}{\partial x^2} + \frac{\partial^2 H}{\partial y^2} + \frac{\partial^2 H}{\partial z^2}\right) + \eta\dot{\gamma}^2 \qquad \text{(I.4-5b)}$$

$$\dot{\gamma} = \sqrt{\left(\frac{\partial V_x}{\partial x}\right)^2 + \left(\frac{\partial V_y}{\partial y}\right)^2 + \left(\frac{\partial V_z}{\partial z}\right)^2} \qquad \text{(I.4-5c)}$$

where x, y and z are the Cartesian coordinates, t is the time, ρ is the density, V_x, V_y and V_z are the velocities in x, y and z directions respectively, P is the pressure, g is the acceleration of gravity, η is the dynamic viscosity, α is the thermal diffusivity, H is the enthalpy and $\dot{\gamma}$ is the shear rate.

From continuity equation with laminar flow and two-dimensional Cartesian geometry, a flow is established if at any point M (x, y) we have (Eq. I.4-6):

$$\frac{\partial V_x}{\partial x} = 0 \qquad \text{(I.4-6)}$$

x being the general direction of the flow and y the perpendicular direction. This assumption means that the component V_x depends only on y: there is an invariance of the velocity profiles along the flow.

An immediate consequence of this definition is that (Eq. I.4-7):

$$\frac{\partial^2 V_x}{\partial x^2} = 0 \qquad \text{(I.4-7)}$$

The implications of condition (Eq. I.4-6 and I.4-7) are important if we consider that the fluid is isochoric (ρ = cte).

1. From the continuity equation $\frac{\partial V_x}{\partial x} + \frac{\partial V_y}{\partial y} = 0$ we deduce (Eq. I.4-8) [5]:

$$\frac{\partial V_y}{\partial y} = 0 \qquad \text{(I.4-8)}$$

Let V_y be independent of y at any point. This is incompatible with the boundary conditions, unless V_y is zero everywhere. We must therefore have V=0, and therefore in particular that the pipeline is rectilinear and of constant section, the generatrices of the wall being parallel to the x-axis: $S_0(x)=S=cte$.

2. Navier Stokes equations (Eq. I.4-9) [5]:

$$\frac{\partial \vec{v}}{\partial t} + (\vec{v}.\vec{\nabla})\vec{v} = -\frac{1}{\rho}\vec{\nabla}P + \frac{1}{\rho}\vec{f}_{v\,ext} + \nu\,\vec{\Delta}\vec{v} \qquad \text{(I.4-9a)}$$

$$\left[\frac{\partial V_x}{\partial t} + V_x\frac{\partial V_x}{\partial x} + V_y\frac{\partial V_x}{\partial y} + V_z\frac{\partial V_x}{\partial z}\right] = -\frac{1}{\rho}\frac{\partial P}{\partial x} + \frac{1}{\rho}f_x + \nu\left[\frac{\partial^2 V_x}{\partial x^2} + \frac{\partial^2 V_x}{\partial y^2} + \frac{\partial^2 V_x}{\partial z^2}\right] \qquad \text{(I.4-9b)}$$

$$\left[\frac{\partial V_y}{\partial t} + V_x\frac{\partial V_y}{\partial x} + V_y\frac{\partial V_y}{\partial y} + V_z\frac{\partial V_y}{\partial z}\right] = -\frac{1}{\rho}\frac{\partial P}{\partial y} + \frac{1}{\rho}f_y + \nu\left[\frac{\partial^2 V_y}{\partial x^2} + \frac{\partial^2 V_y}{\partial y^2} + \frac{\partial^2 V_y}{\partial z^2}\right] \quad \text{(I.4-9c)}$$

$$\left[\frac{\partial V_z}{\partial t} + V_x\frac{\partial V_z}{\partial x} + V_y\frac{\partial V_z}{\partial y} + V_z\frac{\partial V_z}{\partial z}\right] = -\frac{1}{\rho}\frac{\partial P}{\partial z} + \frac{1}{\rho}f_z + \nu\left[\frac{\partial^2 V_z}{\partial x^2} + \frac{\partial^2 V_z}{\partial y^2} + \frac{\partial^2 V_z}{\partial z^2}\right] \quad \text{(I.4-9d)}$$

In permanent flow, the first equation of Navier Stokes (Eq. I.4-9b) becomes:

$$\left[V_x\frac{\partial V_x}{\partial x} + V_y\frac{\partial V_x}{\partial y}\right] = -\frac{1}{\rho}\frac{\partial P}{\partial x} + \nu\left[\frac{\partial^2 V_x}{\partial x^2} + \frac{\partial^2 V_x}{\partial y^2}\right] \quad \text{(I.4-9e)}$$

$$0 = -\frac{1}{\rho}\frac{\partial P}{\partial x} + \nu\left[\frac{\partial^2 V_x}{\partial y^2}\right] \quad \text{(I.4-9f)}$$

The existence of solutions at any point of the flow leads to:

$$\nu\left[\frac{\partial^2 V_x}{\partial y^2}\right] = \text{cte} \quad \text{and} \quad \frac{\partial P}{\partial x} = \text{cte} \quad \text{(I.4-9g)}$$

While, the second Navier Stokes equation (Eq. I.4-9c) becomes:

$$\left[V_x\frac{\partial V_y}{\partial x} + V_y\frac{\partial V_y}{\partial y} + V_z\frac{\partial V_y}{\partial z}\right] = -\frac{1}{\rho}\frac{\partial P}{\partial y} + \nu\left[\frac{\partial^2 V_y}{\partial x^2} + \frac{\partial^2 V_y}{\partial y^2}\right] \quad \text{(I.4-9h)}$$

This is reduced to (Eq. I.4-9i):

$$\frac{\partial P}{\partial y} = 0 \quad \text{(I.4-9i)}$$

where V, P, ρ, ν are the velocity, pressure, density and kinematic viscosity ($\nu=\eta/\rho$), respectively.

That is to say: P=cte on a straight section, since the direction y is perpendicular to the generatrices of the wall.

I.4.4.2. Couette's flow

Couette's experience and its usual diagram: laminar flow of a fluid between two parallel planes, one of which is fixed, and the other animated at a speed V_{xe}. The goal here is to determine the velocity distribution in a straight section, and its relationship with the flow speed and the flow rate of fluid transported [47], [48].

Equations (I.4-9f and g), valid in established flow, can also be written (Eq. I.4-10a):

$$\frac{1}{\rho}\frac{\partial P}{\partial x} = \nu\left[\frac{\partial^2 V_x}{\partial y^2}\right] = cte \qquad \text{(I.4-10a)}$$

This gives by integrating (Eq. I.4-10b):

$$V_x = \frac{1}{2\eta}\frac{\partial P}{\partial x}\, y^2 + C_1\, y + C_2 \qquad \text{(I.4-10b)}$$

The constants C_1 and C_2 are fixed by the boundary conditions:

$$\begin{cases} y = 0\,;\, V_x = 0 \\ y = e\,;\, V_x = V_e \end{cases}$$

Thus obtaining (Eq. I.4-10c):

$$V_x = \frac{1}{2\eta}\frac{\partial P}{\partial x}\, y^2 + \left[\frac{V_e}{e} - \frac{e}{2\eta}\frac{\partial P}{\partial x}\right] y \qquad \text{(I.4-10c)}$$

The speed profile is therefore parabolic (Figure I.4-4b). Its concavity is given by the second derivative $\frac{1}{\rho}\frac{\partial P}{\partial x} = \nu\left[\frac{\partial^2 V_x}{\partial y^2}\right]$ which is of the sign of $\frac{\partial P}{\partial x}$.

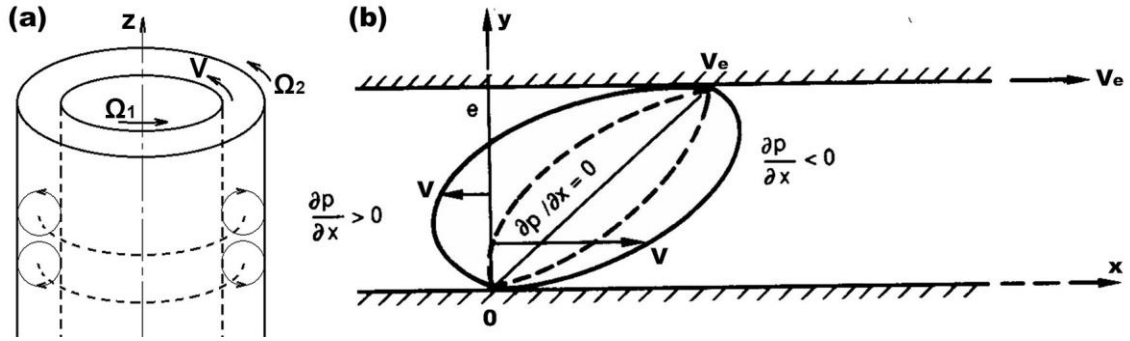

Figure I.4-4: Velocity distribution in a Couette flow.

In the absence of a pressure gradient (dP/dx = 0) the speed distribution between the two planes becomes linear (Eq. I.4-10d):

$$V_x = V_e\,\frac{y}{e} \qquad \text{(I.4-10d)}$$

The shear τ in the flow is then uniformly distributed (Eq. I.4-10e):

$$\tau = \eta\,\frac{\partial V_x}{\partial y} = \eta\,\frac{V_e}{e} = cte \qquad \text{(I.4-10e)}$$

The total flow rate between the two planes is due to both the drive speed and the pressure gradient. By designating by l the width of the fluid vein, the flow rate Q is written, in a section S_0 (Eq. I.4-10f) [47], [48]:

$$Q = \int_{S_0} V_x \, dS = l \int_0^e V_x \, dy \qquad \text{(I.4-10f)}$$

From equation I.4-10c, we obtain (Eq. I.4-10g):

$$Q = l\frac{e}{2}\left[V_e - \frac{e^2}{6\eta}\frac{\partial P}{\partial x}\right] \qquad \text{(I.4-10g)}$$

I.4.4.3. Flow in a flat rectangular duct

In this configuration, the flow is only caused by the pressure gradient, itself imposed by the boundary conditions. But the speed distribution and the flow rate are obtained from the Couette model by simply making $V_{xe} = 0$ since the two planes are fixed. We note that e = 2b the height or (thickness) of the channel (Figure I.4-5) [47], [48].

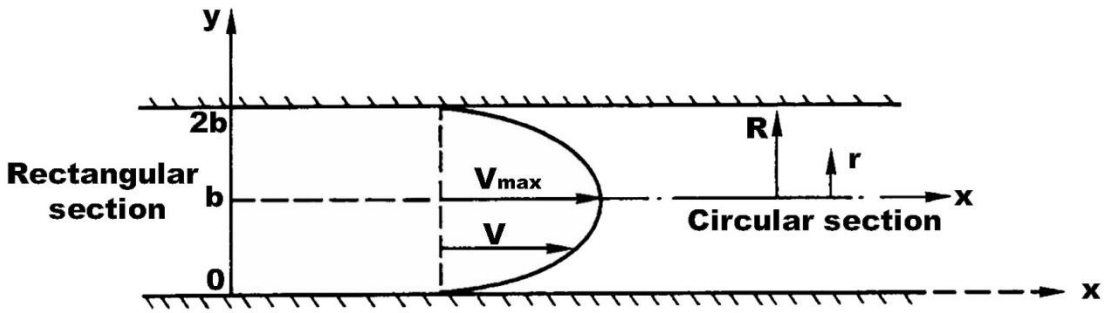

Figure I.4-5: Laminar flow: fluid vein of rectangular or circular section.

This therefore gives:

– For the velocity (Eq. I.4-11a):

$$V_x = \frac{1}{2\eta}\frac{\partial P}{\partial x}(y^2 - 2by) \qquad \text{(I.4-11a)}$$

It is in the middle of the pipe (y=b) that V_x reaches its maximum value V_m (which is obviously logical due to the symmetry) (Eq. I.4-11b) [47], [48]:

$$V_m = \frac{b^2}{2\eta}\frac{\partial P}{\partial x} \qquad \text{(I.4-11b)}$$

Equation I.4-11b further shows that the velocity distribution V_x in the section is parabolic, and that the direction of flow is indeed that of decreasing pressures (V_x is of the opposite sign of dP/dx).

– For the flow rate (Eq. I.4-11c):

$$Q = -\frac{2}{3}\frac{l\, b^3}{\eta}\frac{\partial P}{\partial x} \qquad \text{(I.4-11c)}$$

I.4.4.4. Any section piping

In the general case, the calculations must be made in three dimensions and the results are generally not presented in analytical form. However, in established flow ($\frac{\partial V_x}{\partial x} = 0$, V_y=V_z=0, $\frac{\partial P}{\partial x} = cte$), the flow remains proportional to the pressure gradient $\frac{\partial P}{\partial x}$ [5].

In fact, in direction x, equation I.4-9b is written (Eq. I.4-12a):

$$\frac{1}{\rho}\frac{\partial P}{\partial x} = \nu\left[\frac{\partial^2 V_x}{\partial y^2} + \frac{\partial^2 V_x}{\partial z^2}\right] = cte \qquad \text{(I.4-12a)}$$

So, the velocity can be written in the form of (Eq. I.4-12b):

$$V_x = \frac{1}{\eta}\frac{\partial P}{\partial x}(Ay^2 + Bz^2 + Cyz + Dy + Ez + F) \qquad \text{(I.4-12b)}$$

Where A, B… are constants. The local speed V_x is therefore proportional to the pressure gradient, and the same is true for the flow rate Q.

All these speeds calculate by solving the complete equations of mass, momentum and energy balance in their general form, using the real geometry of the mold, are used mainly for the flow front shape and position prediction. And since, the flow during processing plays a significant role in forming a complex fiber orientation field, the prediction of fiber orientation inside the mold cavity are among the major issues in the molding processes.

I.5. Study of the flow induced fibers orientation

When injecting reinforced thermoplastics, the stresses during the flow and the mold filling have the effect of orienting the fibers preferentially. The flow during filling is done under the fountain effect and thus the competition between the two types of flow (shear and elongation) will tend to orient the fibers. It is possible to determine the properties of composites by knowing the orientation of the fibers in the polymer, which directly affects these properties. In this section, both mechanisms governing fiber orientation and the parameters influencing their orientation will be discussed [26].

I.5.1. Injection orientation mechanisms

This section is devoted to studying the fiber orientation in the suspension during the shaping process. During the filling process, the fibers will be oriented in preferred directions depending on the applied stress. In order to understand the phenomena that govern the orientation of the fibers, their movement will be described once subjected respectively to a shear and elongation flow.

I.5.1.1. A single fiber orientation in a shear flow

Several studies have cited that an isolated fiber, in shear flow with a Newtonian fluid, is animated by a periodic movement [49]. This period T is inversely proportional to the shear rate $\dot{\gamma}$ and approximately proportional to the aspect ratio β of the fiber, defined as being the ratio between the length and the diameter of the fiber (Eq. I.5-1) [49]:

$$T = \frac{2\pi}{\dot{\gamma}} . \beta . (1 + \beta) \qquad \text{(I.5-1)}$$

Thus, the fiber never tends toward an equilibrium position. Indeed, it rotation speed is not constant, it rotates rapidly when the fiber is perpendicular to the direction of the flow and slowly when it's aligned with the flow. In the case of a non-Newtonian flow, the fiber undergoes also a rotation movement [50]. For example, this type of flow is found mainly in the mold feeding channels especially between parallel plates as shown in the figure I.5-1 and in a thin cavity.

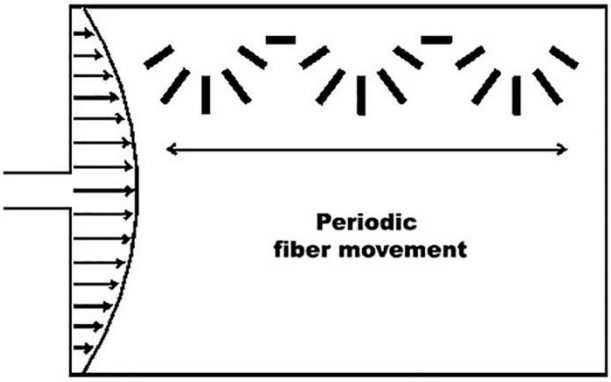

Figure I.5-1: Movement of a single fiber suspended in a Newtonian fluid.

I.5.1.2. A single fiber orientation in an elongation flow

An elongational flow allows a fiber to be oriented parallel to or perpendicular to the direction of flow during filling, this is dependent on rate of elongation whether it is positive or negative. If the elongation rate is positive, the flow is convergent and it is divergent if the elongation rate is negative. In this type of flow, the particles evolve to a stationary state by moving in the stretching direction of the fluid, thus, there is a stable equilibrium position [50]. For instance, this type of flow is found in the axis of a convergent or divergent geometry as illustrated the figure I.5-2.

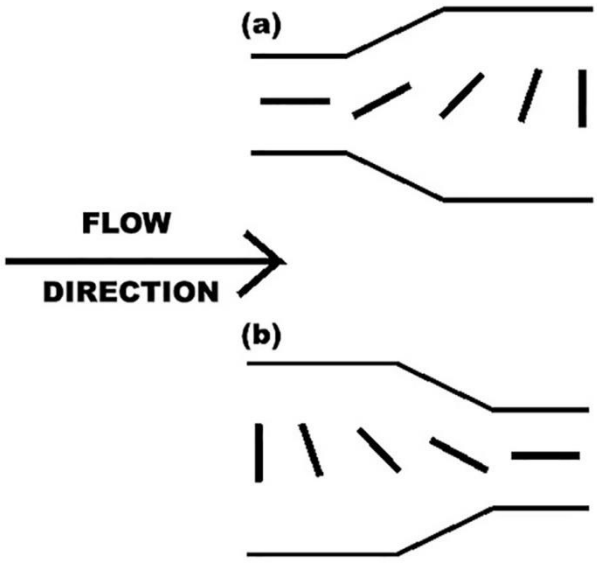

Figure I.5-2: Movement of a single fiber suspended in the elongation flow: (a) Negative elongational flow, (b) Positive elongational flow.

I.5.1.3. Injection orientation mechanisms

In general, the plastic injection molding leads to the realization of a cavity of different thickness, and the obtained piece is classified as thin or thick. Thus, the fiber orientation varies in the thickness of the piece [20] and it is observed that in the thick part, this orientation has a rather special structure, commonly called core-skin structure. Figure I.5-3 illustrates the core-shell-skin structure and the orientation distribution of the fibers throughout the thickness of a disk injected by the center. Several distinct layers are observed and there is symmetry relative to the median plane of the disc (the D layer). Indeed, in the thin skin layer (A), the fiber tends to orient in an isotropic way. In the two layers (B), the fibers are oriented in the flow direction due to the interested stress shear. The core layer (D) is characterized by dominant of elongational stress which means that the fibers tend to orient perpendicular to flow direction. Finally, the layer (C) is a transition layer characterized by a random fiber orientation [51].

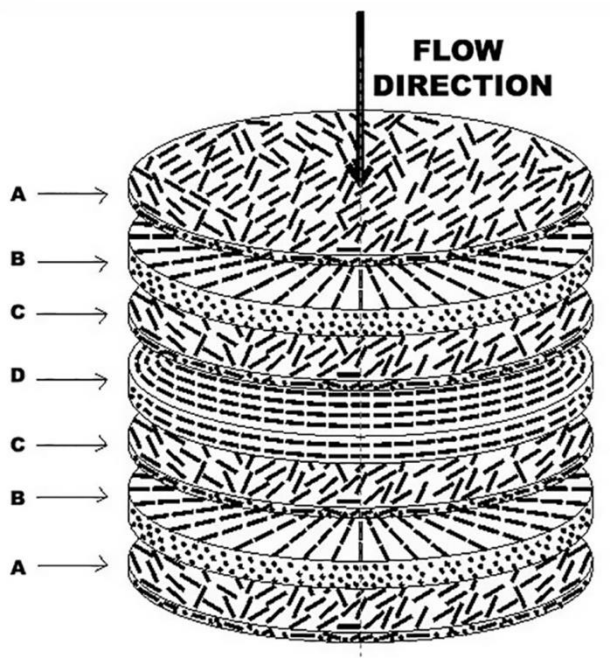

Figure I.5-3: Fiber orientation distribution in a disk injected by the center.

During injection molding process and near the walls, a solidified polymer layer is formed, which allows the fibers not to have a determined orientation. The fountain flow effect has a non-negligible role in term of fibers orientation close to the flow front. In order to further clarify this

phenomenon, it is useful to think of the fountain region as a “machine” that absorbs fibers near the midplane, changes their orientation, and ejects them near the mold wall.

Thus, the fountain flow moves the material of the core layer to skin layer where it is frozen prior to alignment of the fibers in the flow direction by shearing in space. So, the fountain flow effect is the main actor of the formation of the skin layer allowing perpendicular fibers orientation and to the flow direction in the free surface [52]–[54]. Additionally, it creates a divergent flow (stretching flow) near the free surface as shown in figure I.5-4. Between the core and the skin layer a shell layer is formed accounting for the majority of material due to the high shearing, this shear leads to a high orientation in the flow direction. It is worth noting that cooling speed of the polymer allows to more or less accentuating the fountain flow effect. Indeed, if the mold is filled slowly the skin layer appears and the surface orientation freezes contrary to the fast filling which causes the disappearance of the skin layer and the effacement of the fountain flow by the shear flow [52]–[54].

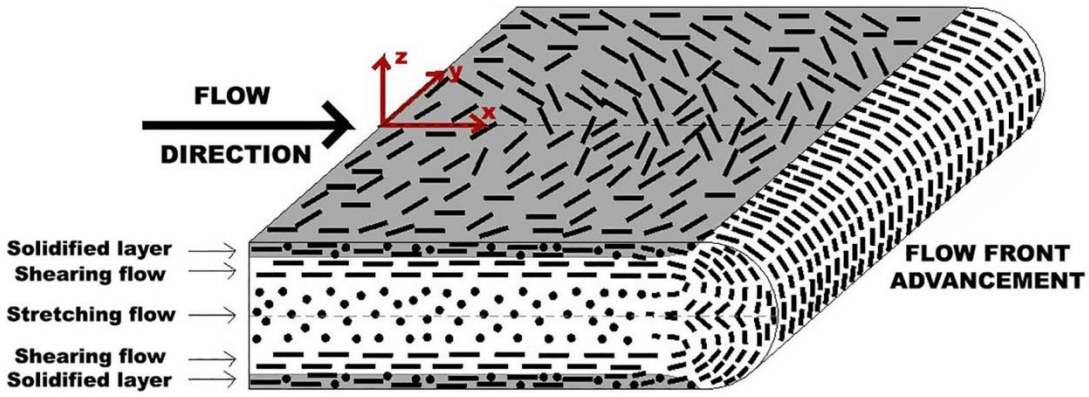

Figure I.5-4: Fountain flow effect.

I.5.2. Analysis of parameters influencing the fibers orientation

For a given geometry, fibers orientation is governed by many factors related to the injection process. Among these factors, we can find the influence of the gate position, the injection parameters, the reinforcement, the matrix and the mold geometry.

I.5.2.1. Influence of gate position

The presence of gates leads, when they are the seat of elongation, to the formation of a core layer with transverse fibers orientation. The gate geometries which not create such a flow (case gate film or carrots injections) facilitate, for their part, the formation of a core region with fibers orientation in the flow direction [55].

P. Shokri et al.[56] tested several asymmetrical gate locations to show their effect on fiber orientation. To infer that, the asymmetric gate position causes an asymmetric viscosity state in the transverse flow direction (width of the mold) leading to asymmetric fiber patterns in the flow plane.

I.5.2.2. Influence of the main injection parameters

- **Influence of mold and melt temperature**

Generally, a decrease of the mold temperature (or the material temperature) increases the solidified polymer layer which induces maximum shear values shifted towards the center of the part. This temperature diminution leads to an increase in the thickness of the shell-skin layer. The phenomena observed are mainly related to the fountain effect, which is accentuated by the cooling rate of the polymer [57].

However, R. Bay et al.[52] when evaluating the effect of a slight variation of mold and melt temperature on fiber orientation for a center-gated disk, they obtained interesting luckily reported. First, fibers orientation was predicted for three mold temperature values: T_w= 337, 347 and 357 K, respectively. Results show that this small temperature variation T_w does not have much influence on fibers orientation, while it can greatly affect the molecular orientation or crystallinity in some polymers. On the other hand, the same procedure was done for three melt inlet temperature values: T_{in}= 540, 550, and 560 K, respectively and it was observed that fibers orientations are not much sensitive to T_{in}, apart from the fact of adjusting the transition layer between the core and shell layers.

- **Influence of filling time and injection speed**

In most cases, a high injection speed causes an increase in the core layer and diminution of the skin layer. Indeed, the fountain flow greatly affects the skin area without giving the fibers time to orient themselves, thus shifting the zone of strong shear towards the walls of the mold [57].

To investigate the effect of the filling time on fibers orientation, R. Bay et al. [52] show the prediction for four filling time values; t_{fill} = 0.5, 2, 2.5 et 3 s, respectively and conclude that fibers orientation and thickness of different layers are controlled by the filling speed. Indeed, for a very fast filling rate, there is virtually no skin layer [52].

For their parts S.T. Chung et al. [58] evaluated the core fibers orientation at different filling time; t= 0.081, 0.255, 0.557 and 0.81 s, respectively for a tensile testing specimen. First, fibers are aligned transversely to the direction of flow due to the strong divergent flow, but as the filling time increases, the fibers tend to align in the flow direction [58].

I.5.2.3. Influence of the matrix

The nature of the speed profile in the mold results from the rheofluidifying nature of the used polymers. The pseudoplastic nature of polymers gives rise to a flow characterized by a much flatter velocity profile than that of Newtonian fluids. It appears that the thickness of the core zone is an increasing function of the pseudo plasticity index of the polymer. At the same time, the addition of fibers increases the pseudo plasticity of the matrix. It must always be remembered that many of these effects acts identically. However, it should also be noted that, in the vast majority of cases, these studies remain qualitative. The matrix viscoelastic nature also affects the periodicity of fiber movement in shear flow. It has been shown that for a non-Newtonian fluid, the period of a particle increases strongly. In addition, it has been observed that this increase in the periodicity of the movement is exacerbated by the shear rate [57].

To explore how the thermal and rheological properties of the polymer matrix could affect fibers orientation, R. Bay et al.[52] simulated the filling of the disk using three polymers with different properties (nylon, polypropylene (PP) and polycarbonate (PC)). The nylon has a smaller heat of fusion and a wider range of freezing, unlike polypropylene has a large heat of fusion and a

narrow range of freezing temperatures, while polycarbonate has no heat of fusion. The viscosity of nylon is sensitive to shear rate and temperature in the range of the experiments, while the polycarbonate is relatively insensitive and the polypropylene is strongly shear thinning and very sensitive to temperature. It was observed that the differences between the velocity profiles of these three matrices lead to different orientation distribution. The flatter velocity profile of polypropylene produces a much thicker core layer and shearing near the wall. On the other hand, the large heat of fusion erases the fountain flow effects, so no skin layer is formed. Nevertheless, the polycarbonate has the same skin layer as Nylon, but the core region is smaller than even the nylon and polypropylene moldings. To conclude, small changes in the speed profile can affect the fibers orientation. An imprecision speed profile prediction inevitably leads to inaccuracy in the fibers orientation. The fountain flow importance is also evoked in terms of the skin layer prediction because the speed profiles can provide only little information [52].

I.5.2.4. Influence of the reinforcement

Several studies have shown that fibers shape factor plays a major role on fibers orientation. Indeed, increasing the aspect ratio leads necessary to increase the core thickness, defined by a transversal fiber orientation. It will be concluded that the core thickness is very sensitive to the increase in the initial fibers length. It's also important to note that more fibers are long more they tend to adopt a planar orientation [59] as shown in figure I.5-5.

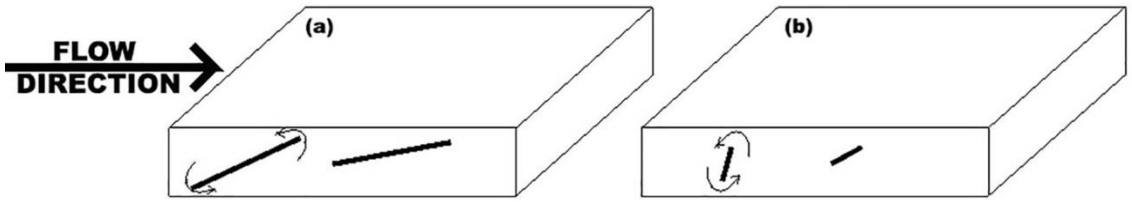

Figure I.5-5: (a) Long fiber orientation. (b) Short fiber orientation.

Otherwise, it seems that the fiber concentration also influences the orientation because its decrease causes the disappearance of the core-skin structure. Whereas, its increase causes the increase of the size of the core zone. Fiber concentration is associated with the aspect ratio of the fibers (L/D), and its volume fraction (V_f) [60].

For a cylindrical particle, the volume fraction is calculated according to the following relation (Eq. I.5-2) [60].

$$V_f = n.\pi.\frac{D^2}{4}.L \qquad \text{(I.5-2)}$$

Where **n** is the number of particles per unit volume.

There are three regimes of concentration:

(1) Dilute solution: It is the regime where there is no interaction between the fibers. It means that, the distance between adjacent fibers is approximately equal to the fiber length and they can turn freely without touching each other. Then the maximum permissible volume fraction V_f verifying the relation below (Eq. I.5-3) [60].

$$V_f \leq \left(\frac{D}{L}\right)^2 \qquad \text{(I.5-3)}$$

(2) Semi-concentrated solution: This characterizes the suspension where the fibers distance is between the fibers length and diameter. In this case, the volume fraction V_f must be verifying the following inequality (Eq. I.5-4) [60].

$$\left(\frac{D}{L}\right)^2 \leq V_f \leq \left(\frac{D}{L}\right) \qquad \text{(I.5-4)}$$

(3) Concentrated solution: It is defined according to following relation (Eq. I.5-5), when the average distance between fibers is lower than the fibers diameter [60].

$$V_f \geq \left(\frac{D}{L}\right) \qquad \text{(I.5-5)}$$

When talking about concentrated or semi-concentrated types, it is important to determine experimentally the interaction coefficient (C_i), which depends on the fiber aspect ratio, L/D, and the volume fraction. An empirical expression (Eq. I.5-6) was proposed by Tucker and Advani to predict approximately the interaction coefficient when the latter is not available experimentally [52], [60], [61].

$$C_i = 0.0184.\exp\left(-0.7148\,.V_f.\frac{L}{D}\right) \quad \text{(I.5-6)}$$

This expression is valid only for concentrated regimes [60].

To demonstrate how the interaction coefficient affects orientation, R. Bay et al.[52] made predictions of C_i = 0.005, 0.01 and 0.05 for the center-gated disk. It is clear that the fiber orientation state approaches the randomized orientation state as the magnitude of C_i increases [52], [60]. Increasing the interaction coefficient leads necessary to random orientation states, whereas low values tend the shell layer to a high orientation in the flow direction and the core layer to a highly transverse orientation. C_i also affects the layered structure, indeed increasing the interaction coefficient decrease the core and increase the shell thicknesses [52].

I.5.2.5. Influence of the geometry of the mold

Some authors have shown for rectangular mold with uniform thickness, via qualitative microscopic observations, that the reduction on the cavity thickness greatly affects the fibers orientation in the core zone. Indeed, more the mold thickness decrease more the core zone disappear, thus resulting in nearly the same planar orientation throughout all the thickness [55], [57].

Generally, two types of molds can be distinguished (Figure I.5-6), thin-walled cavity (less than 1mm) and thick-walled cavity (more than 1mm). M. Vincent et al.[62] evaluated the fibers orientation at different mold thicknesses (1.1, 1.7, 3 and 5 mm). The results revealed the appearance of a skin-core structure above 3 mm as well as the increase and accentuation of the core layer with increasing thickness to 5 mm. On the other hand, it was observed that decreasing the cavity thickness leads necessarily to the decrease in the structure of the core-skin until obtaining one layer where the fibers adopted a specific planar orientation throughout all the thickness. Usually, this converging-diverging flow is more significant in thin parts.

When the plastic contacts the mold surfaces, a frozen layer is immediately formed along the mold walls, where the converging flow tends to flow-align the fibers. Near the center line and due to the decrease of the solid layer , the diverging flow tends to align the fibers perpendicular to the flow thus forming a parabolic shape of fiber orientation [63].

Changing the mold width plays also a major role in the fiber orientation distribution. M. Vincent et al.[62] compared the fibers orientation in a thin rectangular plate for 20 and 40 mm in width. It was observed that reducing mold width leads fibers to orient in the flow direction in the whole thickness whatever the position taken along the plate (Figure I.5-7).

For their part R. Bay et al.[52] reported the fiber orientation measurements for the two injection molding parts center-gated disk and a film-gated strip with the same thickness (3.18mm). It was concluded that both parts have the same layered structure, with outer shell layers of flow-aligned fibers surrounding a central core of either random-in-plane (strip) or transversely aligned fibers (disk), but they also represent significant differences. The center-gated disk core has a transverse orientation much more pronounced than the film-gated strip since the core is formed by the circumferential stretching, which dominates at the mid-plane. Also, a thick frozen layer is formed on the disk walls during filling hence forming the skin layer, in the contrary of the strip where the frozen layer is very small.

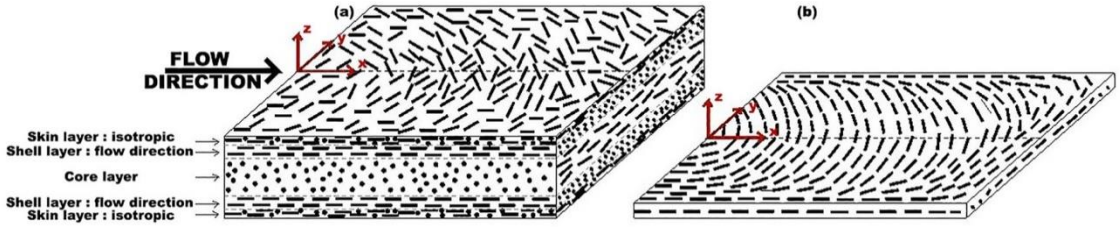

Figure I.5-6: (a) Fiber orientation in thick mold, (b) Fiber orientation in thin mold.

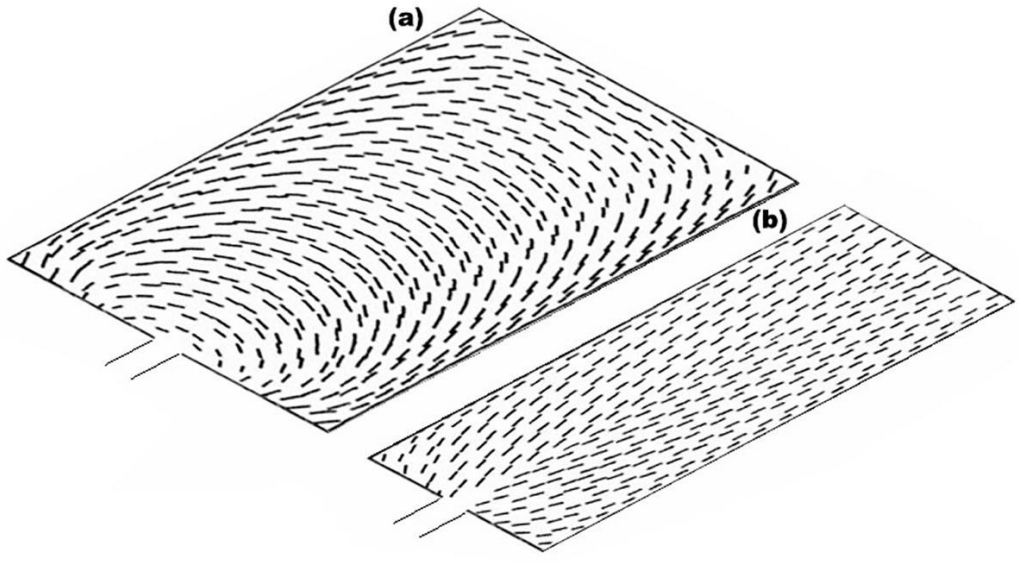

Figure I.5-7: (a) Fiber orientation in large mold width, (b) Fiber orientation in small mold width.

I.5.3. Fibers orientation description

I.5.3.1. Vector representation of a single fiber orientation

A single fiber orientation can be described conventionally according to the Cartesian coordinates of a unit vector representing the main fiber direction or using two angles (θ, φ). As illustrated in figure I.5-8, each single fiber could be represented by a vector P directed along the main axis of the fiber, thereby defining the fiber orientation by its projection in a fixed landmark. It is worth noting that the sense of P is arbitrary due to the two undifferentiated ends. As a result, the orientation description must be unchanged if the transformation (**$\theta \rightarrow \pi - \theta$** and **$\varphi \rightarrow \varphi + \pi$**) is carried out. To conclude the components of this vector P related to angles (θ, φ) are expressed by (Eq. I.5-7) [64]–[66]:

$$\begin{cases} P_1 = \sin\theta \cos\varphi \\ P_2 = \sin\theta \sin\varphi \\ P_3 = \cos\theta \end{cases} \quad \text{(I.5-7)}$$

Where, **θ** is the tilt angles denoted as the angle formed by the Z axis at the direction of the fiber, and **φ** refer to the azimuthal angles. And It is defined in the plane (X, Y) with respect to the axis X. Since a fiber has no orientation sense, the values of **θ** and **φ** are respectively between (0°; 180°) and (-90°; 90°) [64]–[66].

Short fibers composites materials are generally consisting of a very large number of fibers. In order to more concisely describe the orientation distribution of a fibers population, several mathematical representations exist, such as orientation functions, orientation distribution functions, orientation tensors, or Hemans orientation coefficient which will be revealed in the next paragraphs.

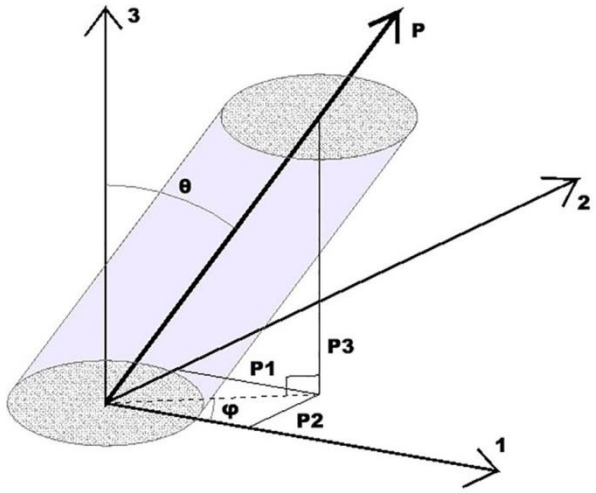

Figure I.5-8: Fiber orientation.

I.5.3.2. Orientation distribution function

A complete description of long or short fibers orientation state requires the calling of an orientation distribution function **Ψ(P,t)** or equivalent **Ψ(θ,φ)** which expresses the probability of obtaining a fiber having a certain orientation 'P' at time 't'.

So, the probability P of finding a fiber between the angles **(θ, θ+dθ)** and **(φ,φ+dφ)** is expressed by the following equation (Eq. I.5-8) [66]:

$$P = \int_{\theta}^{\theta+d\theta} \int_{\varphi}^{\varphi+d\varphi} \Psi(\theta,\varphi) \sin\theta \, d\varphi d\theta \qquad \text{(I.5-8)}$$

This function must satisfy the following conditions [67], [68]:

- It must be unchanged by the P → -P transformation, which translates into equation I.5-9:

$$\Psi(\theta,\varphi) = \Psi(\pi-\theta,\varphi+\pi) \text{ or } \Psi(P) = \Psi(-P) \qquad \text{(I.5-9)}$$

- It must be normalized, that is, the integral of the distribution function on all possible orientations is equal to unity, verifying the equation below (Eq. I.5-10):

$$\int_0^{2\pi} \int_0^{\pi} \Psi(\theta,\varphi) \sin\theta \, d\theta \, d\varphi = 1 \text{ or } \int \Psi(P) \, dP = 1 \qquad \text{(I.5-10)}$$

Where dP is a surface element of the unit sphere.

The orientation distribution function obeys to the Fokker Plank equation, in the case of semi-diluted or concentrated suspensions of fibers, hydrodynamic fibers interaction must be taken into account. Thus, a diffusion coefficient due to Brownian motion of fibers D_r is introduced. If dP = dt denote the matrix derivative of P with respect to time, the evolution equation is written according to equation I.5-11 [69], [70].

$$\frac{\partial \Psi}{\partial t} + \frac{\partial}{\partial P}\left(\Psi \frac{\partial P}{\partial t}\right) - D_r \frac{\partial^2 \Psi}{\partial P^2} = 0 \qquad \text{(I.5-11)}$$

While in dilute suspension (no fibers interaction D_r=0), the orientation distribution function is written as follows (Eq. I.5-12) [69], [70].

$$\frac{\partial \Psi}{\partial t} + \frac{\partial}{\partial P}\left(\Psi \frac{\partial P}{\partial t}\right) = 0 \qquad \text{(I.5-12)}$$

I.5.3.3. Orientation tensor

The orientation distribution function is mostly not explicitly known and difficult to predict, which has lead Hand [71] to introduce a tensor of second order, frequently noted $\overline{\overline{a_2}}$, and defined as the spatial mean of the double tensor product of $\overline{P}$. These tensors are expressed as a function of the vector of orientation P and the orientation distribution function by equation I.5-13 [66], [72] :

$$\overline{\overline{a_2}} = \int \overline{P} \otimes \overline{P}\, \Psi(\overline{P}) d\overline{P} \qquad \text{(I.5-13)}$$

When defining these tensors, one should not neglect the properties of symmetry and the condition of normalization expressed below (Eq. I.5-14) [66], [72] :

$$\begin{cases} a_{ij} = a_{ji} \\ a_{ii} = 1 \quad \text{or} \quad a_{11} + a_{22} + a_{33} = 1 \end{cases} \qquad \text{(I.5-14)}$$

These properties indicate that only 5 of 9 components of $\mathbf{a_{ij}}$ are independent, so there are 5 scalars to describe this tensor in the case of a 3D flow [66].

In an orthonormal base (e_1, e_2, e_3), a_{11}, a_{22} and a_{33}, respectively denote the alignment of the fibers along the directions e_1, e_2 and e_3. In instance, if the component a_{11} = 1 it means that all the fibers are oriented in the direction e_1, whereas if a_{11} = 0 it indicates that all the fibers are perpendicular

to e_1 (they belong to the plane (e_2, e_3)) as explain on figure I.5-9 for a single fiber, and this is valid for the other components too.

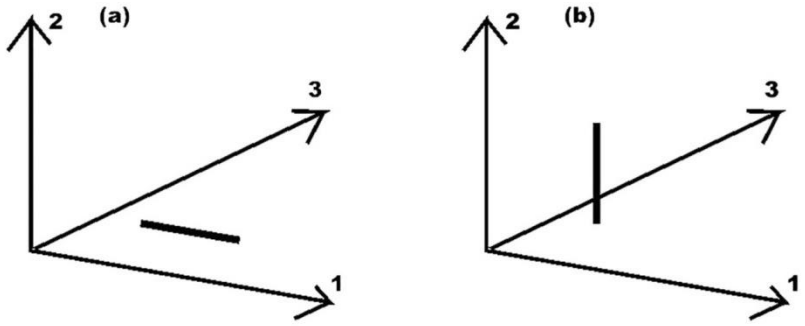

Figure I.5-9: (a) Illustration of the component a_{11}=1. (b) Illustration of the component a_{11}=0.

The components $\mathbf{a_{ij}}$ with i≠j quantify the asymmetry of the orientation distribution with respect to directions $\mathbf{e_i}$ or $\mathbf{e_j}$. Figure I.5-10 (a) and (b) illustrates the values taken by the tensor components for different orientations in the bi-dimensional and three-dimensional cases.

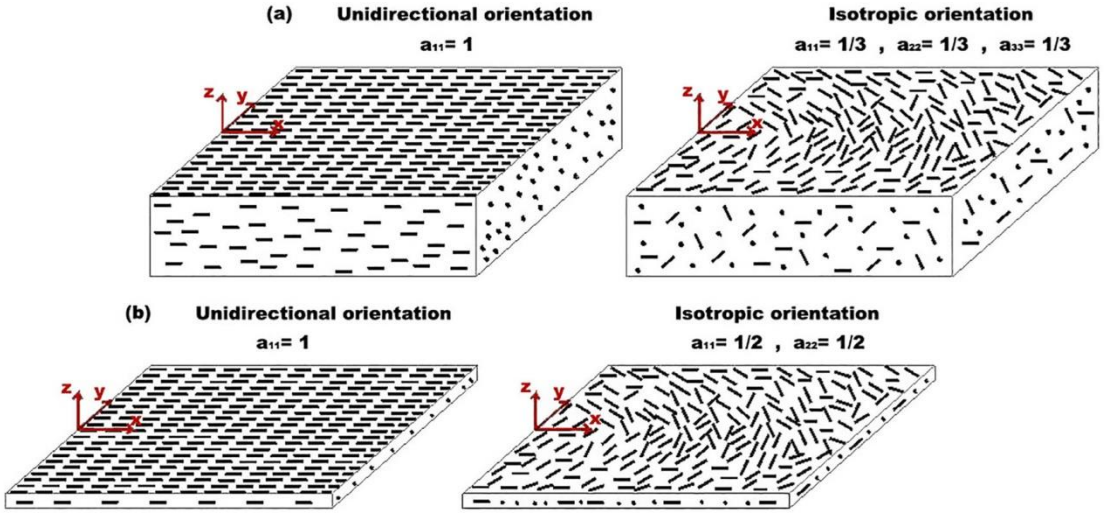

Figure I.5-10: (a) Tensor components values in the bi-dimensional case, (b) Tensor components values in the three-dimensional case.

I.5.3.4. Orientation coefficient of Hermans

The Hermans orientation coefficient could also be used to describe the average reinforcement orientation. Thus, this technique imposes the choice of a reference axis, the orientation of the macromolecules is then defined by an angle with respect to this axis as shown in figure I.5-11.

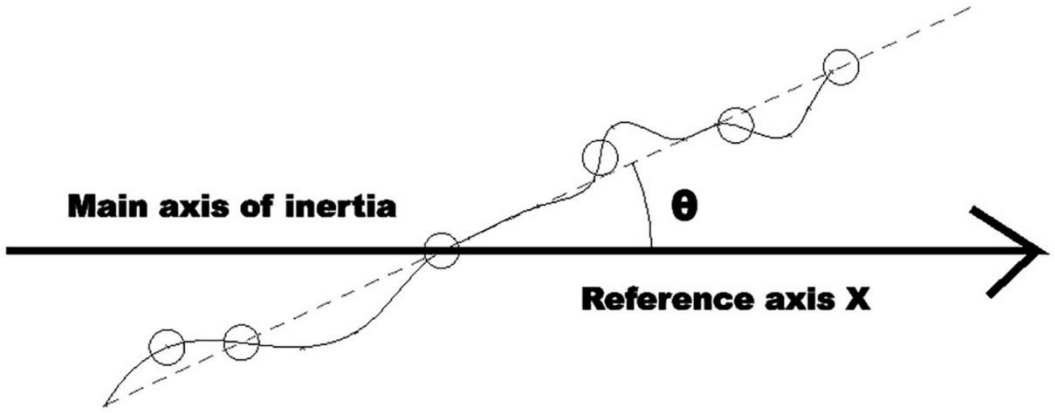

Figure I.5-11: Schematization of Hermans factor.

According to the literature, it is possible to have an idea about the existence of a privileged orientation via the determination of the Hermans factor which is expressed as follows (Eq. I.5-15) [73], [74].

$$f_x = \frac{3}{2} < \cos^2\varphi_x > -\frac{1}{2} \quad \text{(I.5-15)}$$

Where,φ_x is the angle between the fiber and the reference axis x.

Theoretically, the value of f_x can range from 1, for perfectly oriented molecules, to zero for an isotropic material$<\cos^2\varphi_x>=1/3$, and it's equal to -1/2 when the fiber orientation is transverse to the reference axis [74].

This method doesn't allow to determinate the fiber orientation state with precision, it only allows to qualitatively determining the existence of an orientation axis or not. The mathematical tools that provide more concrete information about the orientation state are the 2nd and 4th order tensor and the orientation distribution functions.

I.5.4. Modeling of the fibers orientation in flow

I.5.4.1. Evolution model of a single fiber

Jeffrey [75] was the first to propose a theoretical work describing the orientation evolution in the case of diluted solutions of rigid spheroidal particles immersed in a Newtonian fluid. The main hypothesis is that the particle sizes are small enough that the deformation velocity field is

homogeneous at a great distance. The speed of the undisturbed fluid is then a linear function of the position, and the inertial forces are neglected. Jeffrey's model is thus given by the equation I.5-16 [76], [77]:

$$\frac{D\overline{P}}{Dt} = \Omega(V)\,\overline{P} + \lambda[\varepsilon(V)\,\overline{P} - (\varepsilon(V) : \overline{P}\otimes\overline{P})\,\overline{P}] \qquad \text{(I.5-16)}$$

Where $\frac{D\overline{P}}{Dt}$ is the matrix derivative of $\overline{P}$ defined by the equation I.5-17. It takes into account the displacement of the center of gravity of the particle and its evolution as a fluid particle [76].

$$\frac{D\overline{P}}{Dt} = \frac{\partial\overline{P}}{\partial t} + V\nabla\overline{P} \qquad \text{(I.5-17)}$$

$\varepsilon(V)_{ij}$ and $\Omega(V)_{ij}$ are respectively the volume averaged vorticity and the strain rate tensors which are express by the equation I.5-18. They contribute to the particle orientation change due to the deformation and the rotation of the fluid [76].

$$\varepsilon(V)_{ij} = \frac{1}{2}\left(\frac{\partial u_i}{\partial x_j} + \frac{\partial u_j}{\partial x_i}\right) \qquad \text{(I.5-18a)}$$

$$\Omega(V)_{ij} = \frac{1}{2}\left(\frac{\partial u_i}{\partial x_j} - \frac{\partial u_j}{\partial x_i}\right) \qquad \text{(I.5-18b)}$$

V is the local speed field and λ is a function of the fiber form ratio β given by equation I.5-19. Concerning the symbol "**:**" it denotes the tonsorial product twice contracted [77].

$$\lambda = \frac{\beta^2-1}{\beta^2+1} \qquad \text{(I.5-19)}$$

In order to calculate the evolution of the vector $\overline{P}$ over time for a particle with an infinite form ratio (λ=1), Hand [71] introduce in the Jeffrey equation a Brownian motion via the insertion of a diffusion coefficient D_r. He gets the equation I.5-20:

$$\frac{D\overline{P}}{Dt} = \Omega(V)\,\overline{P} + \lambda[\varepsilon(V)\,\overline{P} - (\varepsilon(V) : \overline{P}\otimes\overline{P})\,\overline{P}] - \frac{D_r}{\Psi}\frac{\partial\Psi}{\partial\overline{P}} \qquad \text{(I.5-20)}$$

Knowing that: $\overline{P} = \begin{Bmatrix} P_x \\ P_y \\ 0 \end{Bmatrix}$

Projection on the axes (ox) and (oy) leads to the equation I.5-21:

$$\begin{cases} \frac{\partial P_x}{\partial t} + V_x \frac{\partial P_x}{\partial x} = -\frac{1}{2} P_y \left(\frac{\partial V_y}{\partial x} - \frac{\partial V_x}{\partial y} \right) + \lambda P_x \frac{\partial V_x}{\partial x} \left(1 - P_x^2 - P_y^2 \right) + \frac{1}{2} \lambda P_y \left(\frac{\partial V_x}{\partial y} - \frac{\partial V_y}{\partial x} \right) \left(1 - P_x^2 - P_y^2 \right) \\ \frac{\partial P_y}{\partial t} + V_y \frac{\partial P_y}{\partial y} = -\frac{1}{2} P_x \left(\frac{\partial V_y}{\partial x} - \frac{\partial V_x}{\partial y} \right) + \lambda P_y \frac{\partial V_y}{\partial y} \left(1 - P_x^2 - P_y^2 \right) + \frac{1}{2} \lambda P_x \left(\frac{\partial V_x}{\partial y} - \frac{\partial V_y}{\partial x} \right) \left(1 - P_x^2 - P_y^2 \right) \end{cases} \quad \text{(I.5-21)}$$

The direct orientation calculation of the movement of each fiber in reinforced thermoplastics has proved very expensive and consumes computer resources. That's why it was more legitimate to use a compact notation of the fibers orientation (orientation tensors) and to develop macroscopic models to follow the evolution of these tensors. Lipscomb et al. [78] used Jeffrey's equation to model the state of fiber orientation. This equation was homogenized in volume and combined with the Fokker-Plank equation (Eq. I.5-11). So, Jeffery's analysis can also be written in terms of the second- and fourth-order orientation tensors as follows (Eq. I.5-22) [76], [77]:

$$\frac{D\overline{\overline{a_2}}}{Dt} = [\Omega(V)\overline{\overline{a_2}} - \overline{\overline{a_2}}\Omega(V)] + \lambda[\varepsilon(V)\overline{\overline{a_2}} + \overline{\overline{a_2}}(\varepsilon(V) - 2\varepsilon(V) : \overline{\overline{a_4}}] \quad \text{(I.5-22)}$$

I.5.4.2. Evolution models of a fiber population

In non-dilute suspensions, taking into account the interaction between the fibers is more complex. The evolution of orientation in such environments has been the subject of several studies and few macroscopic models are likely to take into account this evolution during the flow. Folgar and Tucker [50] modified the Jeffrey equation (Eq. I.5-22) by adding a diffusion Brownian coefficient D_r in order to consider the interaction between fibers as shown in equation I.5-23 [76], [77]:

$$\frac{D\overline{\overline{a_2}}}{Dt} = [\Omega(V)\overline{\overline{a_2}} - \overline{\overline{a_2}}\Omega(V)] + \lambda[\varepsilon(V)\overline{\overline{a_2}} + \overline{\overline{a_2}}(\varepsilon(V) - 2\varepsilon(V) : \overline{\overline{a_4}}] + 2D_r(\overline{\overline{I}} - 3\overline{\overline{a_2}}) \quad \text{(I.5-23)}$$

The Brownian diffusion coefficient proposed by these authors is defined by (Eq. I.5-24):

$$D_r = C_I \dot{\bar{\varepsilon}} \quad \text{(I.5-24)}$$

Where C_I is the interaction coefficient and $\dot{\bar{\varepsilon}}$ is the magnitude of the strain-rate tensor. The major difficulty in this model lies in the interaction coefficient determination. The choice of this coefficient has a significant impact on the orientation profile. In the general case, it is suggested to take a coefficient interaction value between 10^{-3} and 10^{-2}, to have a good agreement with experience [77]. For the determination of the Brownian diffusion tensor, no complete study has been developed until today. Nevertheless, the numerical estimation allows establishing the value of this tensor. This description is easier to use than the orientation distribution function in equation I.5-22, but cannot be solved from its evolution equation in which the tensor of order 6 intervenes and so on. This scheme is thus repeated for higher order tensors. To circumvent this difficulty and allow a complete description of the behavior, a closure approximation has been called to give an approximation of the tensor $\overline{\overline{a_4}}$ as a function of the tensor $\overline{\overline{a_2}}$ and to substitute the result in the equation I.5-23 [76].

I.6. Conclusion

Injection molding of natural fibers reinforced thermoplastic matrices are gaining interest due to their potential mechanical properties, processing advantages, environmental and economic benefits. The performance of natural fiber-reinforced composite can be affected by many factors, leading us to present a general overview of the different models developed for the composite mechanical properties prediction. Since, the fiber orientation field during the process is the main factor affecting the material performance, this chapter highlights the different models existing in the literature for the characterization of the flow induced fiber orientation, as well as the orientation complexity phenomena. We demonstrate the formation of a core-skin structure characteristic of fiber reinforced composites. The origin of these arrangements is complex, it is linked to a number of interactions that appear during the flow. The difficulty lies in highlighting these interactions. In fact, hydrodynamic fiber-fluid interactions, fiber-fiber and fiber-wall interactions, the nature of the flow, the concentration of particles are all phenomena that can be responsible for the final orientation of the particles.

Also, this chapter detailed the major challenges of the injection molding processes (often using fiber-filled polymeric suspensions) from a rheological point of view. The flow is transient, non-Newtonian and non-isothermal with ongoing solidification as the molten polymer flows through

the mold cavity. An important characteristic of the problem is the existence of a continually moving boundary, i.e. the melt front, the location of which is not known a priori. Furthermore, the process is highly nonlinear because of the convective terms and the strong dependence of viscosity on the shear rate and temperature. While the fact that most injection molded parts are 'thin walled' allows for an approximation of the flow to a two-dimensional problem, the temperature distribution in the fluid remains fully three-dimensional with significant gradients occurring near the mold walls.

This literature review allows understanding the complex interactions between the flow field and the fiber orientation, to be able to accurately study the injection molding process by taking into account all those factors. Thus, in the following chapters, we will present our simple mathematical models developed in order to predict the whole material mechanical performance and optimize the mold design and processing variables.

Chapter II. Mechanical properties prediction of polypropylene/Short coir fibers composites using a self-consistent approach

F. Semlali Aouragh Hassani et al., "Mechanical Properties Prediction of Polypropylene/Short Coir Fibers Composites Using a Self-Consistent Approach", Polym. Compos., vol. 40, no. 5, pp. 1919–1929, 2019.

II.1. Abstract

Short coir fibers composite of thermoplastic polypropylene (PP) matrix was successfully prepared by using a twin-screw extruder and an injection molding machine. In order to provide a better understanding of the effect of fiber orientation and concentration (2.5, 5, and 10 wt%) on the mechanical properties of short coir fibers reinforced PP, a self-consistent approach was developed based on a modified Hirsch model by taking the empirical parameter (x) proportionally to the fiber orientation factor (α). Finally, the results are com- pared with other models (Hirsch and Tsai-Pagano) and validated with experimental data. Overall, our approach was found to better predict the mechanical results in terms of Young's modulus, tensile strength and torsion modulus.

II.2. Résumé

Afin de mieux comprendre l'effet de l'orientation et de la concentration des fibres (2,5, 5 et 10% en poids) sur les propriétés mécaniques du PP renforcé par des fibres courtes de coco, une approche auto-cohérente a été développée sur la base de schéma auto-cohérent couplé au modèle de Hirsch modifié en prenant le paramètre empirique (x) proportionnel au facteur d'orientation des fibres (α). Finalement, les résultats ont été comparés à d'autres modèles (Hirsch et Tsai-Pagano) et validés avec les données expérimentales. Globalement, notre approche s'est avérée mieux pour prédire les résultats mécaniques en termes de module d'Young, de résistance à la traction et de module de torsion. Le mélange fibres de coco et matrice PP a été préparé par voie fondue en utilisant une extrudeuse bi-vis suivi de moulage par injection pour la fabrication des échantillons standards pour les différents tests.

II.3. Introduction

Nowadays, thermoplastics can be found in a wide range of applications and fields due to their relatively low cost and easy processing, especially by injection molding. But most commodity polymers, such as polypropylene (PP), have relatively low mechanical properties limiting their use to non-structural applications [79], [80]. Nevertheless, the addition of short natural fibers in these matrices was shown to substantially improve their mechanical performance without compromising their processability. This is related to natural fibers advantages such as good specific mechanical properties, low densities, low production costs, non-toxicity, high specific properties, and easy recycling [81]–[83].

Several studies have shown that the mechanical properties of a composite are strongly related to the matrix nature, fiber morphology, aspect ratio, fiber-matrix interface quality, as well as fiber type, concentration and orientation distribution [52], [84]–[86]. For example, the fibers in a thin plate tend to orient parallel to the flow direction near the walls due to shear stresses, while they tend to align perpendicular to the flow in the central zone [8], [57], [63].

To predict the longitudinal and transversal composites tensile properties, a wide variety of models have been proposed based on different assumptions. The simplest and most obvious way to predict the Young's modulus and tensile strength is to assume that the fibers and the matrix are organized in parallel or series as done for the Voigt and Reuss models, respectively [87]. These models only account for the fiber and matrix moduli, as well as the fiber volume fraction. On the other hand, models like Hirsch include other parameters such as fiber orientation and stress concentration effects (fiber ends). These parameters mainly influence an empirical factor (x) introduced by Hirsch to account for the relative contributions of both Voigt and Reuss models [28], [29], [34]. Furthermore, the Tsai-Pagano model (T-P) accounts for fiber orientation and stress concentration effects at the fiber ends, as well as the fiber aspect ratio (ratio between fiber length and diameter). The model includes both the longitudinal (3/8) and transversal (5/8) contribution [27], [28], [33]. Several other techniques and models have been developed, but the self-consistent approach was mostly used to predict the mechanical properties of spherical/spheroidal inclusions [88].

So, the aim of this work is to develop a self-consistent approach to predict the composite properties while considering the effect of reinforcement content and orientation. Thus, a modified Hirsch model is proposed by taking the empirical parameter (x) to depend on the fiber orientation factor (α). The self-consistent approach is based on the iterative insertion of a family of fiber orientation; thus, the first category of fibers was included in the matrix to constitute an equivalent homogeneous material which, in turn, is integrated into an infinite composite. The work also presents a theoretical approach based on experimental results for the torsion modulus prediction at a given weight fraction and frequency.

II.4. Materials and methods

II.4.1. Materials

The matrix used was an extrusion grade of polypropylene (PP) supplied by Exxon Mobil chemicals. This polymer has a melt flow index (MFI) of 3.4 (g/10 min), a density of 0.90g/cm^3 and a melting temperature of 165 °C. The reinforcement was coir fibers with an initial length of 150-200 mm and extracted from the shell of walnut fruits grown in Ivory Coast.

II.4.2. Fibers preparation

Coir fibers (150-200 mm) were first carefully washed with tap water and air-dried for 24 h to be grinded using a Fritsch Pulverisette-19 with a sieve opening of 4 mm and finally sieved through a 200 µm opening. The fiber diameters were evaluated using optical microscopy (Nikon Eclipse LV100ND Microscope) as shown in figure II.4-1a. About 200 fibers were analyzed using a digital camera under a white LED backlight illuminator (Figure II.4-1a) and the measurements were analyzed using the ImageJ software. The results gave an average diameter of 290 µm (Figure II.4-1b).

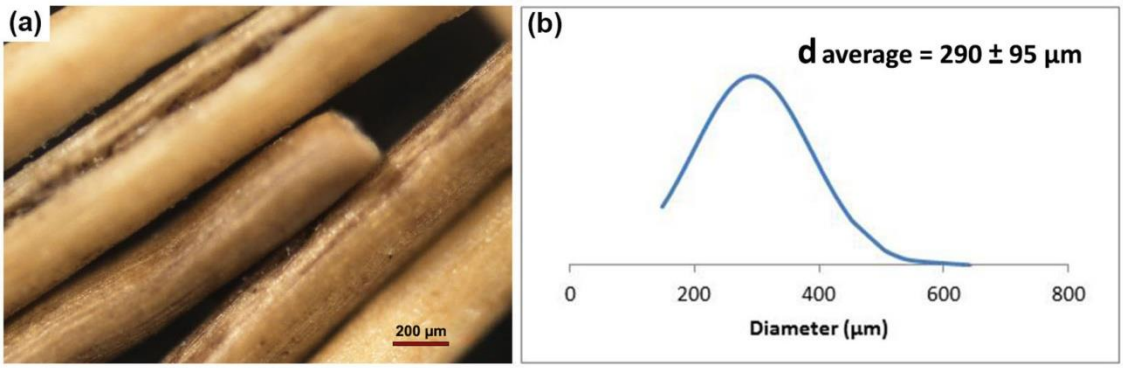

Figure II.4-1: Measurement of coir fibers diameter: (a) typical optical image and (b) diameter distribution.

II.4.3. Composites preparation

The polypropylene was firstly mechanically blended with 10 wt.% coir fibers to produce a preliminary masterbatch using a Leistritz ZSE-18 twin-screw extruder (Leistritz Extrusion Technik GmbH, Germany) at a screw speed of 125 rpm. The extruder temperature profile was set at 200, 200, 200, 200, 190, 190, 190, and 190 °C from the feed hopper to the die exit [89]. The compounds were cooled in a water bath and then manually cut into pieces with an average length of 15 mm to avoid as much as possible fibers length degradation.

To evaluate the extrusion process effect on fiber length, some parts (100 mm) of the compounds coming out of the extruder were laid side by side, then pressed together using an automatic hot press (Carver inc., USA) with two heated platens (190 °C), after which a pressure of 4 MPa was applied. Then, the same procedure as for fiber diameter was used to determine the average fiber length. The procedure was also applied on the injection molded samples to get the final fiber dimensions.

Injection molding was used to produce square plates with dimensions of 100×100×1 mm^3 at different fiber concentrations (10, 5 and 2.5 wt.%) using an Engel e-Victory machine. The injection barrel temperature profile was constant at 200 °C with a nozzle temperature at 190 °C, while the mold was set at 45 °C.

II.4.4. Fiber orientation measurement

To determine the fiber orientation in the molded samples, a digital camera under white LED backlight illuminator was used to take pictures. It was observed that similar fiber orientations were obtained for the different fiber concentrations used (2.5 to 10 wt.%). As shown in figure

II.4-2, it can be assumed that fiber concentrations up to 10 wt.% do not affect fiber orientation due to the low concentration (limited fiber-fiber interactions). To avoid edge effects, the first 10 mm from both extremities was discarded. So, the final specimen geometry used for the calculation is reduced to 100 mm in the transversal (0°) direction and 90 mm in the longitudinal (90°) direction as reported in figure II.4-3.

For the measurements, a mesh of 10 x 10 mm^2 was applied on five samples and the average of 10 fibers by mesh was considered to get a total of 900 fibers by plates as shown in Fig. 3). Then, the ImageJ software was used to calculate the final fiber orientation state.

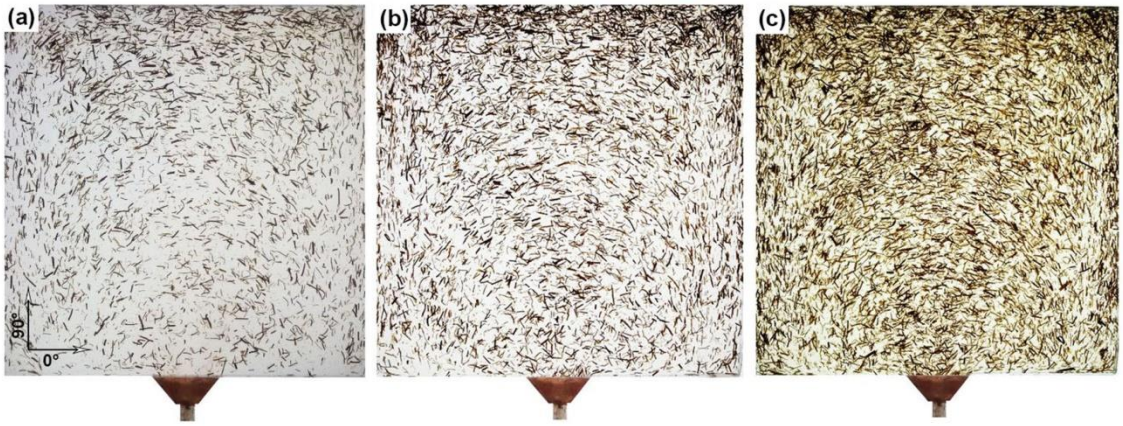

Figure II.4-2: Square plates images (100 x 100 mm^2) of the molded PP composites at different coir fiber concentrations: (a) 2.5, (b) 5, and (c) 10 wt.%.

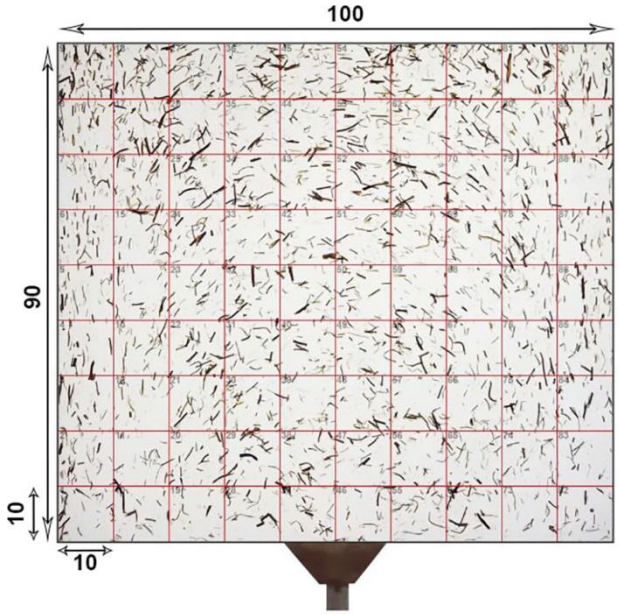

Figure II.4-3: Typical image used for modeling the mechanical properties/fiber orientation of PP/coir fiber bio-composites in a plate of 100x90 mm^2 (2.5 wt.%).

II.4.5. Functional Characterization

The fiber morphology was observed by a scanning electron microscope (SEM) model FEI Quanta 200-ESEM operated at 20 kV. Prior to imaging, the samples were cryo-fractured in liquid nitrogen to obtain a clear break and precise fracture faces. Since all the materials are non-conductive, a gold coating was applied via sputtering.

Regarding mechanical trials, Tensile tests were performed on a universal testing machine Tinius Olsen Horizon H10KT at a crosshead speed of 5 mm/min using a 5 kN load cell according to ISO 527-5 [90]. Assuming, that the composite is isotropic, the samples were cut into pieces of 10 x 80 mm^2 in the longitudinal direction with respect to the mold flow direction as shown in figure II.4-4. The first 10 mm from both sides was discarded to avoid edge effects. For each fiber content an average of five specimens was used to report representative values.

The torsion (shear) tests were performed on an ARES-LS rheometer (TA Instruments) using the torsion rectangular mode. The samples were cut in the same way as for tensile testing (figure II.4-4). The torsion modulus (G*) was obtained via small amplitude oscillatory tests (deformation of 0.002) performed at room temperature using frequency sweeps (0.1 to 40 Hz).

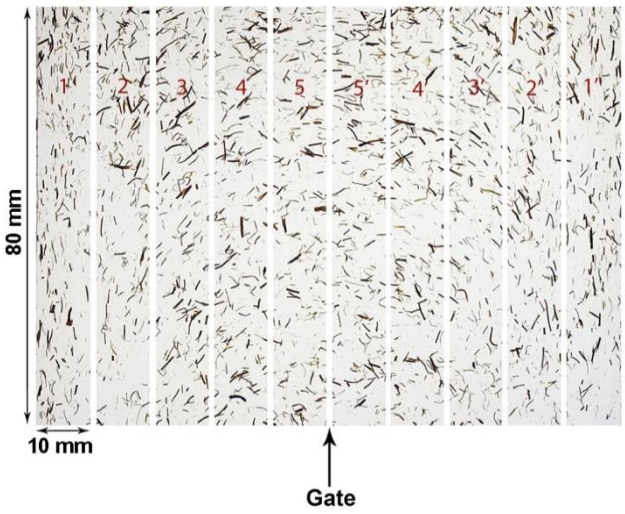

Figure II.4-4: Example of sample preparation for tensile and torsion testing.

II.5. Results and discussion

II.5.1. Morphological structure

The typical coir fibers surface aspect is illustrated in figure II.5-1. As shown, the fibers have a circular cross-section and are composed of several micro-fibrils with an average diameter of 12 µm.

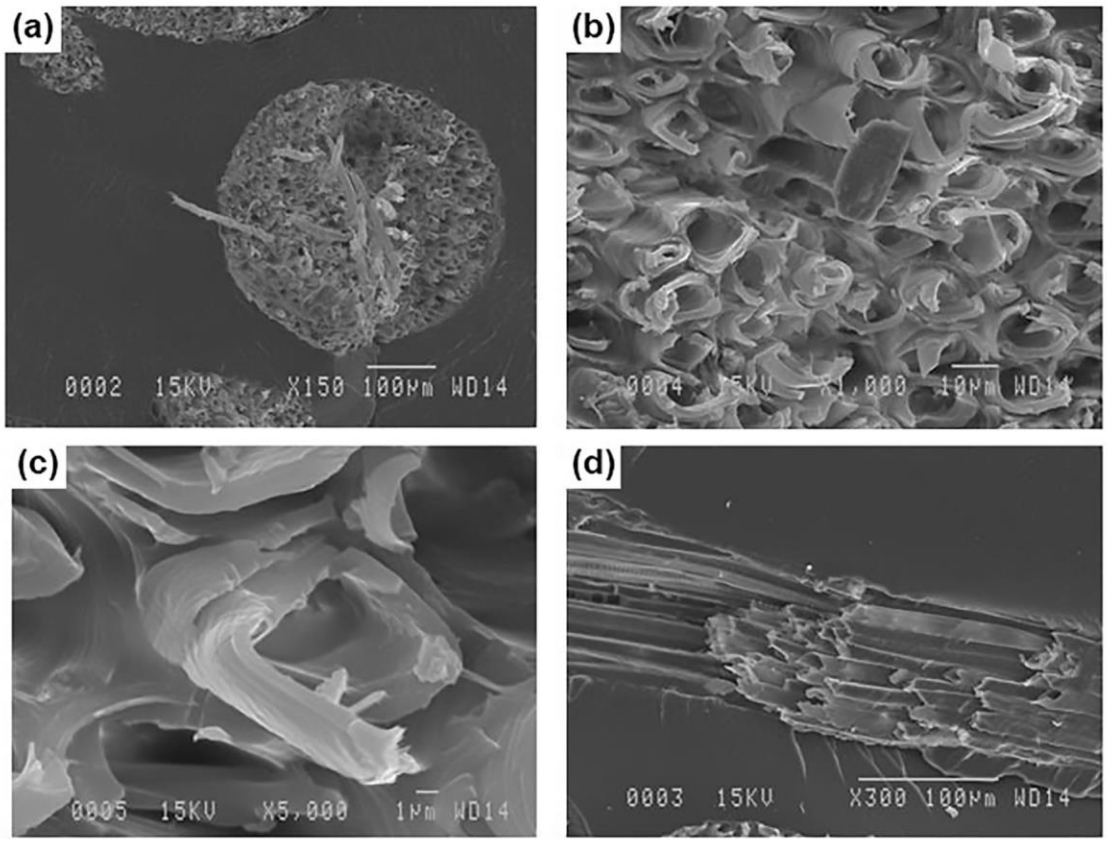

Figure II.5-1: Typical SEM micrographs of the coir fibers at different magnifications and directions: (a) coir fiber cross-section, (b) micro-fibril agglomeration, (c) micro-fibril cross-section, and (d) coir fiber longitudinal section.

II.5.2. Fiber orientation and fiber length

Most investigations generally consider that fiber orientation is not random because of the combination of converging and diverging flow and the fountain flow effect in most injection molded parts [84]. As figure II.5-2 illustrates, the fiber orientation distribution for 1 mm thick parts follow this rule. In our case, 9 orientation families were considered (no significant differences were obtained using a higher number). It can be seen, that near the walls, the

orientation is very close to 90° indicating that the shear flow aligns a large number of fibers along the flow direction [91]–[93]. On the other hand, fiber orientation has a parabolic orientation distribution as most fibers closer to the central part tend to orient perpendicularly reaching 0° along the center-line. As expected, this implies that the velocity profile controls the short fibers orientation [91]–[93]. Figure II.5-3 presents the fiber length and orientation results at 2.5 wt.%. As expected, fiber length degradation occurred through the different processing steps involved. The first one was that fiber length decreased from an initial value of 150-200 mm to an average of 4.55 mm after grinding and sieving. Then, the fibers passed through extrusion compounding to get homogeneous samples. The latter reduced the fibers length by half to get an average of 2.50 mm. Finally, the extruded compound was cut into pieces and mixed with a required amount of PP to be injection molded (100x100x1 mm^3). This process slightly decreased the fibers length to a final value of 2.25 mm. So, it is clear that the extrusion step is the important one in terms of fiber length reduction.

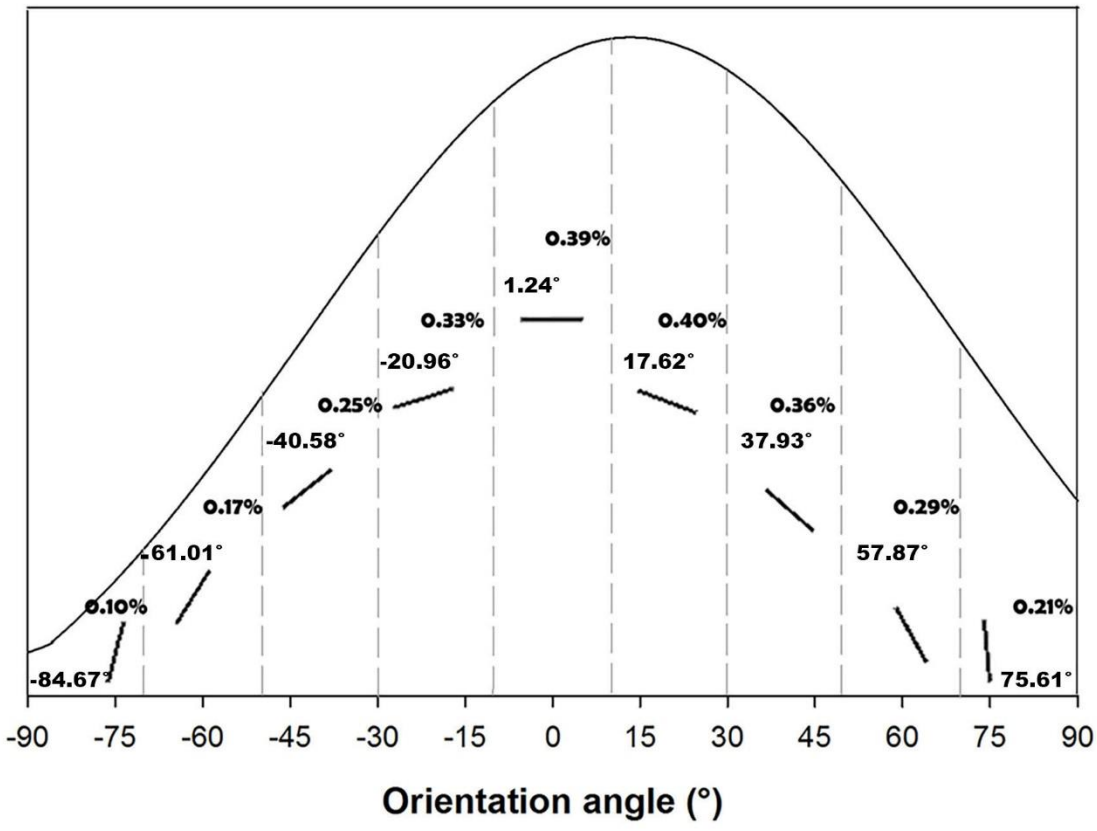

Figure II.5-2: Average fiber orientation in molded plates of 2.5 wt.% (100x100 mm^2).

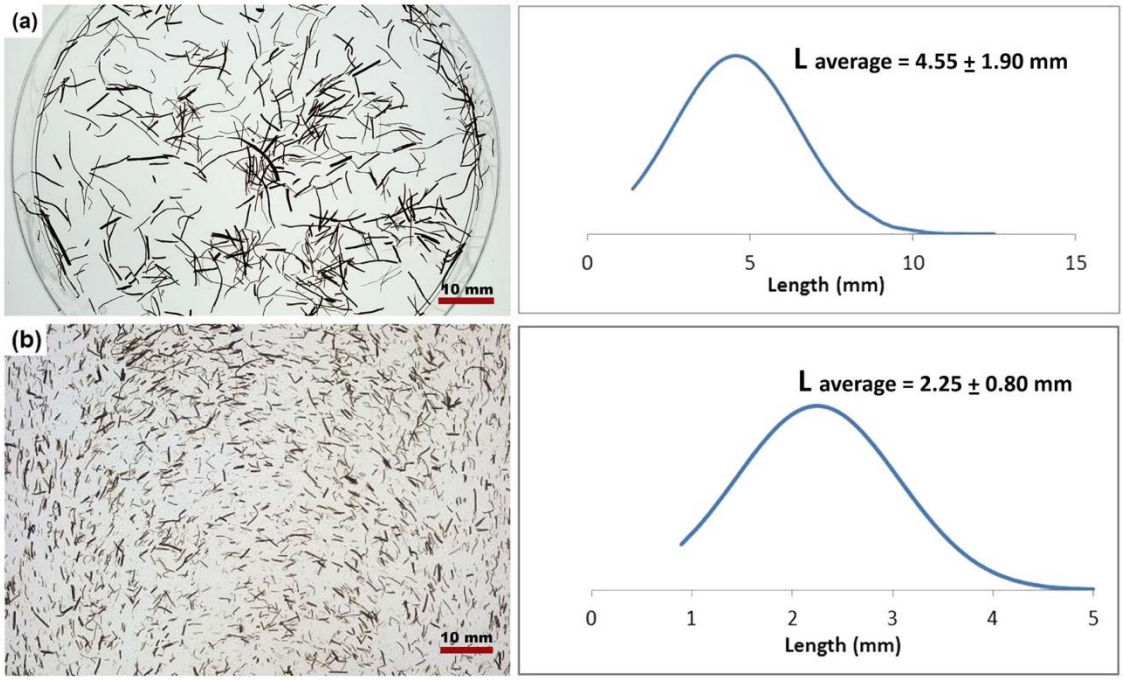

Figure II.5-3: Fiber length distribution: (a) after grinding/sieving and (b) after injection molding.

II.5.3. Tensile properties

Figure II.5-4 presents the tensile properties in terms of tensile strength, Young's modulus and strain at yield as a function of fiber content. It can be seen in figure II.5-4a that increasing the fiber concentration leads to an important improvement (17 %) in Young's modulus (from 1253 MPa for the neat PP to 1470 MPa at 10 wt.%). It can be seen, that the presence of coir fibers effectively improves the PP mechanical properties due to their high tensile modulus [94], [95]. Figure II.5-4a also shows that the tensile strength was almost constant (about 30 MPa) with fiber loading indicating a good mechanical anchorage between matrix and fibers, as well as good fiber dispersion was achieved to uniformly distribute/transfer the stresses to the fibers [96]. On the other hand, figure II.5-4b shows that the composite ductility decreases with increasing fiber content. This trend can be related to the rigid but fragile character of coir fibers decreasing the possibility of plastic energy absorption/dissipation in the composites [81], [94].

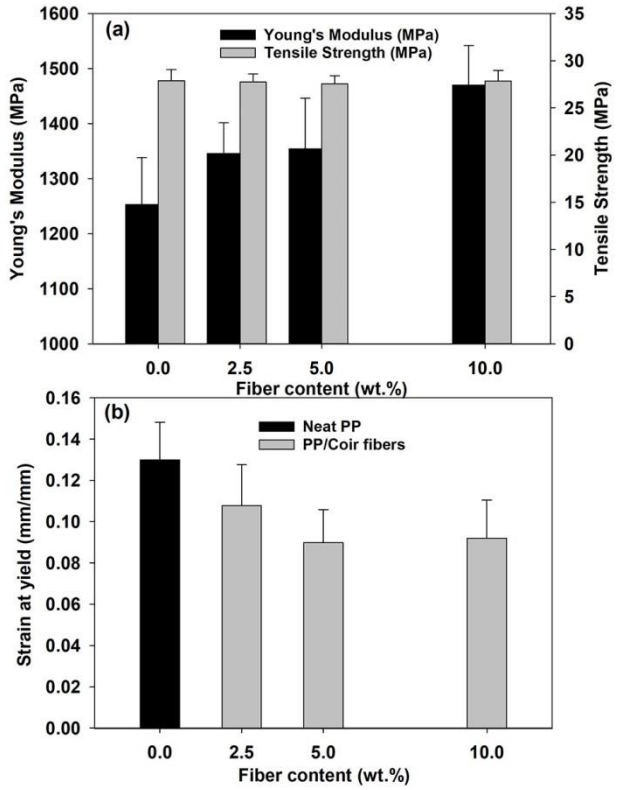

Figure II.5-4: Tensile properties of PP/coir fibers bio-composites: (a) Young's modulus and tensile strength; (b) strain at yield.

II.5.4. Torsion properties

The complex torsion modulus (G*) is given by:

$$|G^*| = \sqrt{G'^2 + G''^2} \qquad \text{(II.5-1)}$$

Where G' and G" are respectively the storage and loss moduli. Another parameter of interest is the loss factor (tanδ) which is the ratio between the loss and storage moduli as:

$$tan\delta = \frac{G''}{G'} \qquad \text{(II.5-2)}$$

Figure II.5-5a presents the torsion modulus as a function of frequency and fiber content. It can be seen that the plots have different trends above and below 2.5 wt.% of coir fibers indicating that a critical fiber content exists. This percolation threshold indicates that under deformation, the fibers rotate sufficiently to support a part of the load. Figure II.5-5a also shows that the values increase with frequency as the materials are viscoelastic; i.e. the composites behave more like elastic solids as frequency increases [81], [97]. On the other hand, the fact that the curves are parallel

indicates that one can be obtained from a simple translation of another, so the values of the matrix (G_0^* = torsion modulus at 0 wt.%) are used for the analysis and the results are plotted as a function of frequency (f) in figure II.5-5b. The data were fitted to get:

$$|G_0^*| = 50\ log(f) + 456 \qquad \text{(II.5-3)}$$

Figure II.5-5c shows a slight loss factor decrease from 0.1 to 40 Hz with increasing fiber content. This can be explained by the dominating elastic part in the composites which confirms that the materials mostly behave as elastic solids. This elasticity is mainly related to the coir fibers reinforcement leading to a more elastic composite behavior compared to the neat matrix [81], [94].

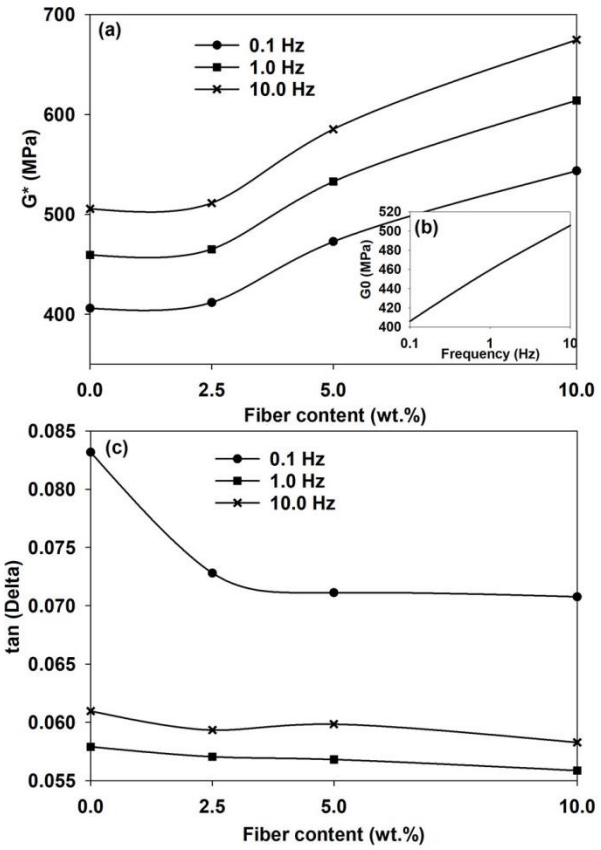

Figure II.5-5: (a) Experimental results of PP/coir fibers torsion modulus as a function of fiber content and frequency. (b) Torsion modulus of the neat PP (G0) as a function of frequency. (c) Loss factor as a function of fiber content.

II.6. Modeling

This section presents a self-consistent approach based on a modified Hirsch model to predict the composites Young's modulus, tensile strength and torsion modulus by considering fiber orientation. The model will be validated with the experimental results presented above and compared with the original Hirsch and Tsai-Pagano models.

Several models have been developed to predict the mechanical properties of fiber reinforced thermoplastic composites using a combination of Voigt and Reuss models (Eq. II.6-1 and Eq. II.6-2) defined as:

Voigt model:

$$E_v = V_f E_f + (1 - V_f) E_m \quad \text{(II.6-1a)}$$

$$\sigma_v = V_f \sigma_f + (1 - V_f) \sigma_m \quad \text{(II.6-1b)}$$

$$G_v = V_f G_f + (1 - V_f) G_m \quad \text{(II.6-1c)}$$

Reuss model:

$$E_r = \frac{E_f E_m}{V_f E_m + (1 - V_f) E_f} \quad \text{(II.6-2a)}$$

$$\sigma_r = \frac{\sigma_f \sigma_m}{V_f \sigma_m + (1 - V_f) \sigma_f} \quad \text{(II.6-2b)}$$

$$G_r = \frac{G_f G_m}{V_f G_m + (1 - V_f) G_f} \quad \text{(II.6-2c)}$$

Where E is the Young's modulus, σ is the tensile strength and G is the torsion modulus, while indices v, r, m and f refer to the Voigt, Reuss, matrix and fiber, respectively. Finally, V_f and (1-V_f) are the fibers and matrix volume fraction, respectively.

The Voigt model assumes a parallel fiber arrangement in the matrix (in the applied stress direction), while the Reuss model assumes that the fibers are normal to the applied stress [98].

To compare the proposed model prediction ability, a comparison was first done with the Hirsch model (Eq. II.6-3). The latter assumes that the fibers are randomly oriented in the matrix and introduces an empirical parameter "x" ($0 < x < 1$) which represents the relative contribution of the

parallel and series models. It is also assumed that the fiber orientation and the stress concentration effects (fibers end) can be combined into this lumped parameter "x". A value of x = 0.4 has been proposed for a random fiber orientation [28], [29], [34]. Unlike the Hirsh model, the Tsai-Pagano model (Eq. II.6-4) includes the reinforcing fibers length and diameter. The model also assumes a random filler orientation in the matrix as well as good dispersion and perfect fiber-matrix interfacial adhesion. In this case, the longitudinal and transversal contributions are 3/8 and 5/8, respectively [28], [29], [34].

Hirsch model

$$E_h = x\,E_v + (1 - x)\,E_r \qquad \text{(II.6-3a)}$$

$$\sigma_h = x\,\sigma_v + (1 - x)\,\sigma_r \qquad \text{(II.6-3b)}$$

$$G_h = x\,G_v + (1 - x)\,G_r \qquad \text{(II.6-3c)}$$

Tsai-Pagano model

$$E_{tp} = \frac{3}{8}\,E_v + \frac{5}{8}\,E_r \qquad \text{(II.6-4a)}$$

$$\sigma_{tp} = \frac{3}{8}\,\sigma_v + \frac{5}{8}\,\sigma_r \qquad \text{(II.6-4b)}$$

$$G_{tp} = \frac{3}{8}\,G_v + \frac{5}{8}\,G_r \qquad \text{(II.6-4c)}$$

Where, the indices h and tp refer to the Hirsch and Tsai-Pagano models, respectively. Finally, x and (1-x) are the contribution of the parallel and series models, respectively.

Both Hirsch and Tsai-Pagano models have been developed and optimized for a random fiber orientation, but their performance may be different if orientation effects are included. This led to develop a self-consistent approach to predict the Young's modulus, tensile strength and torsion modulus for a specific average fiber orientation "θ". This was done by modification of the Hirsch model by taking the empirical parameter (x) to be proportional to the fiber orientation factors (α), which can also range between 0 and 1 to give a best fit (Eq. II.6-5), as (α) and (l-α) represent the relative contributions of the parallel (uniform strain) and series (uniform stress) models as shown in figure II.6-1. The values for α are determined from a linear interpolation in the range of [-90°,

90°] according to Eq. II.6-6, where α = 1 implies a longitudinal fiber orientation (-90° and 90°) and α=0 refers to a transversal fiber orientation (0°).

The modified Hirsch model:

$$E_h = \alpha E_v + (1 - \alpha) E_r \quad \text{(II.6-5a)}$$

$$\sigma_h = \alpha \sigma_v + (1 - \alpha) \sigma_r \quad \text{(II.6-5b)}$$

$$G_h = \alpha G_v + (1 - \alpha) G_r \quad \text{(II.6-5c)}$$

$$\alpha = \frac{|\theta|}{90°} \quad \text{(II.6-6)}$$

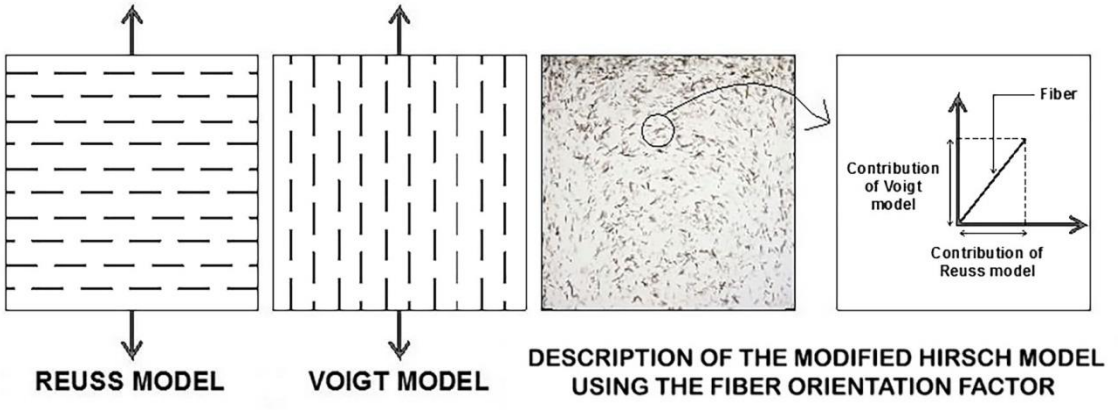

Figure II.6-1: Schematic representation of the modified Hirsch's model as a combination of the Voigt and Reuss models.

The self-consistent approach is based on the iterative incorporation of the fiber orientation families according to their volume fraction in the matrix (Figure II.5-2). To take into account the interaction between the inclusions, the proposed scheme assumes that each inclusion is embedded into the homogenized material and seen as second inclusions embedded into the matrix as illustrated in figure II.6-2.

Figure II.6-2 presents the details of the self-consistent formulation proposed. The first fiber orientation family (θ_1, V_{f1}, E_f, σ_f, G_f) was introduced in the homogeneous polypropylene matrix (E_0, σ_0, G_0) to predict the Young's modulus, tensile strength and torsion modulus using Voigt (E_{v1}, σ_{v1}, G_{v1}), Reuss (E_{r1}, σ_{r1}, G_{r1}) and modified Hirsch (E_{h1}, σ_{h1}, G_{h1}) models. Then, the second family (θ_2, V_{f2}, E_f, σ_f, G_f) was embedded into the first equivalent homogenous material (E_{h1}, σ_{h1}, G_{h1}) to get (E_{v2}, E_{r2}, E_{h2}, σ_{v2}, σ_{r2}, σ_{h2}, G_{v2}, G_{r2}, G_{h2}). The same steps were repeated until the final

fiber family (θ_n, V_{fn}, E_f, σ_f, G_f) was added to the mixture ($E_{h(n-1)}$, $\sigma_{h(n-1)}$, $G_{h(n-1)}$), enabling to obtain the homogenous composite properties (E_{hn}, σ_{hn}, G_{hn}). The index (1, 2…n) refers to the fiber orientation family where in our case n = 9 (see Figure II.5-2).

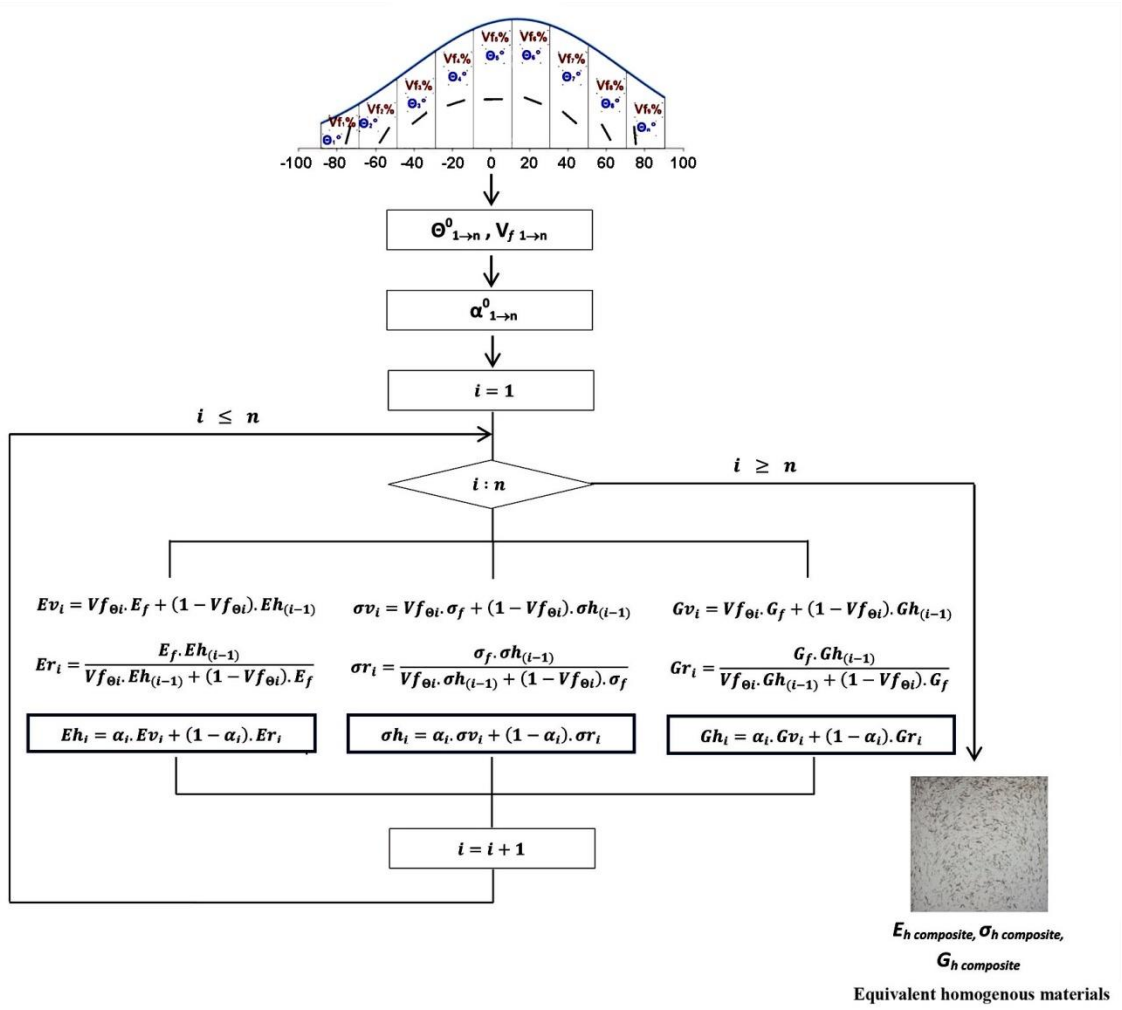

Figure II.6-2: Summary of the resolution steps for the modified Hirsch model coupled with the self-consistent approach.

II.7. Application

Prediction of the Young's modulus, tensile strength and torsion modulus for the Hirsch and Tsai-Pagano models, as well as the proposed self-consistent approach will be compared to the experimental values. For the calculations, the raw materials properties were taken from the experimental results as:

$E_f = 5\,695$ MPa and $E_m = 1\,253$ MPa

$\sigma_f = 234$ MPa and $\sigma_m = 28$ MPa

$G_f = 2589$ MPa and $G_m = 406$ MPa

The intrinsic elastic modulus of alkali treated fibers was determined experimentally by using the RSA in the rectangular tension/compression geometry (monofilament) [99], [100]. The measured value was 5695 MPa, which is very close to the Young's modulus of natural fibers reported in the literature [99], [100].

Assuming, that the fibers mechanical properties are isotropic, their torsion modulus G_f can be calculated from E_f by taking a Poisson's ratio ($\nu = 0.1$) generally used for natural fibers [101] to give:

$$G = \frac{E}{2(1+\nu)} \quad \text{(II.7-1)}$$

Figure II.7-1a compares the experimental and predicted elastic modulus of the PP/coir fibers bio-composites. By increasing fiber content, the experimental as well as the theoretical elastic modulus increased. Generally, when the fibers have much higher strength and stiffness than the polymer matrix, the composites tensile properties are substantially improved by fibers addition. The improvement can also be related to good fiber-matrix adhesion [102]. However, the Hirsch model (x=0.4 for random orientation) shows the highest value for the Young's modulus prediction, while the values for the self-consistent approach and Tsai-Pagano model were closer to the experimental ones. It seems that the absence of specific fiber morphology in the Hirsch model had a small effect on the calculations. For better comparison, the deviations are reported in figure II.7-1b. There is a slight difference ranging from 1.7% for the self-consistent approach to 2.7% for the Hirsch model, but it is clear that the self-consistent approach based on the modified Hirsch model provided better estimations than the original Hirsch model. On the contrary, the Tsai-Pagano model and self-consistent approach deviations were approximately at the same level and very close to the experimental result. This may be due to the fact that the Tsai-Pagano model explicitly accounts for the fiber morphological properties. On the other hand, it was noted for the experimental results that, only the composites with a fiber concentration less than 5 wt.%, have experimental Young's modulus slightly higher than the predictions.

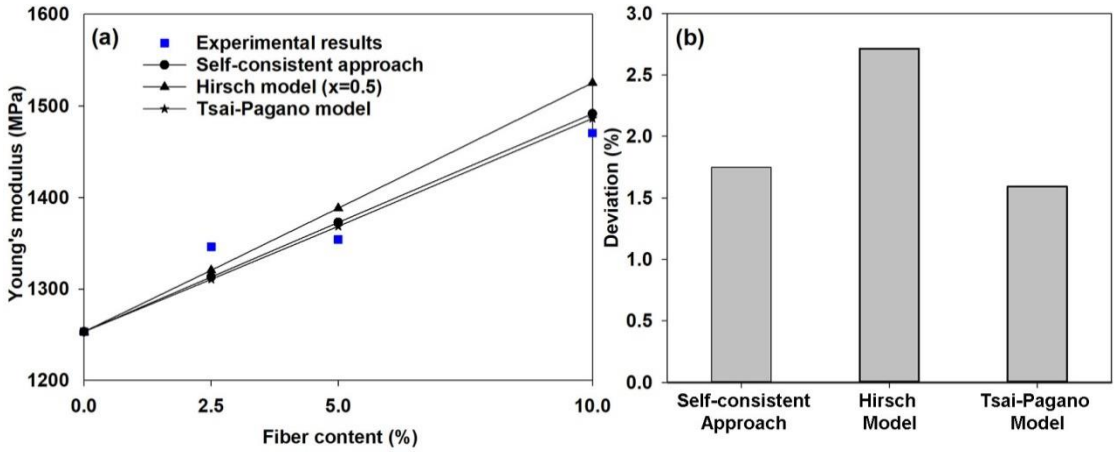

Figure II.7-1: Comparison between the model prediction and the experimental Young's modulus.

On the other hand, figure II.7-2a clearly indicates that all the models overestimate the tensile strength compared to the experimental values. This may indicate that the assumption of either uniform stress (Reuss) or uniform strain (Voigt) is an oversimplification. In our case, short fibers were chosen as reinforcement for a thermoplastic matrix meaning that the stress transfer mostly depends on fiber orientation and concentration [103]. It was also seen in all the models that at low fiber content, the predicted tensile strength is close to the experimental one, but higher deviations are observed as fiber concentration increases. This can be attributed to good fiber dispersion and distribution in the polymer matrix at low concentration, but as fiber content increases their wettability by the matrix may be more limited leading to some agglomeration [34], [103]. This effect is not included in our calculations. Nevertheless, referring to the error bars presented in figure II.7-2b, it can be seen that the Hirsch model shows the highest deviation (24.6%) compared to other models (21.3% for the self-consistent approach and 20.3% for the Tsai-Pagano model). To conclude, the self-consistent approach based on a modified version of the Hirsch model gives better tensile strength results compared to the original Hirsch model. As mentioned earlier for the Young's modulus results, the precision of the Tsai-Pagano model can be attributed to the morphological parameter included.

Finally, figure II.7-3a, b and c show that the torsion modulus significantly increases with increasing fiber content and frequency. This indicates that the composites are more rigid/elastic [97]. According to the deviation presented on figure II.7-3d, it appears that the deviation increases with increasing frequency, but in all cases the Hirsch model gives better results than the self-consistent approach and the Tsai-Pagano model. This probably means that other factors play

a major role in the torsion behavior than orientation. It can have said that with increasing frequency, apart from the degree of orientation, simultaneous morphology and molecular mobility changes occur, both of which affect the torsion properties [104]. So, additional work is needed to better understand the different parameters controlling this property.

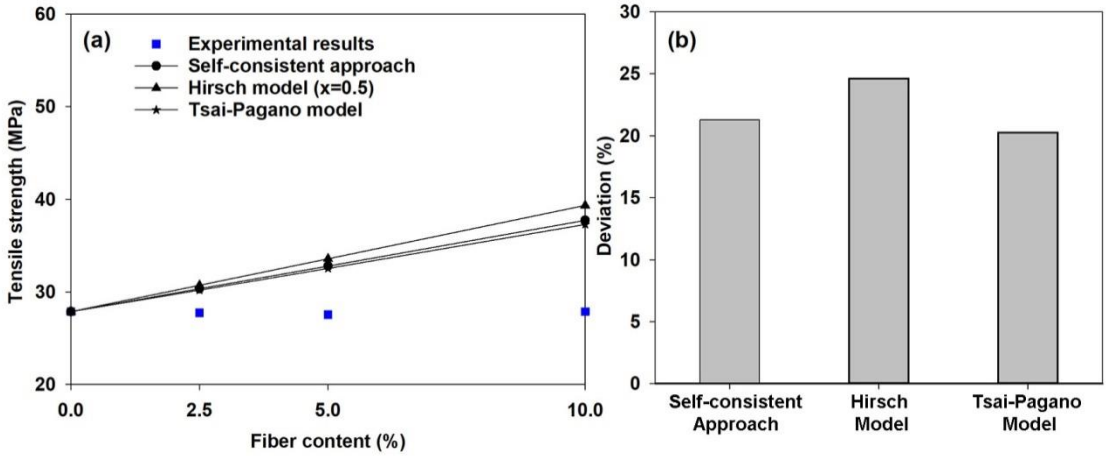

Figure II.7-2: Comparison between the model prediction and the experimental tensile strength.

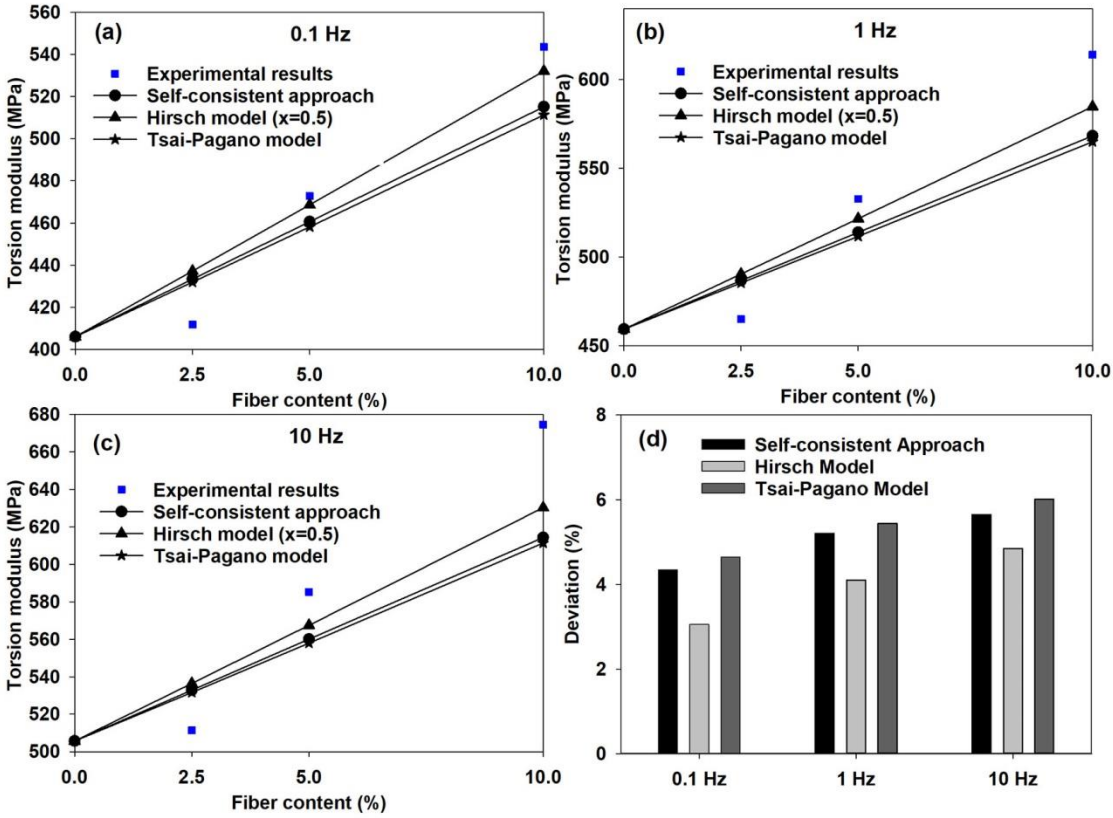

Figure II.7-3: Comparison between the model prediction and the experimental torsion modulus at different frequency.

II.8. Conclusion

This work investigated the effect of coir fiber content and orientation on the tensile/shears properties of polypropylene composites. The specimens were prepared by twin-screw extrusion and injection molding. It was found that mechanical properties increased with fiber content (0, 2.5, 5 and 10 wt.%). In the final samples, fiber length and orientation were determined for different positions to get a full distribution and extract an average value with standard deviation.

Also, this work proposed a modified Hirsch model for which the empirical parameter x was related to fiber orientation. Based on a self-consistent approach, the new model was found to give better overall predictions of the experimental data compared to the original Hirsch and Tsai-Pagano models. Nevertheless, more work needs to be done to account for higher fiber content and other type of deformation.

Chapter III. Injection molding of short coir fiber polypropylene bio-composites: Prediction of the mold filling phase

F. Semlali Aouragh Hassani et al., "Injection Molding of Short Coir Fiber Polypropylene Biocomposites : Prediction of the Mold Filling Phase", Polym. Compos., vol. 40, no. 10, pp. 4042–4055, 2019.

III.1. Abstract

The mold-filling phase in injection molding is the most important one because the material flow behavior controls the final part structure. In this work, the effect of melt rheology on the flow front progression of coir fiber (2.5, 5, 10, and 15 wt%) filled polypropylene is investigated. The flow behavior is predicted using the incom- pressible Navier–Stokes equations to determine the flow front shape and position and the model proposed is in good agreement with the experimental results for the range of conditions studied. Finally, to provide a better understanding of the effect of different processing conditions (pressure, melt, and mold temperature) on the flow front evolution, several simulations were per- formed using Autodesk Moldflow Insight.

III.2. Résumé

Dans ce travail, l'effet de la rhéologie à l'état fondu sur la progression du front d'écoulement du polypropylène renforcé par des fibres de coco (2,5, 5, 10 et 15% en poids) a été étudié. Tandis que la prédiction de la forme et position du front d'écoulement a été faite en se basant sur les équations de Navier–Stokes. Globalement, le modèle proposé est en bon accord avec les résultats expérimentaux pour la gamme de conditions étudiées. Finalement, pour mieux comprendre l'effet des différentes conditions de mise en œuvre (pression, température de fusion et du moule) sur l'évolution du front d'écoulement, plusieurs simulations ont été effectuées à l'aide d'Autodesk Moldflow Insight.

III.3. Introduction

Injection molding represents one of the most important process to manufacture plastic parts, especially for complex geometries because of its high productivity, with high precision and low cost [2], [105], [106]. For a specific injection molding machine, thermoplastic resin and mold, the process can be decomposed into three distinct stages: filling, post-filling and cooling [25], [105]. Firstly, a polymer melt is injected into an empty cavity under high pressure to form a plastic part. After solidifying and cooling, the part is ejected out of the mold and a new cycle begins [6], [105]. The filling stage is very complex because several phenomena occur such as momentum and heat transfer. This coupling can lead to problems like jetting or the inability to completely fill the mold cavity, especially for thin sections where the polymer rapidly solidifies upon contact with cold walls [4], [105]. Although the mold temperature can be increased, this will increase the cooling cycle time so a compromise must be made. The distance that the material can flow (short shot) is also related to the processing conditions taking into account the rheological properties of each material [107], [108]. An optimized injection molding process require an accurate control of several parameters such as the melt temperature, melt viscosity, shear rate, mold temperature, injection speed, injection pressure and switch over point for speed and pressure to reduce the cycle time [107], [108]. These factors must be controlled for each formulation and requires a multidisciplinary/multivariable approach to optimize the final product performances [107]. These complex interactions between all the parameters must be related to the mold geometry and the melt flow properties. So engineers must develop methods/techniques to accurately predict the flow front progression during injection molding. This enables to improve parts quality as well as reducing production cost and time. Fortunately, experimental design can be used to reduce/eliminate lengthy experimental testing (trials and error) [4], [107], [109].

Nowadays, numerical simulations are more and more being used because several models have been developed and material information (physical properties) is available. Several studies aimed at the mathematical modeling of the different steps involved in injection molding, but more precisely the flow front progression. For complex parts, a three-dimensional analysis is necessary not only to predict the position and shape of the flow front, but also to evaluate the most important parameters influencing parts quality. So the development of effective computer-assisted techniques to replace lengthy experimental methods are now common [108]. This

procedure provides information about the tooling design and the processing conditions [110]. Commercial softwares such as Moldflow are widely used for plastic injection molding simulations as they allow for a careful and complete analysis of the materials while proposing practical solutions to be implemented [109].

This study firstly presents the effect of fiber concentration (2.5, 5,10 and 15 wt.%) on the flow front progression of polypropylene melts and then explains in details the effect of temperature, viscosity and shear rate on the flow front shape and position. Secondly, the flow behavior is studied by developing a three-dimensional model for the non-isothermal and non-Newtonian mold filling prediction. The incompressible Navier-Stokes equations are simplified into a single Poisson equation, and then solved to estimate the flow velocity which under a constant flow rate allows the flow front shape and position prediction for the composites. The simulations are finally compared with experimental data to confirm that the model is able to provide good prediction. Finally, the Moldflow software is used to further understand the effect of processing conditions such as pressure, as well as melt and mold temperature on the flow front behavior.

III.4. Materials and methods

III.4.1. Materials

The polymer used was polypropylene (PP) PPH03BPM (TASNEE, Saudi Arabia) supplied by Exxon Mobil with a density of 903 kg/m^3 and a peak melting temperature of 165°C. The coir fibers (C), with an average density of 1548 kg/m^3, an initial length of 150-200 mm and an average diameter of 300 µm were obtained from coconut shells extracted from Ivory Coast and used as natural reinforcements. The fibers were prepared in three steps. Firstly, the coir fibers were carefully washed with tap water and air-dried for 24 h. Secondly, the fibers were ground with a 4 mm sieve opening using a Pulverisette-19 (Fritsch GmbH, Germany). Finally, the fibers were sieved using a 200 µm opening to get rid of fine particles.

III.4.2. Samples preparation

Samples PP, PP/C 2.5, PP/C 5, PP/C 10 and PP/C 15, which denote the PP/C bio-composites with 2.5, 5, 10 and 15 wt.% coir content respectively, were prepared on a Leistritz ZSE-18 twin-screw extruder (LEISTRITZ EXTRUSIONSTECHNIK GmbH, Germany) at a screw speed of

125 rpm. The temperature profile was set to 200, 200, 200, 200, 190, 190, 190 and 190°C from the feed hopper to the die. The extrudates were immediately quenched in water and cooled in air to be manually cut into pieces (average length of 15 mm) to limit fibers length degradation.

Injection molding was performed in rectangular molds (100x100x1 mm^3) using an Engel e-Victory machine (ENGEL GmbH, Austria). The standard molding conditions were: a flow rate of 80 cm^3/s, a maximum injection pressure of 24 MPa and a filling time of 4 s. The temperature was set at 200°C for the first three heating zones, while the nozzle temperature was set at 190°C with a mold temperature of 45°C. The conditions were selected to produce short shots every 1 cm in the injection direction as shown in figure III.4-1.

III.4.3. Measurements

The (x) axis denotes the injection direction where x = L is the mold length, while the y and z axes refer to the mold width (y = 2l) and height (z = 2h), respectively. The overall flow pattern or the advancing front profiles were determined by a series of short shots. Pictures of selected samples were taken using a white LED backlight illuminator equipped with a digital camera. Since extrusion and injection molding are known to mechanically degrade the fibers, their final dimensions were measured with the ImageJ software (National Institutes of Health, USA) and gave an average length of 2.25 mm. Then, to establish accurate comparison of the flow front pattern, pictures of the short shots were superimposed (figure III.4-1) to get a complete profile. Finally, the images were digitalized using the Plot Digitizer software (ver. 2.6.6.0) to evaluate the flow front correlation between samples.

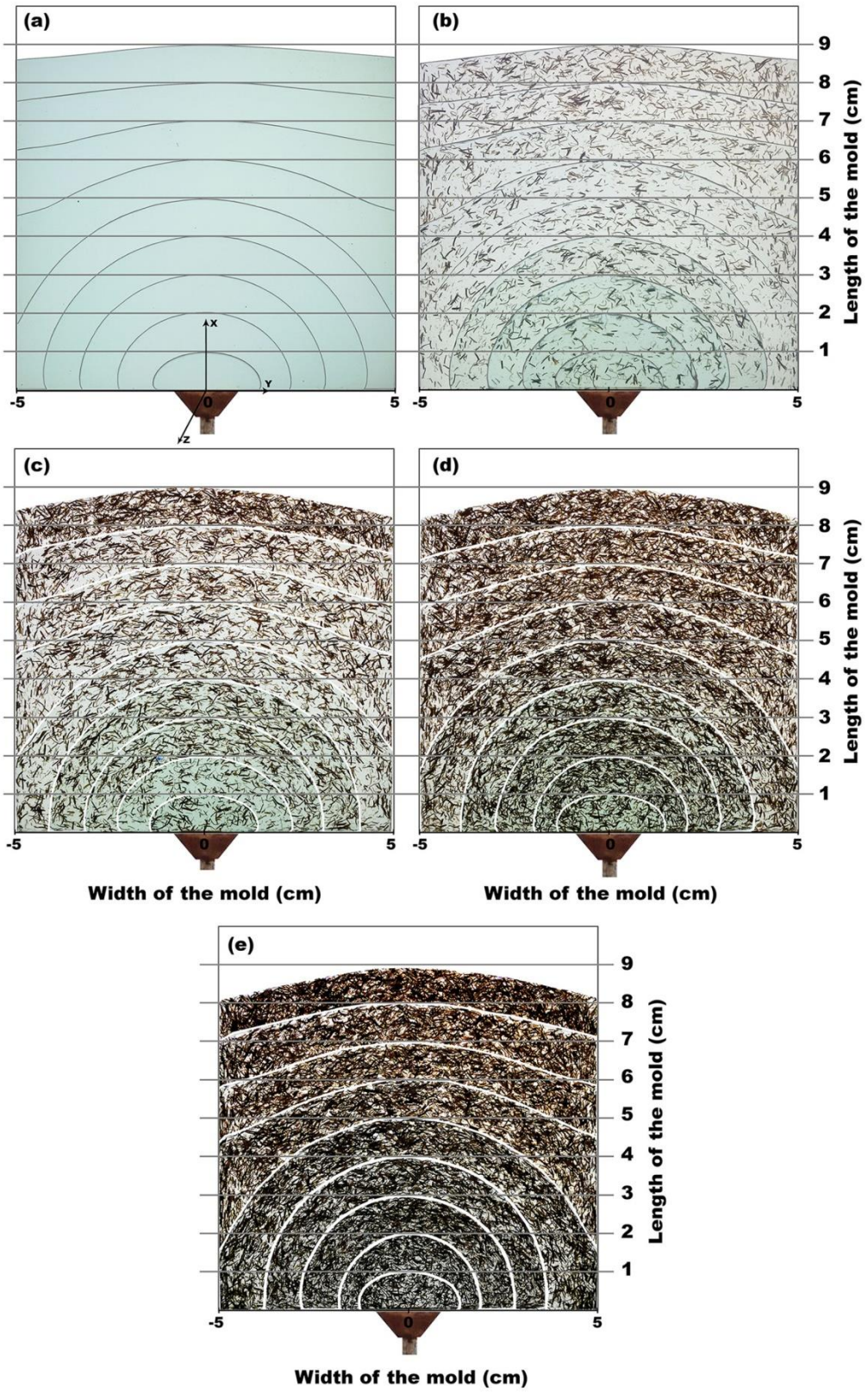

Figure III.4-1: Superposition of short shot images to get a complete flow front profile for: (a) PP, (b) PP/C 2.5, (c) PP/C 5, (d) PP/C 10 and (e) PP/C 15.

III.4.4. Rheological testing

To characterize the rheological properties in the melt state, small amplitude oscillatory tests were performed on a MCR 500 (Physica, Germany) rheometer equipped with a CTD600 device. The measurements were carried out using a 30 mm parallel plate geometry with 1 mm thick samples at 190°C (injection temperature) using frequency sweeps between 0.05 and 500 Hz at a strain of 5% (linear viscoelastic regime was confirmed via strain sweeps).

III.4.5. Moldflow analysis

Numerical simulations were performed to investigate the effect of the processing conditions on the flow front behavior. The parts (100x100x1 mm^3) were modeled using the Autodesk SimStudio Tools 2016 R2 software (Autodesk, USA). This application was used to create the CAD surface and solid models to simplify or repair existing CAD models. Then, the mold was imported into Autodesk Moldflow Insight 2019 (Compilation 20180406.1525) software (Autodesk, USA) to study the flow behavior in the mold cavity during injection molding. The injection was done directly through one gate using the same processing conditions and material as in the experimental work. According to the finite-element/finite-difference scheme used by the software, the cavity was meshed into elements and nodes as shown in figure III.4-2.

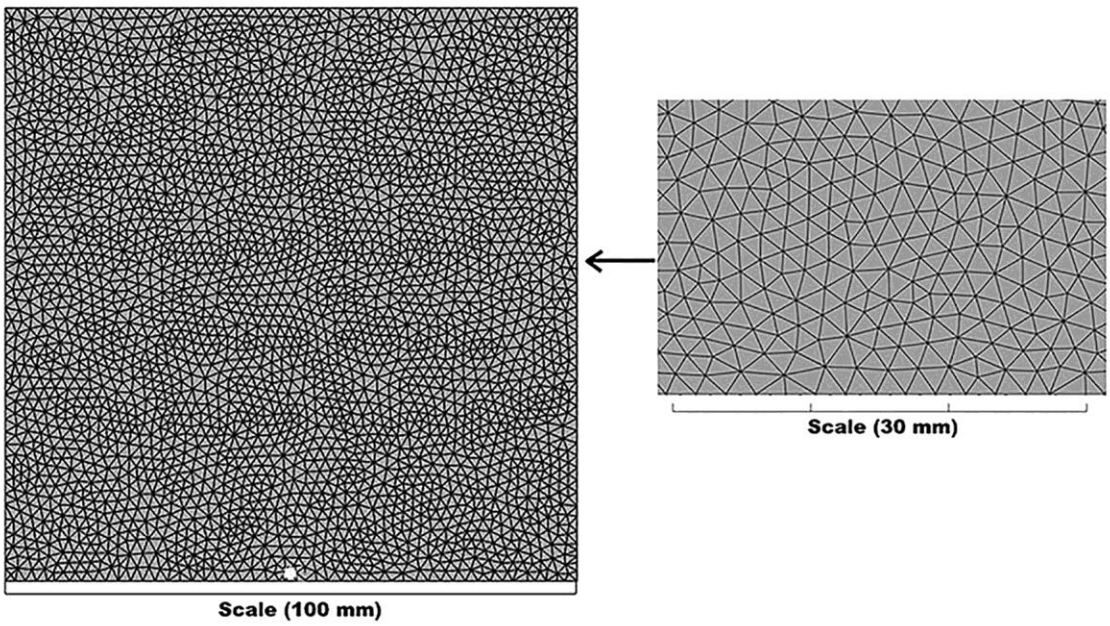

Figure III.4-2: The mesh configuration and part dimensions used for the simulations using Autodesk Moldflow.

III.5. Results and discussion

III.5.1. Experimental studies

The objective of this experimental study is to determine the effect of each parameter on the flow front pattern in terms of reinforcement content, melt temperature, melt viscosity and shear rate. By comparing the flow front behavior of the neat polypropylene and the composites (PP/C 2.5, PP/C 5, PP/C 10 and PP/C 15) every 1 cm (x axis position), it was observed that the flow front profiles for the five samples are initially a series of semi-circles, but switched towards curved lines as the front progressed (Figure III.5-1a). This observation led to conclude that the flow front goes through three phases (Figure III.5-1b). At the cavity entrance (gate), the melt progresses in a radial pattern to fill the mold width. Then, as the melt comes into contact with the walls, a transition occurs where the flow front changes from a circular shape to a new steady shape. The front distorts into a parabolic shape with a pronounced degree of curvature at the centerline, but this curvature decreases as the flow front progresses to become almost flat. This new steady pattern continues until the mold is filled [111],[112],[113]. Even if the five samples have similar front behavior, it can be seen that fiber addition decreases the flow front progression at the mold surface (c). For example, the PP/C 15 flow front position is 2-13% less before the melt reaches the corners (phase 1), while the value is 2-7% after the corners are filled (phases 2 and 3) when compared to the neat PP.

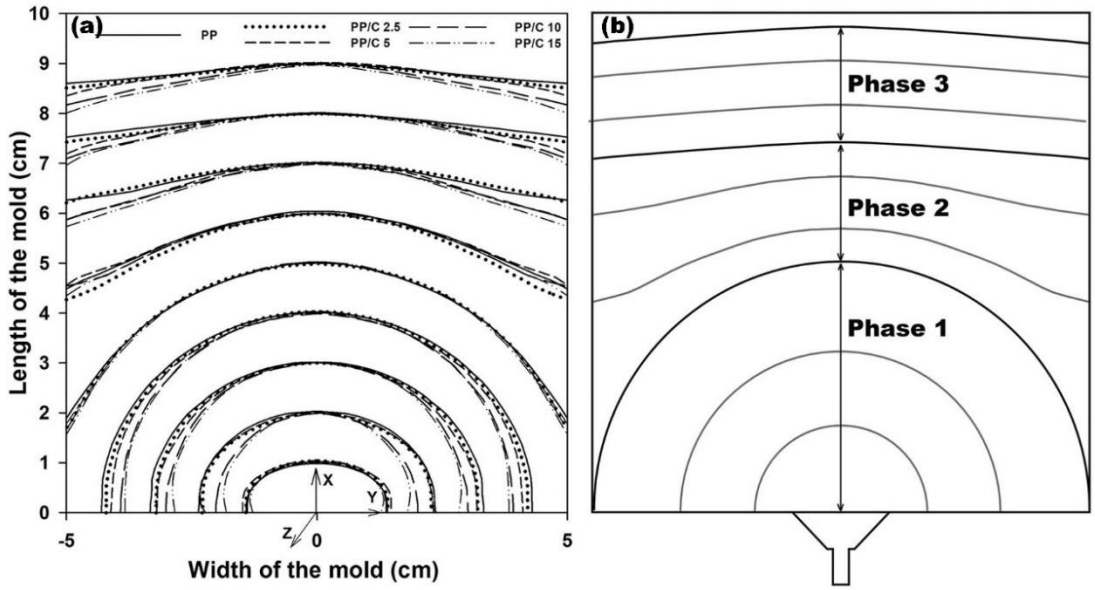

Figure III.5-1: (a) Superposition of flow front progression of all samples after digitalization. (b) Schematic representation of the three phases associated with mold cavity filling.

Changes in the flow front progression speed are related to different rheological properties (viscosity) with increasing fiber content. This effect is further enhanced by heat transfer decreasing the melt temperature with increasing filling time. So the effect of temperature on the melt viscosity is presented in figure III.5-2. From the results of figure III.5-2a,a', several observations can be made. Firstly, the viscosity decreases with increasing frequency indicating a non-Newtonian pseudoplastic behavior of the materials. Secondly, the viscosity increases with fiber addition due to their rigid structure and strong hydrogen interactions (higher number of interacting chains) as the fibers begin to form a network structure. This explains the drop in the flow front position with increasing fiber content [96]. As expected, viscosity also decreases with increasing temperature (Figure III.5-2a,a'), especially at low frequency while the effect is less important at higher values.

To provide a better understanding of the effect of each parameter, the viscosity at different frequency was plotted on a representative flow front curve, according to the temperature along a normalized width of the mold (approximation of 190°C in the center and 185°C at the surface). As shown for all the samples in figure III.5-2b, c, d, e and f, the temperature decreases when the material enters the cold cavity leading to a higher local viscosity close to the mold walls. When the melt reaches the mold surfaces, a frozen layer rapidly forms along the mold walls where the velocity drops to zero. This brings the melt in the central region to flow more rapidly due to its lower viscosity (Figure III.5-3). The solidified polymer layer at the walls combined with the expanded central material leads to the pronounced curvature of the flow front centerline [107],[114]. It was also observed that the viscosity tends to be constant along the mold width as shear rate increases. Since the viscosity at higher frequency (above 10 Hz) is less affected by the temperature, viscosity variations are negligible [108]. So high shear rate (frequency) is more favorable for injection molding [108].

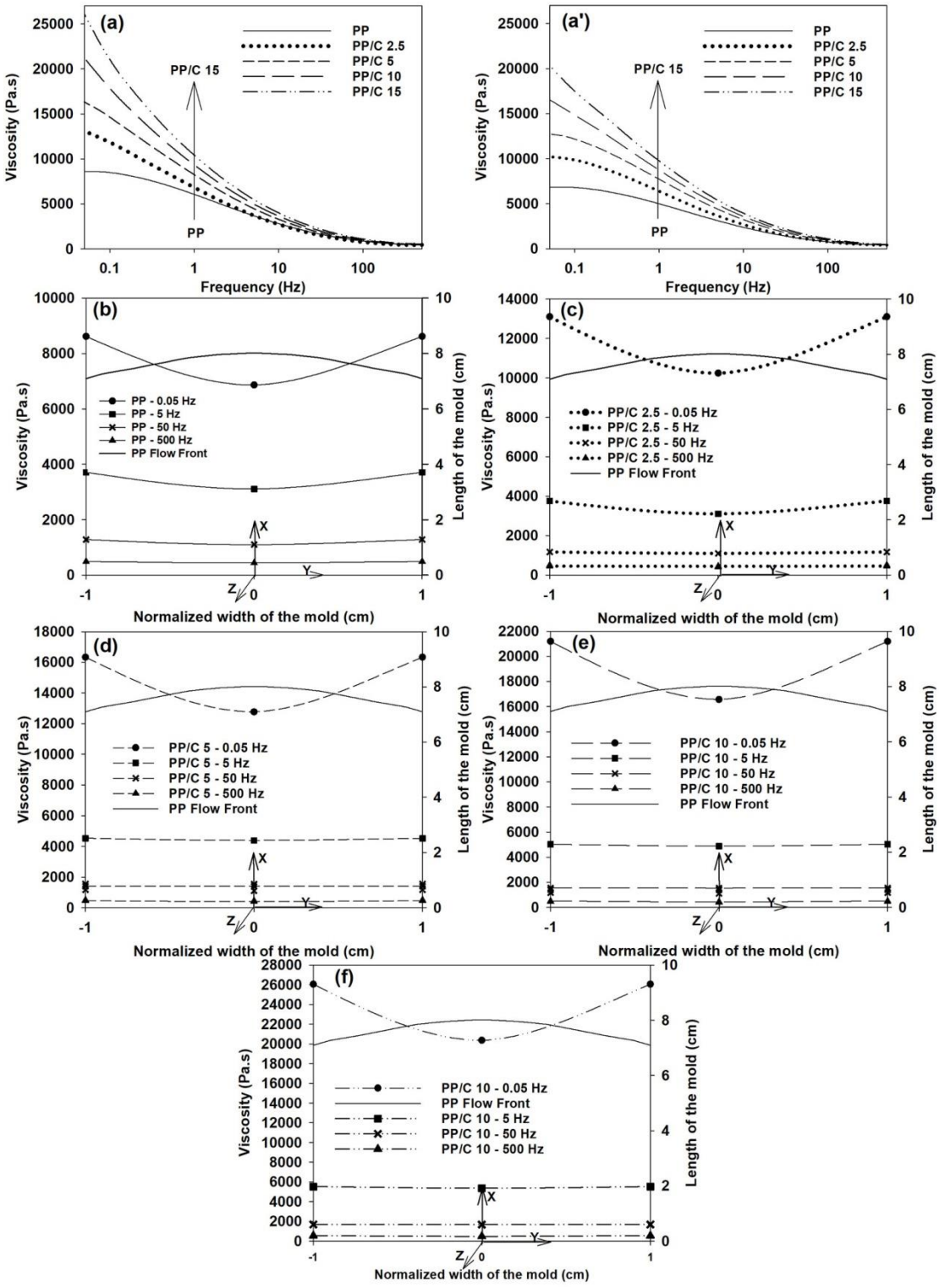

Figure III.5-2: Viscosity of the samples at: (a) 185°C and (a') 190°C. Variation of the viscosity as a function of the normalized mold width for: (b) PP, (c) PP/C 2.5, (d) PP/C 5, (e) PP/C 10 and (f) PP/C 15.

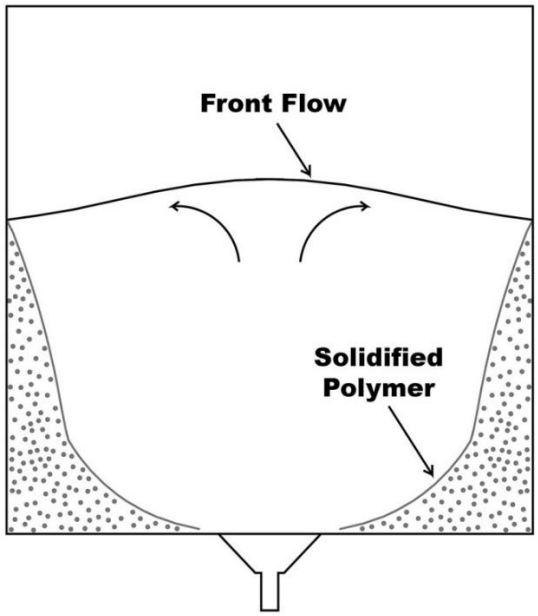

Figure III.5-3: Schematic representation of a polymer melts filling a cold mold.

Based on these experimental observations, a theoretical approach was developed to predict the flow front behavior. Figure III.5-4a presents the evolution of the centerline flow front position as a function of its position at the wall, before filling of the corners (phase 1). The five samples show a linear evolution which can be approximated by:

$$Y = (-0.01\, w_f + 0.95)\, x + (0.0036\, w_f + 0.43) \qquad \text{(III.5-1)}$$

Where, w_f is the fiber weight fraction. Figure III.5-4b reports a maximum deviation of 16% between the predictions and the experimental results indicating that equation III.5-1 provides very good estimation.

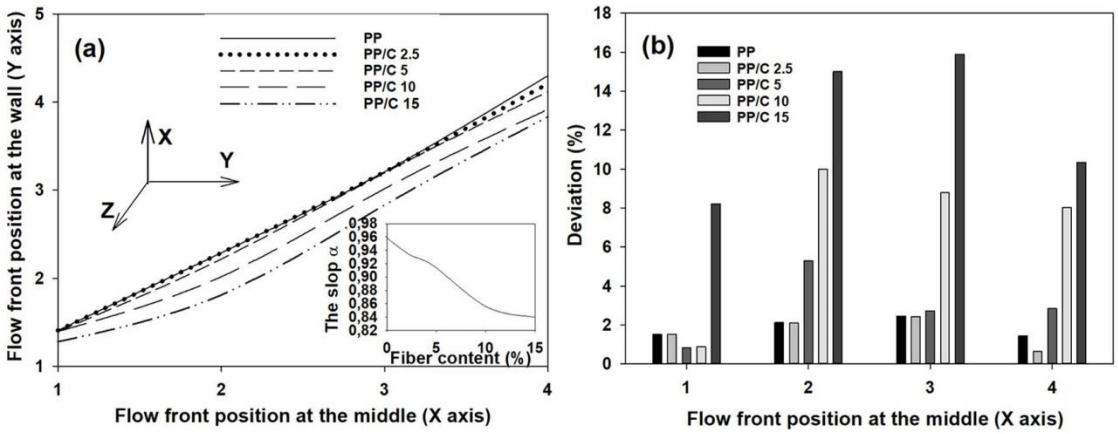

Figure III.5-4: (a) Position of the flow front at the wall as a function of its position at the centerline for all samples. (b) Deviation between the predicted and experimental results.

III.5.2. Mathematical model

The aim of building a mathematical model is to solve the governing equations to predict the flow front position and shape. A three-dimensional (3D) study of a viscous flow in a rectangular channel includes solving the Navier-Stokes equation:

$$\frac{\partial \vec{v}}{\partial t} + (\vec{v}.\vec{\nabla})\vec{v} = -\frac{1}{\rho}\vec{\nabla}P + \frac{1}{\rho}\vec{f}_{v\,ext} + \nu\,\vec{\Delta}\vec{v} \qquad \text{(III.5-2)}$$

Where, V, P, ρ, ν are the velocity, pressure, density and kinematic viscosity, respectively.

To solve the problem, the following simplifying assumptions are introduced:

- Incompressible flow : $\mathrm{div}\,\vec{v} = \vec{0}$
- Steady flow : $\frac{\partial \vec{v}}{\partial t} = \vec{0}$
- Laminar flow : $(\vec{v}.\vec{\nabla})\vec{v} = \vec{0}$
- External volume forces are neglected with respect to the viscous force : $\vec{f}_{v\,ext} = \vec{0}$
- Pressure on the flow front : $P_{front} = P_{atmosphere}$
- Pressure at the gate : $P = P_{inj}$
- Non-isothermal flow with an imposed temperature at the mold entrance.
- Symmetry with respect to the geometry median plane.
- Flow along the x axis: $\vec{v} = \overrightarrow{v_x}(y,z)$

Referring to the origin location and the above assumptions, the flow governing equations are simplified into a single Poisson equation as [115], [116]:

$$\frac{\partial P}{\partial x} = \eta\left(\frac{\partial^2 v_x}{\partial y^2} + \frac{\partial^2 v_x}{\partial z^2}\right) \qquad \text{(III.5-3)}$$

Where η is the dynamic viscosity.

Since the left-hand side $(\frac{\partial P}{\partial x})$ only depends on x while the right hand side $(\frac{\partial^2 v_x}{\partial y^2} + \frac{\partial^2 v_x}{\partial z^2})$ only depends on y and z, the only solution is that both sides are constant in the whole domain ∀(x,y,z). This enables to suppose that the pressure (Eq. III.5-4) varies linearly with position (x) as:

$$\frac{\partial P}{\partial x} = cte < 0;\ \frac{\partial P}{\partial x} = -a \qquad \text{(III.5-4)}$$

Equation III.5-5 which is a particular form of a Poisson equation [117], must be solved with appropriate boundary conditions. In the case of a rectangular geometry, the equation can be analytically solved to give:

$$v_x(y,z) = -\frac{a}{\eta}\,[Ay^2 + Bz^2 + Cyz + Dy + Ez + F] \qquad \text{(III.5-5)}$$

The boundary conditions imposed are no-slip at the wall and symmetry:

- $v_x(\pm l, 0) = 0$ (III.5-5a)
- $v_x(0, \pm h) = 0$ (III.5-5b)
- At $y = 0$; $\frac{\partial v_x(y,z)}{\partial y} = 0$ (III.5-5c)
- At $z = 0$; $\frac{\partial v_x(y,z)}{\partial z} = 0$ (III.5-5d)

Since the flow is unidirectional and symmetric in the z direction, the shear stress can be written as:

- $\tau_{z,x} = -\eta \frac{\partial v_x(y,z)}{\partial z}$ (III.5-6a)

Where $\tau_{z,x}$ is the shear stress representing the friction force per unit surface area applied tangentially between the fluid layers. In the absence of mechanical work provided by the system, other equations are obtained as:

- $dP = -\frac{dF}{2h\,2l}$; $dF = \tau_{z,x}\,dS$ (III.5-6b)

In our case, the shear stress on the sides is neglected because of the small thickness approximation ($h < l$).

Solving equation III.5-5 gives:

$$v_x(y,z) = \frac{a\ h^2}{\eta}\,\left[1 - \left(\frac{y}{l}\right)^2 - \left(\frac{z}{h}\right)^2\right] \qquad \text{(III.5-7)}$$

Equation III.5-7 shows that the velocity profile in a rectangular channel is elliptical, and the pressure decreases linearly in the flow direction (Equation III.5-4).

After the velocity field has been calculated at each time step, the interface position needs to be determined. For this, the analytical solution for the flow front position (x_f) under constant flow rate can be written as [114], [118]:

$$x_f = \frac{Q}{h\,l}\,t \qquad \text{(III.5-8)}$$

where t denotes the filling time and Q is the flow rate obtained from [117]:

$$Q = \int_{-l}^{l} \int_{-h}^{h} v_x(y,z)\, dz\, dy \qquad \text{(III.5-9)}$$

It is important to emphasize that for the earlier filling stages (phase 1), significant deviation between the predicted and experimental results may be found due to the imposed boundary conditions. The first inaccuracy is the imposed temperature at the mold entrance; i.e. the inlet temperature is equal to the nozzle temperature because some cooling may occur inside the injection channel [119]. Another cause of deviation may be related to neglect the extensional stresses acting on the melt moving from smaller to larger areas [119].

For this reason, the flow motion has been predicted based on equations III.5-7, III.5-8 and III.5-9 from the time it reaches the mold corners and compared with the experimental observations reported in Figure III.5-5. The results indicate very good qualitative agreement with good correlation coefficients ($r^2 > 0.99$) for the five samples. The curves (theoretical and experimental) are more curved near the centerline. However, a slight difference is observed at the front position near the walls. This deviation of the melt front shape and position at the contact point (melt–air–solid) may be related to the artificial imposition of viscosity values as they were assumed from rheological tests and also the assumption of constant wall temperature. On the other hand, the wall boundary conditions (no-slip) can also influence the position of this triple point [115]. Consequently, it can be assumed that the proposed theoretical model is successful in predicting short shots based on the experimental results. In addition, the parabolic shape of the surface velocity field during a short shot clearly shows that in regions of higher temperature, the velocity is also higher. Conversely, decreasing the temperature decreases the velocity down to zero. Thus, as the polymer melt fills a cold cavity, the velocity is minimum close to the walls due to the no-slip boundary conditions and much higher (above the average value) at the centerline [111], [116]. The front curvature at the centerline correlates with the fast fluid flow and this central region moves out towards the cavity walls producing the “fountain flow” effect (Fig. 6). Consequently, its velocity in the flow direction is decreased and a cross-flow velocity component is created [113], [115].

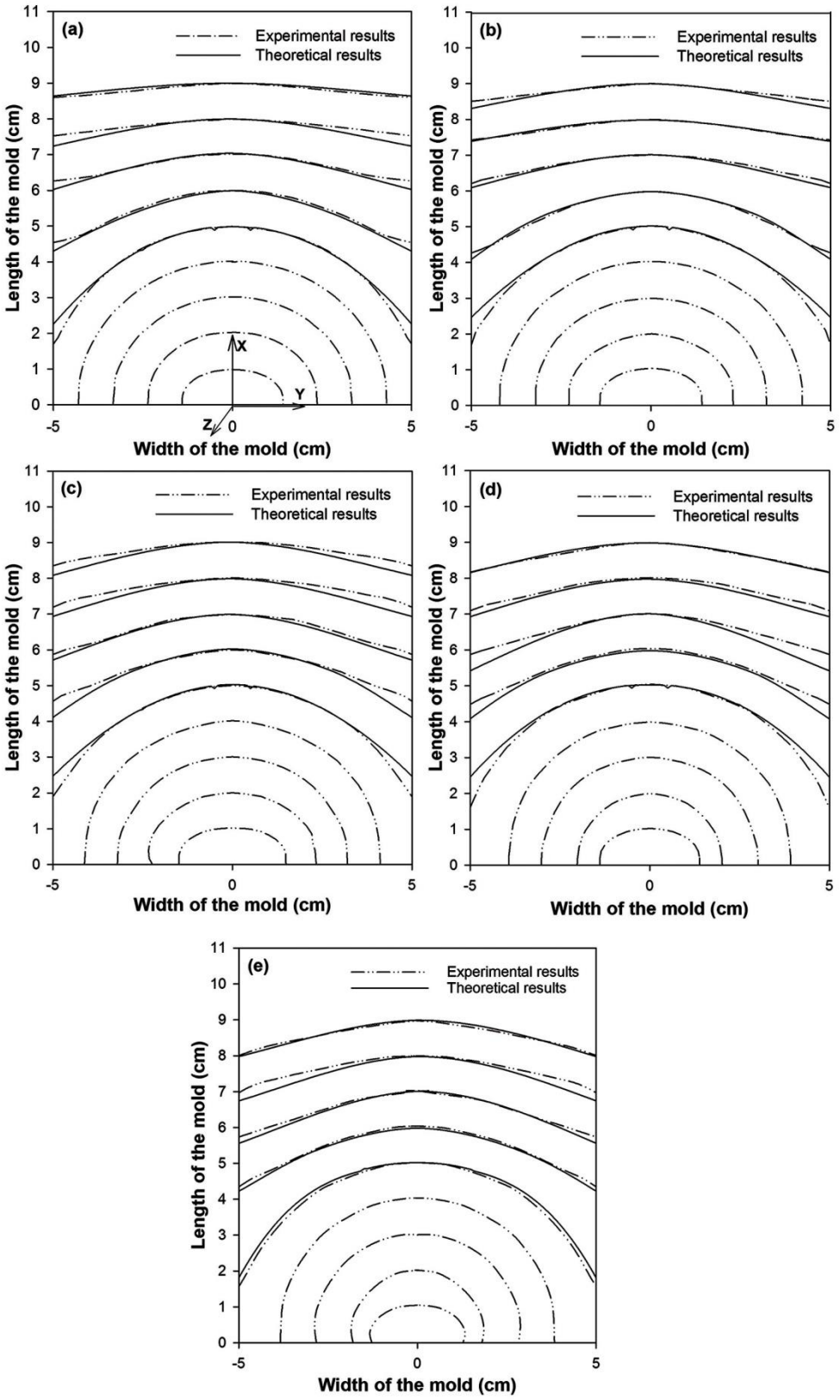

Figure III.5-5: Predicted and experimental front flow pattern at the same position for all samples: (a) PP, (b) PP/C 2.5, (c) PP/C 5, (d) PP/C 10 and (e) PP/C 15.

III.5.3. MoldFlow simulation

The simulation of the five samples (PP, PP/C 2.5, PP/C 5, PP/C 10 and PP/C 15) was carried out using the commercial software Autodesk Moldflow Insight 2019 which simulated the cavity filling phase during injection molding (Figure III.4-2). This software was used because it accounts for the necessary processing conditions during the molding processes such as temperature distribution, pressure distribution, melt velocity, flow front advancement, etc. The mold filling problem involves the solution of the conservation equations (mass, momentum and energy) governing the flow of incompressible fluids [120]:

Mass conservation (continuity):

$$\frac{\partial \rho}{\partial t} + \frac{\partial(\rho V_x)}{\partial x} + \frac{\partial(\rho V_y)}{\partial y} + \frac{\partial(\rho V_z)}{\partial z} = 0 \qquad \text{(III.5-10)}$$

Momentum conservation:

$$\rho\left(\frac{\partial V_x}{\partial t} + V_x\frac{\partial V_x}{\partial x} + V_y\frac{\partial V_x}{\partial y} + V_z\frac{\partial V_x}{\partial z}\right) = -\frac{\partial P}{\partial x} + \eta\left(\frac{\partial^2 V_x}{\partial x^2} + \frac{\partial^2 V_x}{\partial y^2} + \frac{\partial^2 V_x}{\partial z^2}\right) + \rho g_x \qquad \text{(III.5-11a)}$$

$$\rho\left(\frac{\partial V_y}{\partial t} + V_x\frac{\partial V_y}{\partial x} + V_y\frac{\partial V_y}{\partial y} + V_z\frac{\partial V_y}{\partial z}\right) = -\frac{\partial P}{\partial y} + \eta\left(\frac{\partial^2 V_y}{\partial x^2} + \frac{\partial^2 V_y}{\partial y^2} + \frac{\partial^2 V_y}{\partial z^2}\right) + \rho g_y \qquad \text{(III.5-11b)}$$

$$\rho\left(\frac{\partial V_z}{\partial t} + V_x\frac{\partial V_z}{\partial x} + V_y\frac{\partial V_z}{\partial y} + V_z\frac{\partial V_z}{\partial z}\right) = -\frac{\partial P}{\partial z} + \eta\left(\frac{\partial^2 V_z}{\partial x^2} + \frac{\partial^2 V_z}{\partial y^2} + \frac{\partial^2 V_z}{\partial z^2}\right) + \rho g_z \qquad \text{(III.5-11c)}$$

Energy conservation:

$$\left(\frac{\partial H}{\partial t} + V_x\frac{\partial H}{\partial x} + V_y\frac{\partial H}{\partial y} + V_z\frac{\partial H}{\partial z}\right) = \alpha\left(\frac{\partial^2 H}{\partial x^2} + \frac{\partial^2 H}{\partial y^2} + \frac{\partial^2 H}{\partial z^2}\right) + \eta\dot{\gamma}^2 \qquad \text{(III.5-12a)}$$

$$\dot{\gamma} = \sqrt{\left(\frac{\partial V_x}{\partial x}\right)^2 + \left(\frac{\partial V_y}{\partial y}\right)^2 + \left(\frac{\partial V_z}{\partial z}\right)^2} \qquad \text{(III.5-12b)}$$

Where x, y and z are the Cartesian coordinates, t is the time, ρ is the density, V_x, V_y and V_z are the velocities in x, y and z directions respectively, P is the pressure, g is the acceleration of gravity, Ƞ is the viscosity, α is the thermal diffusivity, H is the enthalpy and $\dot{\gamma}$ is the shear rate.

The viscosity is an important function to provide into the injection molding flow analysis. To describe the composites rheological behavior, the Cross-WLF viscosity model is used according

to equation III.5-13 [25]. This rheological model is well-known to predict the viscosities of polymer melts at different temperatures, pressures, and shear rates via:

$$\eta(\dot{\gamma}, T, P) = \frac{\eta_0(T,P)}{1+(\frac{\eta_0\dot{\gamma}}{\tau^*})^{1-n}} \quad \text{(III.5-13)}$$

Where:

- $\eta_0(T,P) = D_1 \exp\left[-\frac{A_1(T-T^*(P))}{A_2+(T-T^*(P))}\right]$, $T>T^*$ (III.5-14a)
- $\eta_0(T,P) = \infty$, $T \leq T^*$ (III.5-14b)
- $T^*(P) = D_2 + D_3 P$ (III.5-14c)
- $A_1 = A_2 + D_3 P$ (III.5-14d)

T^* and $\tau*$ are the glass transition temperature and the shear stress at the transition between the Newtonian and power-law region, respectively. η_0 is the zero-shear-rate viscosity with temperature and pressure dependent factors. D_1, D_2, D_3, A_1, A_2, n and $\tau*$ are seven material constants given by the experimental measurements of the Moldflow Software.

To start, a comparison between the experimental flow front and the one provided by Moldflow for the five samples was done by imposing the same input parameters (T_{mold}=45°C, T_{melt}=190°C) and according to the simulation an injection pressure of 50 MPa is enough for complete mold filling. As shown on figure III.5-6, the flow front progression of the experimental results and Moldflow at several representative positions are very close. It can be concluded that MoldFlow can successfully predict the flow front shape for our samples. However, a slight difference was observed near the mold wall for all the composites which is probably due to the surface tension and melt shrinkage, along with the phase change problem as these parameters may not be accounted for in the simulation [4].

This good agreement between the results enables a good understanding of the parameters affecting the flow front as well as complete mold filling. It is well known that a wrong injection temperature or pressure, low flow rate, insufficient shot volume or resin burnout may generally cause defects such as incomplete mold filling [107]. For this analysis, several simulations were carried out by changing one factor while keeping the others constant.

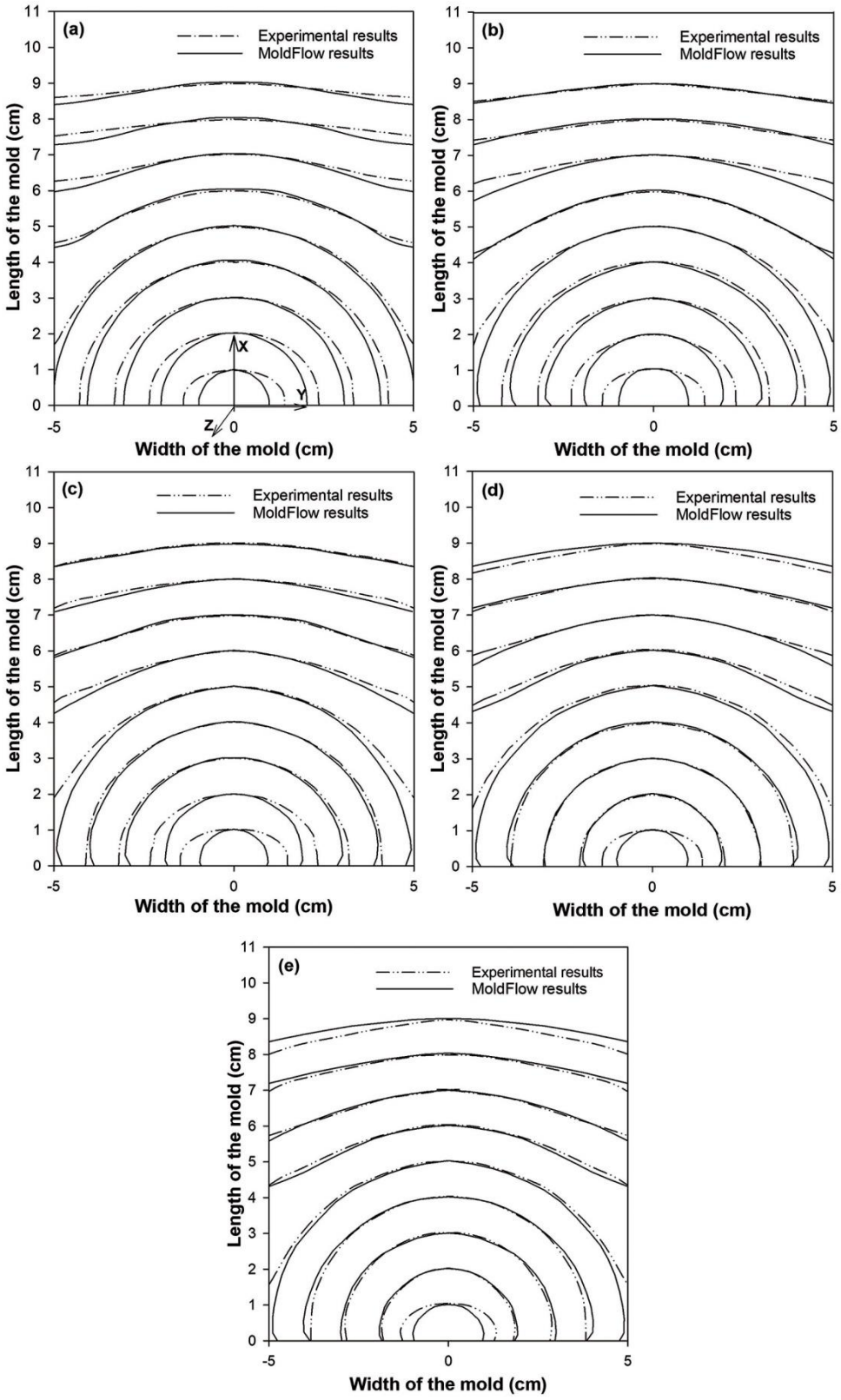

Figure III.5-6: Comparison between the experimental results and the Moldflow simulation for the flow front progression at different time: (a) PP, (b) PP/C 2.5, (c) PP/C 5, (d) PP/C 10 and (e) PP/C 15.

Figure III.5-7 and III.5-8 present the effect of injection pressure and melt temperature on the state of mold filling for the five materials. It can be seen that imposing a low injection pressure or melting temperature leads to a short shot. Figure III.5-7 shows that the filling distance increases with increasing injection pressure from 10 to 50 MPa because the injection pressure is the main driving force pushing the melt into the mold. High injection pressure allows the melt to advance rapidly to fill the mold cavity before solidifying [121]. It was also observed from figure III.5-7f that fiber addition leads to a more linear flow evolution by increasing the pressure.

On the other hand, Figure III.5-8 shows that the mold cavity cannot be completely filled when decreasing the melt temperature while keeping the mold temperature and the injection pressure unchanged. This behavior is associated to decreasing the melt temperature leading to a rapid solidification of the polymer which does not leave enough time to fill the mold cavity [120], [121].

Figure III.5-9 presents the effect of the mold temperature on the melt front progression for the five materials studied. The first series was done by keeping the same processing parameters (T_{melt} = 190°C and P_{inj} = 50 MPa) while only changing the mold temperature. It was observed that by increasing the mold temperature from 10 to 45°C, the flow front begins to advance until filling the cavity. So increasing the mold temperature decreases the cooling rate and thus slows the polymer solidification [105], [121].

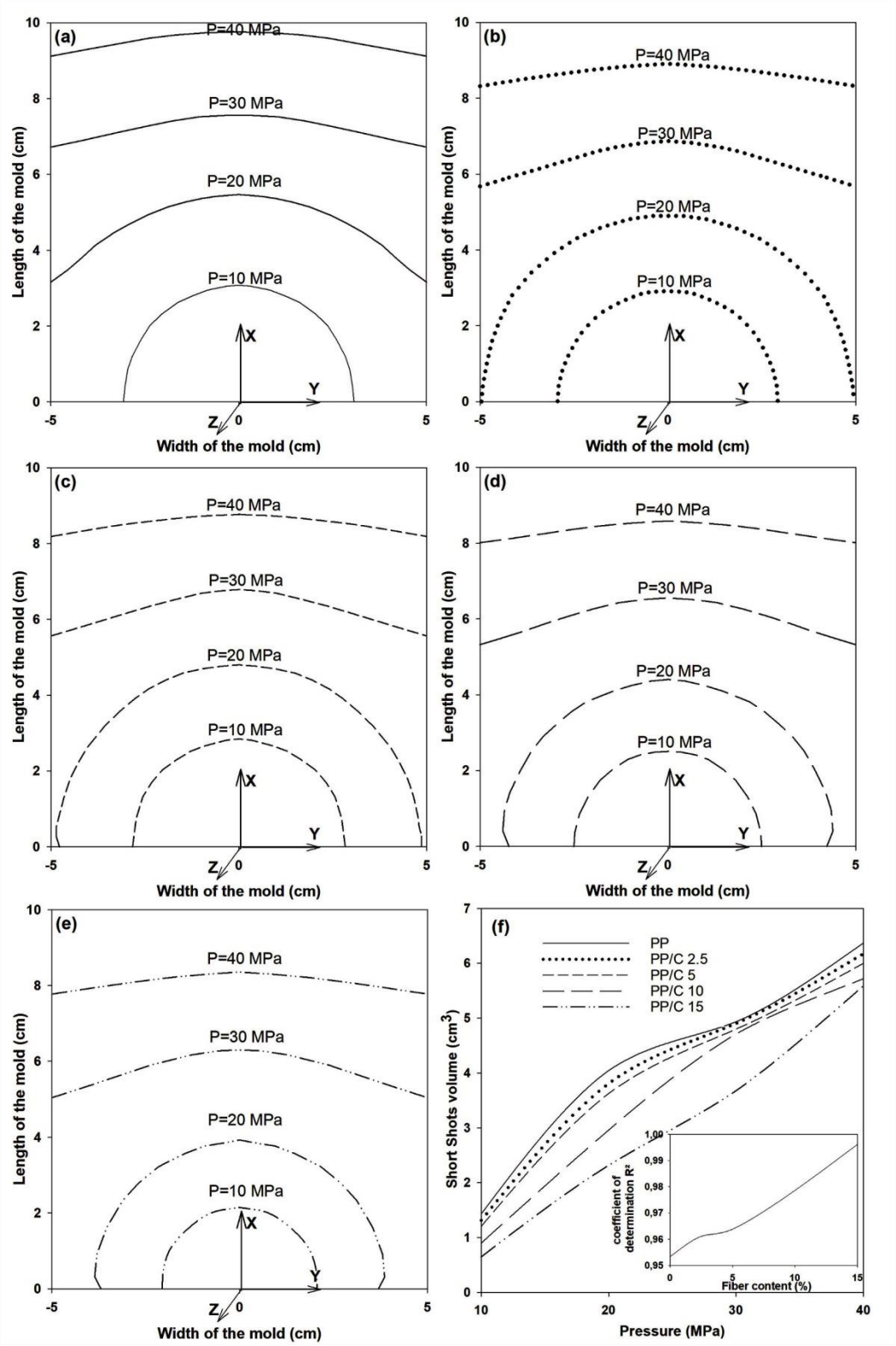

Figure III.5-7: Effect of injection pressure on the flow front progression at Tmold=45°C and Tmelt=190°C for: (a) PP, (b) PP/C 2.5, (c) PP/C 5, (d) PP/C 10 and (e) PP/C 15. (f) Short shot evolution with increasing the injection pressure.

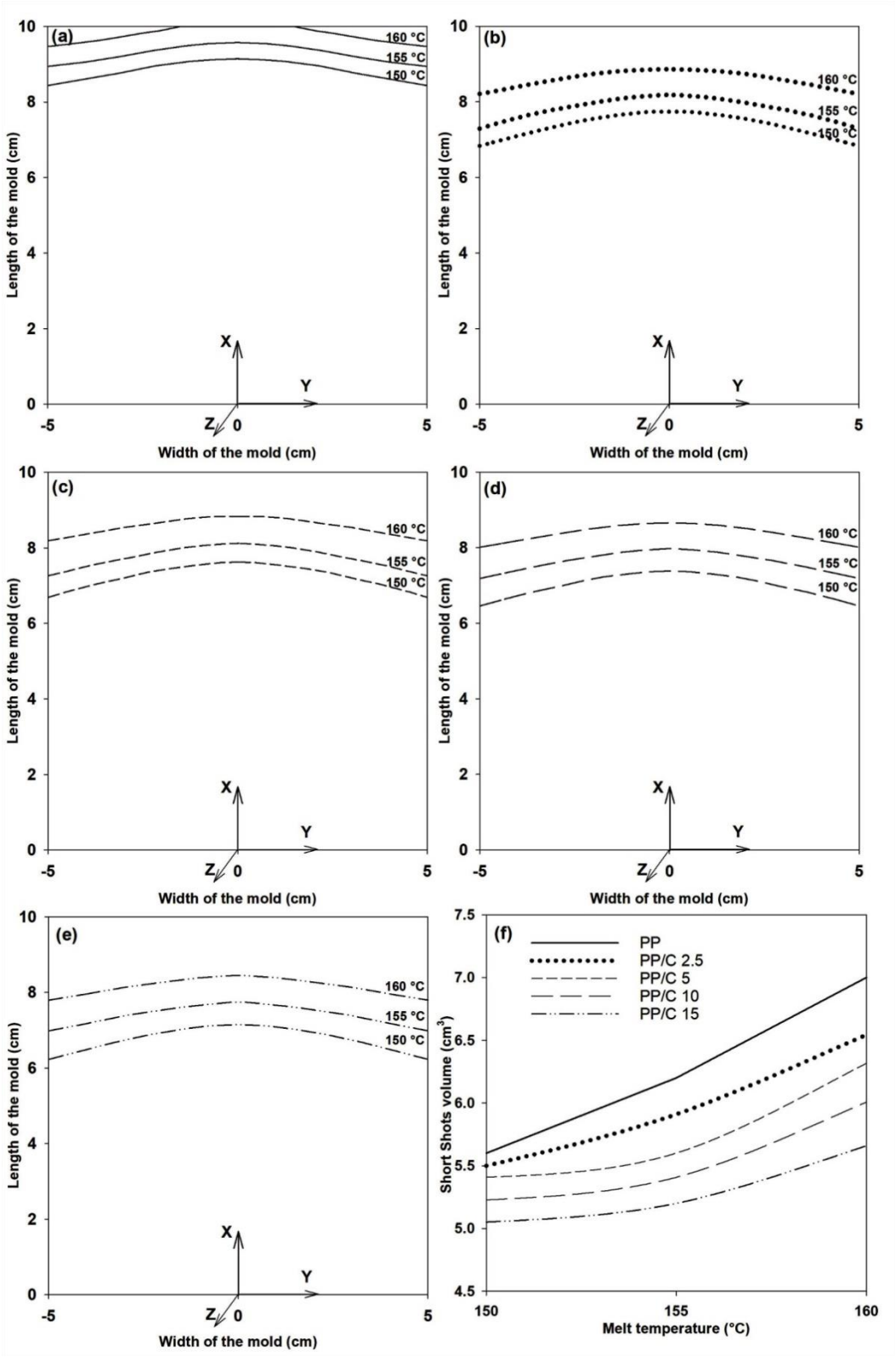

Figure III.5-8: Effect of the melt temperature on the flow front progression at Tmold = 45°C and Pinj = 50 MPa for: (a) PP, (b) PP/C 2.5, (c) PP/C 5, (d) PP/C 10 and (e) PP/C 15. (f) Short shot evolution with increasing the melt temperature.

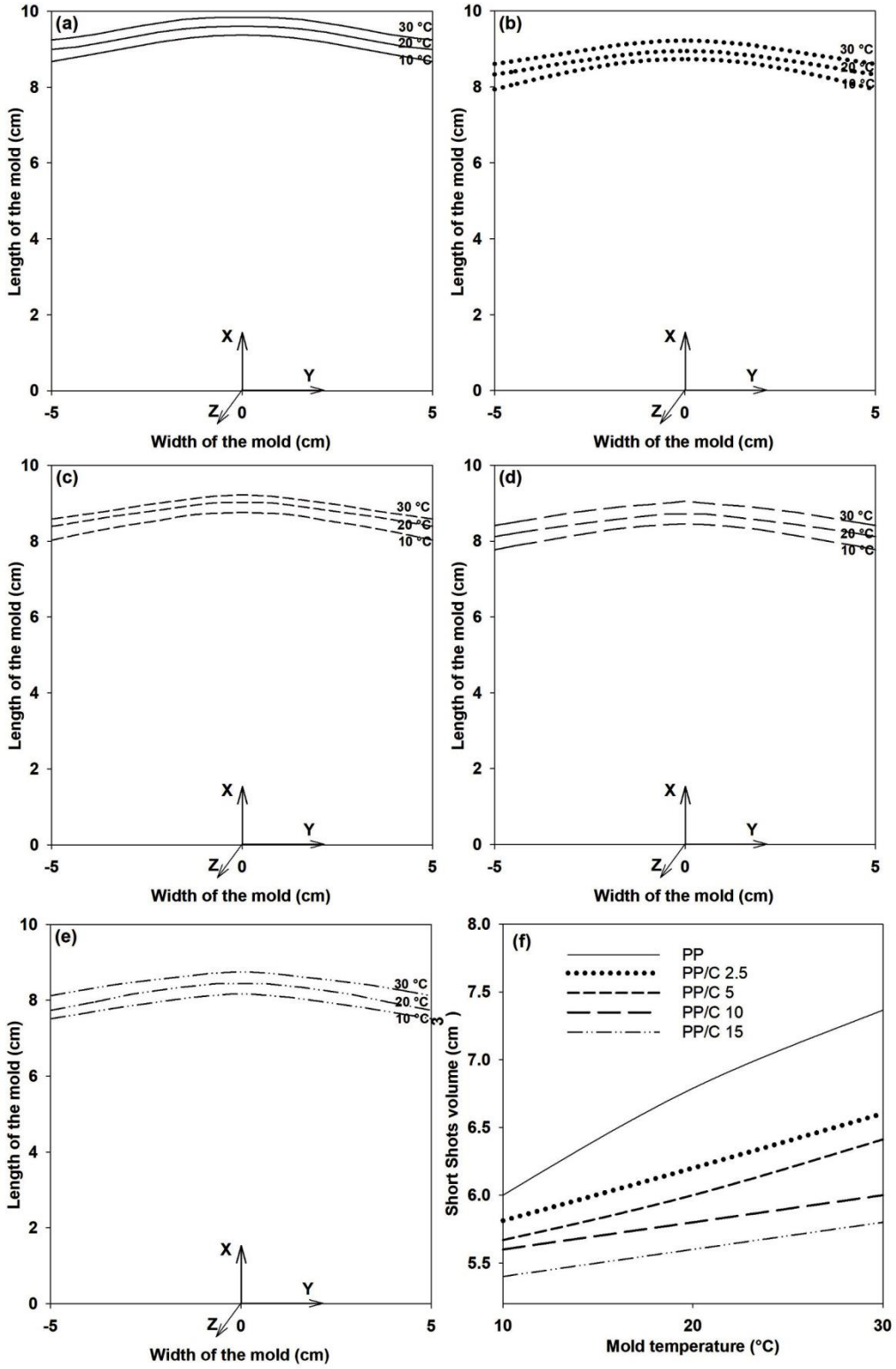

Figure III.5-9: Effect of the mold temperature on the melt front progression at Tmelt = 190°C and Pinj = 50 MPa for: (a) PP, (b) PP/C 2.5, (c) PP/C 5, (d) PP/C 10 and (e) PP/C 15. (f) Short shot evolution with increasing the mold temperature.

III.6. Conclusion

This work investigated the effect of several parameters affecting the progression of the polypropylene flow front inside a mold cavity for biocomposites produced via injection molding. In the experimental part, the effect of coir fibers (0-15 wt.%) was investigated. As expected, increasing the fiber content linearly decreased the flow front position for the low concentrations used.

In the second part, a mathematical model based on the Navier-Stokes equations was developed for the flow front shape and position. The simple model proposed was found to be in good agreement with experimental observations to predict short shots.

Finally, the effect of injection pressure, as well as melt and mold temperature were studied using numerical simulations performed via the Moldflow software. As expected, the filling position was found to increase by increasing all these parameters, but to different extent related to fiber concentration.

Based on these results, more work needs to be done to include fiber-fiber interactions, especially when working at higher fiber concentrations.

Chapter IV. Injection molding of short fiber thermoplastic bio-composites: Prediction of the fiber orientation

F. Semlali Aouragh Hassani *et al.*, "Injection molding of short fiber thermoplastic bio-composites: Prediction of the fiber orientation" *J. Compos. Mater.*, vol. 54, no. 30, pp. 1–11, 2020.

IV.1. Abstract

Injection molding of short fiber reinforced thermoplastic polymer results in a preferential fiber orientation in the part, which leads to an anisotropy in the material mechanical properties. To anticipate the molded part performances, it is necessary to predict the fiber orientation pattern. Our goal is to have a practical tool that accurately predicts fiber orientation patterns, and to use that information to estimate the final product properties. Consequently, an efficient way to determine the flow induced fiber orientation for different flow cases under real injection molding conditions is presented. The proposed approach allows the average orientation angle prediction in a section by considering the close interaction between the fibers and the flow rheology, the fibers aspect ratio and the mold geometry. Finally, to validate the model, experimental data were taken with different matrices, fibers and mold geometries, where good agreements ($R^2 \geq 0.8$) were obtained for the fiber orientations measurements. At the end of this chapter the predicted fiber orientation were introduced to the self-consistent approach developed in chapter 2 in order to deduce the whole material mechanical performance before design.

IV.2. Résumé

Le moulage par injection de polymère thermoplastique renforcé de fibres courtes se traduit par une orientation préférentielle des fibres dans la pièce, ce qui conduit à une anisotropie des propriétés mécaniques du matériau. Afin d'anticiper les performances des pièces moulées, il est nécessaire de prédire l'orientation des fibres dans la matrice polymérique. L'objectif est d'avoir un outil pratique qui prédit avec précision l'orientation des fibres afin d'utiliser ces informations pour estimer les propriétés finales du produit. Par conséquent, un moyen efficace de détermination de l'orientation des fibres induites par l'écoulement pour différents cas d'écoulement dans des conditions de moulage par injection réelles a été présenté. L'approche proposée permet la prédiction de l'angle d'orientation moyen dans une section, en considérant l'interaction étroite entre les fibres et la rhéologie de l'écoulement, le rapport d'aspect des fibres et la géométrie du moule. Enfin, pour valider le modèle, des données expérimentales ont été prises avec différentes matrices, fibres et géométries de moule, où de bons accords ($R^2 \geq 0.8$) ont été obtenus pour les mesures d'orientations des fibres. À la fin de ce chapitre, l'orientation prédite des fibres a été introduite dans l'approche auto-cohérente développée au chapitre 2 afin de déduire les performances mécaniques du matériau entier avant la conception.

IV.3. Introduction

Injection molding is one of the most widely used polymer processing methods. This is especially the case for thermoplastics reinforced with short natural fibers, due to its ability to produce net-shaped materials with high dimensional stability in a relatively short cycle time [63], [84]. For these bio-composites, the overall performances (high strength-to-weight ratio, high stiffness, and possibility to control anisotropy) are important, but a successful composite design requires a good estimation of the produced part properties before production [63], [84].

The final product mechanical properties depend strongly on the process itself, the filled polymer rheological properties and the fibers orientation. During injection molding, flow of a fiber suspension results in a preferential short fibers orientation. Typically, fibers tend to align perpendicular to the flow near the mid-plane of the part, but in flow direction near the mold wall. The short fibers are then frozen into the matrix, and this anisotropic flow-induced fiber orientation becomes a key feature of the finished product anisotropic performance [2]. However, it is very difficult to predict the fiber orientation state during the molding process because the physical mechanisms that orient the fibers are not yet fully understood [10], [122]. For example, the flow of fiber filled thermoplastics in the molten state is modified by the presence of fibers while the fiber motion and rotation is affected by the flow. So a close interaction between them exists and must be investigated via the materials rheological properties [10]. Also, changing the mold geometry and fiber aspect ratio play a major role in the final fiber orientation distribution. It is thus mandatory to get good fiber orientation prediction from the system kinematics in the mold; i.e. processing conditions and materials properties.

The first work studying the fiber motion dates from 1922 where Jeffery relate the rotation rate of a rigid ellipsoidal particle immersed in a Newtonian fluid by solving the equations of motion for dilute suspensions (no fiber-fiber interaction) [75]. His study enabled to compute the fiber orientation evolution by decoupling it from the flow field which can lead to some important deviations. What prompted several researchers to use his model to generate general constitutive equations for the fiber orientation prediction. Okawaga, et al. [123], Mason and Manley and Goldsmith and Mason have extensively studied the classical Jeffery's equations for a number of flow configurations and for several particle shapes. In addition to analytical studies, they have performed various experimental investigations on the important parameters influencing the

rotations of ellipsoids and stresses on particles [123]–[125]. Later, Givler et al. [49] integrate Jeffery's orientation equations along the streamlines obtained on the basis of the finite element method, to develop a numerical scheme for the fiber orientation state determination in dilute suspensions. They present numerical solutions of the fiber orientation state for the simple shear flow, the fountain flow and the flow in an infinite expansion. Folgar and Tucker [50] add a diffusion term to the Jeffery's equations in order to account for fiber-fiber interactions and thus developing a model for the fiber orientation prediction of concentrated suspensions. After that, Rosenberg et al. [126] addressed a coupling solution between the flow field and fiber orientation in the case of a dilute suspension and short fiber only. Their studies show that, coupling orientation and flow are problems are very difficult to solve [127]. However according to Pontes et al. [60], no complete theory is available to predict the fiber orientation distribution resulting from the injection molding process [2], [60].

The aim of this work is to present an efficient way to predict the anisotropic distribution of the flow induced fibers orientation under real injection molding conditions, using the classical Jeffery's equation. The first section reviews the theory describing the fiber orientation states and provides evidence concerning the factors influencing the fiber orientation during the injection molding process. It is clearly understood that decoupling the fiber orientation function from the flow field relies on a number of strong hypotheses that may invalidate the procedure in practical applications. So, in the following section, a model for the fiber orientation prediction that couples a nonisothermal mold filling flow and fiber orientation in arbitrary plane flow is presented. The proposed approach allows the prediction of the average orientation angle in a section as a function of the filled polymer rheological properties, the fibers aspect ratio and the mold cavity geometry. Finally, another application of this model was investigated to study the effectiveness of our approach using another polymer and fibers in more complex mold geometries. To complete the injection molding study, the developed fiber orientation values are introduced to the self-consistent approach developed in chapter 2 in order to deduce the material mechanical properties before design. Very qualitative agreements were obtained when comparing the experimental and the theoretical results with a correlation factor higher than 0.9.

IV.4. Materials and methods

IV.4.1. Materials

The polymers used in this study were polypropylene (PP) PPH03BPM (TASNEE, Saudi Arabia) and high density polyethylene (HDPE) (extrusion grade HD F0455). The PP was supplied by Exxon Mobil with a density of 0.903 g/cm^3 and a melting temperature of 165°C, while the HDPE was purchased from SODEVIC (Morocco), with a density of 0.959 g/cm^3 and a melting temperature of 135°C. As reinforcements, coir (Co) and cactus (Ca) fibers were used. The coir fibers (Co), with an average density of 1.548 g/cm^3 and an initial length between 150-200 mm were obtained from coconut shells extracted from Ivory Coast. They were firstly carefully washed with tap water, air-dried for 24 h, grinded with a 4 mm sieve opening using a Pulverisette-19 (Fritsch GmbH, Germany), then sieved using a 200 µm opening to get rid of fine particles. On the other hand, the cactus fibers (Ca) with an average density of 1.625 g/cm^3 were extracted from *Opuntia ficus indica* rackets (300-350 mm length, ≈200 mm wide and ≈20 mm thick) collected from the region of Essaouira (Morocco). These rackets were washed with tap water while removing their spines, air dried, chopped into pieces to be grinded with a 2 mm sieve and finally sieved using a 200 µm opening to get rid of fine particles.

IV.4.2. Samples preparation

The samples prepared were PP, PP/Co 2.5, HDPE and HDPE/Ca 2.5, where 2.5 represents the fiber content (wt.%). The Extrusion was done on a Leistritz ZSE-18 twin-screw extruder (LEISTRITZ EXTRUSIONSTECHNIK GmbH, Germany) at a screw speed of 125 rpm. The temperature profile was set to 200, 200, 200, 200, 190, 190, 190 and 190°C from the feed hopper to the die. The extrudates were immediately quenched in water and cooled in air to be manually cut into pieces (average length of 15 mm) to limit fiber length degradation.

Injection molding was performed in rectangular (100x100x1 mm^3) and circular molds (diameter of 25 mm) for the PP composites, as well as in a rounded rectangle mold with four different widths (15×50×1; 10×50×1; 5×50×1 and 3×50×1 mm^3) and two injection points for the HDPE composites. The mold geometry consists of two congruent semicircles and two parallel segments, generally called an oval (Figure IV.4-1). The injection process was done using an Engel e-Victory machine (ENGEL GmbH, Austria) according to the following molding conditions: a flow

rate of 80 cm^3/s, a maximum injection pressure of 24 MPa and a filling time of 4 s. The temperature was set at 200°C for the first three heating zones, while the nozzle temperature was set at 190°C for the PP composites and 200°C for the HDPE composites with a mold temperature of 45°C.

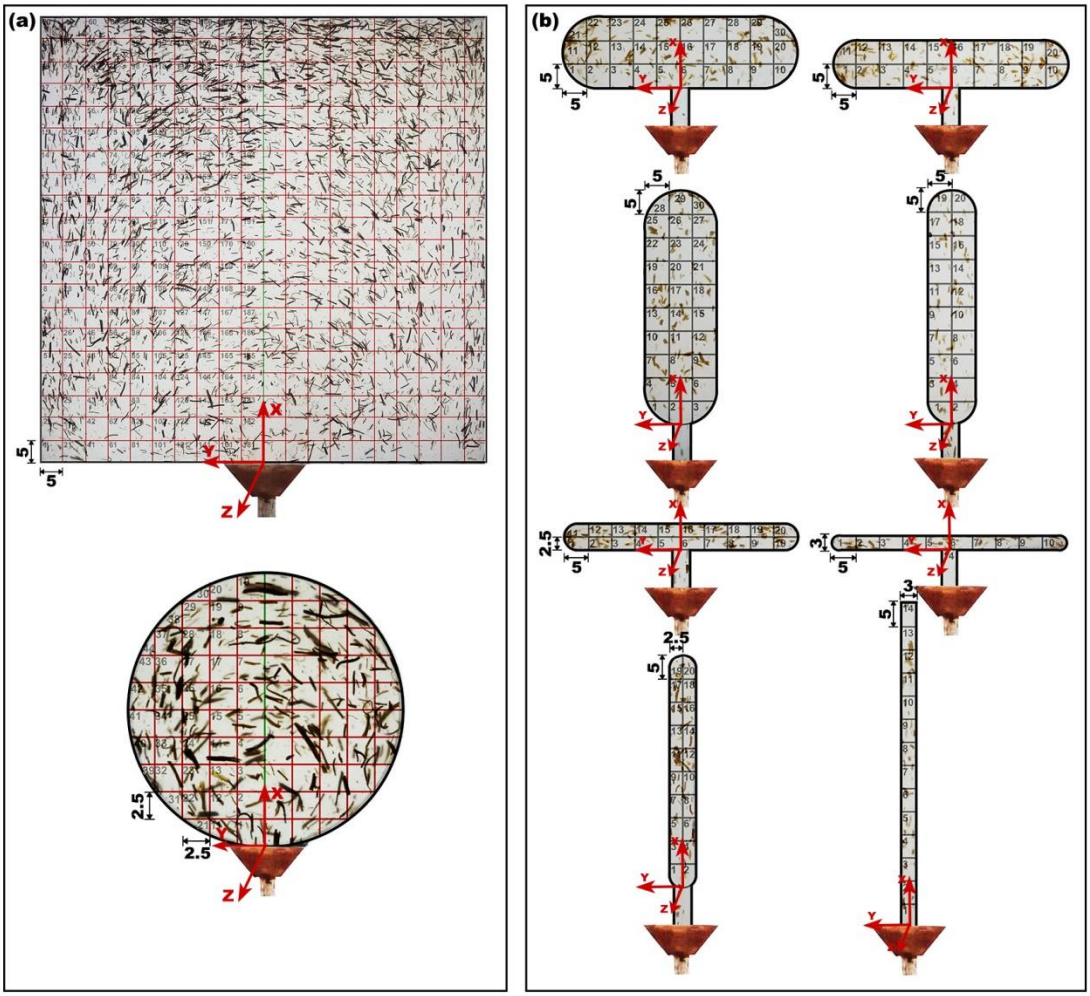

Figure IV.4-1: Typical examples for the mesh configuration used and the parts dimensions (in mm) for the fiber orientation measurements. (a) PP/Co 2.5 and (b) HDPE/Ca 2.5 composites.

IV.4.3. Fiber orientation measurement

For the fiber orientation measurements, pictures of the molded composites PP/Co 2.5 and HDPE/Ca 2.5 were taken using a white LED backlight illuminator equipped with a digital camera (Nikon D5300, Japan). The selected samples were meshed as finely as possible depending on the mold shape as shown in figure IV.4-1. Then, the orientation angle as well as the length of a minimum 3 fibers by mesh was measured using the ImageJ software (National Institutes of

Health, USA), and the average was represented in each section (Figure IV.5-1). Since extrusion and injection process are known to mechanically degrade the fibers length, the obtained average lengths are 2.25 mm and 2.00 mm for the coir and cactus fibers, respectively (Figure IV.4-2a',b'). On the other hand, the fiber diameters were evaluated using optical microscopy (Nikon Eclipse LV100ND, Japan) by taking an average of 50 fibers as a representing values to give values of 290 µm and 465 µm for the coir and cactus fibers, respectively (Figure IV.4-2a,b). For the coir fiber dimensions, the results are similar as obtained from our previous work [5]. For the measurements, it was assume that the fiber has the same orientation through thickness due to the thin mold cavity thickness (1mm). The x-axis denotes the injection direction where x = L is the mold length, while the y and z axes refer to the mold width (y = 2l) and height (z = 2h), respectively.

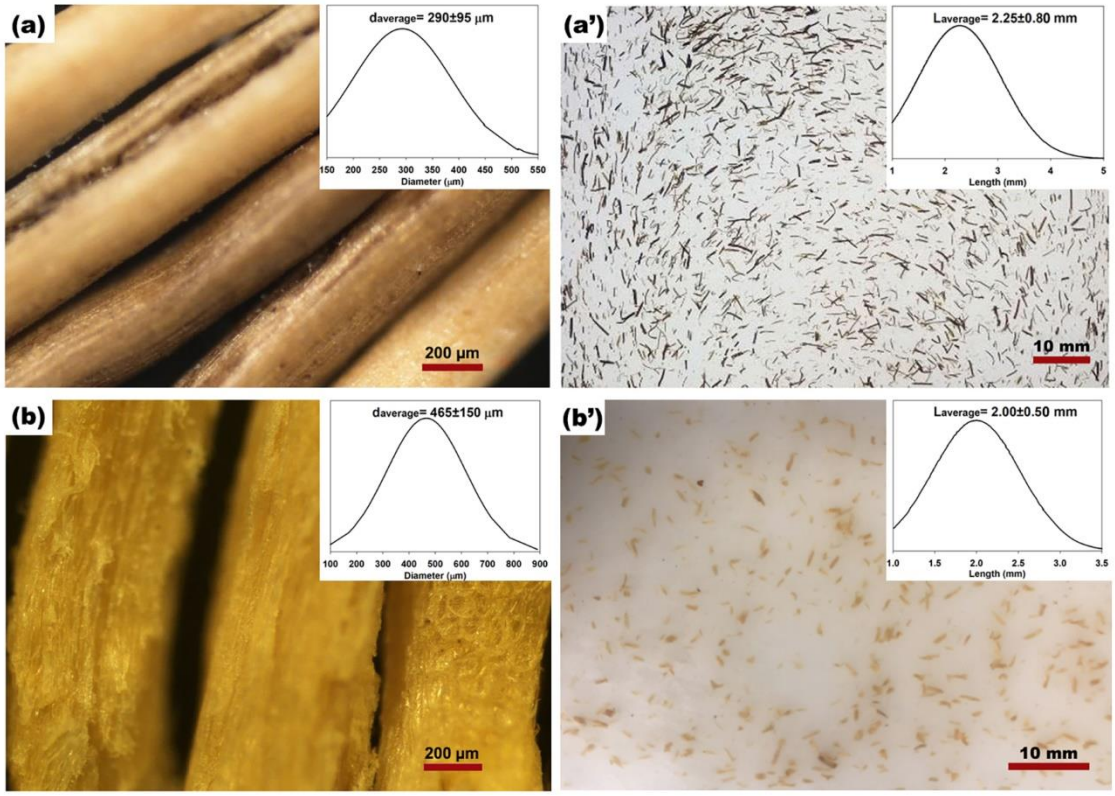

Figure IV.4-2: Fiber diameter and length distribution for: (a,a') PP/Co 2.5 and (b,b') HDPE/Ca 2.5 composites.

IV.4.4. Rheological characterization

To characterize the rheological properties in the melt state, small amplitude oscillatory tests were performed on a MCR 500 (Physica, Germany) rheometer equipped with a CTD600 device. The

measurements were carried out using a 25 mm parallel plate geometry with 1 mm thick samples between 190ºC and 200°C (injection temperature) using frequency sweeps between 100 and 0.1 Hz at a strain of 5% (linear viscoelastic regime was confirmed via previous strain sweeps).

IV.5. Results and discussion

IV.5.1. Experimental Investigations

The goal of this experimental investigation is to provide evidence concerning the dynamic processes controlling the fiber orientation inside dilute suspensions. Thus, the obtained average fiber orientation states of the PP/Co 2.5 composite injected in rectangular and circular molds are analyzed (Figure IV.5-1). It can be seen that for a thin-walled cavity (1 mm), the fibers tend to adopt a specific planar orientation throughout the whole thickness [26]. For a rectangular mold (Figure IV.5-1a), once the melt comes in contact with the cold mold surfaces, a frozen layer is immediately formed along the mold walls leading the converging flow to flow-align fibers, while the diverging flow in the central zone tend to align the fibers perpendicularly [2], [26]. On the other hand, the stretching (diverging) flow is highly significant near the gate in a circular mold (Figure IV.5-1b). Consequently, this shearing/stretching nature of the flow tend to align the fibers transversely near the mid-plane and along the circumferential direction close to the mold surfaces [63], [128].

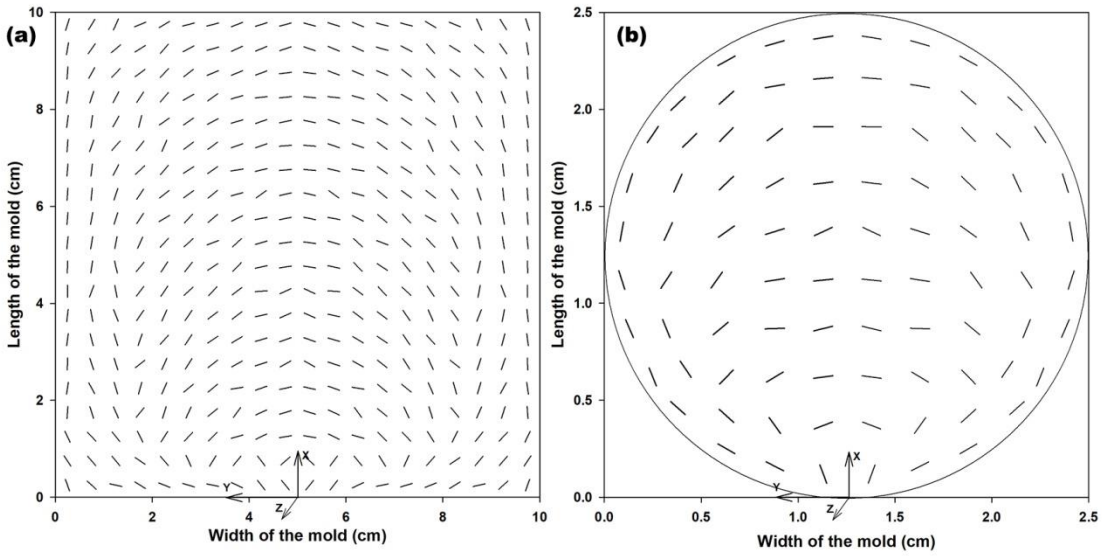

Figure IV.5-1: Average orientation state of the PP/Co 2.5 composite: (a) rectangular mold and (b) circular mold.

Independent of the mold geometry and the fibers aspect ratio (β = L/D), several other factors related to the injection molding process governed the fiber orientation, such as the materials rheological properties and the flow field conditions [26].

The rheological properties of fiber reinforced polymer melts still remains challenging as the presence of fibers modifies the flow of fiber filled thermoplastics in the molten state while the flow affect the fiber motion and rotation [10]. Since the melt temperature decreases once the material reaches the cold cavity, it was assumed that the melt temperature is approximately equal to 190 °C in the center and to 185 °C at the mold surface. Thus the first step was to study the effect of the temperature on the melt viscosity at the two temperatures (185 and 190°C). From figure IV.5-2a it can be clearly seen that for both temperatures, the viscosity decreases with increasing frequency which is an indication of the materials non-Newtonian pseudo-plastic behavior [5]. While, the increase of the viscosity with the fibers addition can be explained by the fibers rigid structure and the strong hydrogen interactions formed between the matrix and the reinforcement [5]. Also, from figure IV.5-2a, it was observed that viscosity decreases with increasing the temperature from 185 to 190°C, especially at low frequency while the effect is less important at higher values. So, the interactions between the viscosity, melt temperature, flow field and fiber orientation is studied in our case by plotting the viscosity at crescent frequency on a representative PP/Co 2.5 flow front curve, according to the temperature along a normalized mold width (190°C in the center zone and to 185°C at the mold surface), and the results are taken from our previous work [5] and reported in figure IV.5-2b.

Generally, in the case of rectangular mold, the melt begin to advance in a radial shape until reaching the mold corner. Then, the front distorts into a parabolic shape with a pronounced degree of curvature at the centerline, which decreases as the flow front progresses to become almost flat until filling the mold [5]. This flow behavior is can be explain by the decrease in temperature when the material enters the cold cavity leading to a higher local viscosity close to the mold walls. Indeed, once reaching the mold surface, a frozen layer forms rapidly which brings the melt in the central region to flow more rapidly due to its lower viscosity, thus resulting in the pronounced curvature of the flow front centerline [5]. Also from figure IV.5-2b, it can be seen that the viscosity of the PP/Co 2.5 tends to be constant along the mold width as shear rate increases. Thus, the fibers orientation depends on the flow rate. At higher shear rates most of the shearing flow takes place near the mold wall leading the fibers to be strongly aligned along the

wall. While, in the central region, the material is relatively unsheared and no fiber-fiber contact occur, so the flow field coupled with the lower viscosity induces a perpendicular fiber alignment, thus forming a parabolic fiber orientation state [5], [35], [129]. To conclude, high shear rate (frequency) is more favorable for injection molding [5].

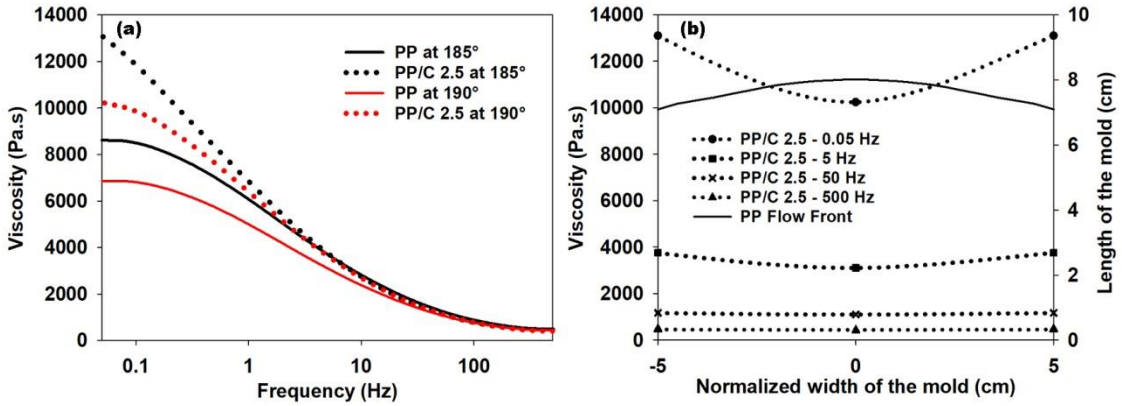

Figure IV.5-2: (a) Viscosity of the samples. (b) Variation of the viscosity as a function of the normalized mold width for the PP/Co 2.5 composite.

The fiber aspect ratio (β = L/D) is known to play a major role on fiber orientation, due to the sensitivity of the core thickness to the fiber length [26]. Hence, increasing the fiber aspect ratio leads to an increase in the core thickness defined by a transversal fiber orientation. Consequently, more the fibers are long, more they tend to adopt a planar orientation because their length prevents them from rotating freely [26]. Also, changing the mold geometry by varying the mold thickness or width also strongly affects the fiber orientation. In fact, decreasing the cavity thickness decreases the core zone until it disappears, thus resulting in nearly the same planar orientation throughout the thickness. On the other hand, decreasing the mold width leads to flow-align fibers across the whole thickness, whatever the position taken along the mold [26], [62].

IV.5.2. Mathematical Model

Modeling the injection process requires general constitutive equations to represent the materials behavior for each flow case. For thermoplastic composites reinforced with short fibers, the fiber orientation distribution is related to the angle between each fiber and the flow direction with respect to physical, mechanical and rheological properties. It is well known that the fiber orientation during the injection molding filling stage is determined principally by the flow field, the fiber aspect ratio and the mold geometry as reported in the experimental section.

An accurate description of the flow induced fiber orientation represents an important challenge because of the necessity to account for fiber-fiber, fiber-fluid, and fiber-boundary interactions [130], [131]. Thus, the first work studying the fiber motion dates from 1922 where Jeffery established the equation for the orientation evolution of a single ellipsoidal particle [75]. However, the fluid streamlines in this investigation were computed by assuming that the presence of fibers do not change the stress field; i.e. the flow field was limited to dilute suspensions (non-interacting systems) in a Newtonian suspending fluid [75]. To model the flow of injection molded composites, Jeffery decoupled the fiber orientation evolution from the flow field. Consequently, the fiber orientation field is not influenced by the material rheological properties or the flowing dynamics, which can lead to important deviations. There are two fundamental problems with these assumptions. Firstly, the orientation distribution function measurement is possible only by repeated calculation for different initial configurations. Secondly, the assumption that the presence of the fibers do not affect the streamlines is important even at very low fiber concentrations [130], [131].

Here, we propose a way to predict the fiber motion and rotation by considering the close interaction between the fiber orientation and the flow field. Our formulation involves using the classical Jeffery's equation to generate more general and accurate 2D constitutive equations for the flow induced fiber orientation prediction.

Let's first start by describing the flow field during injection molding. For a three-dimensional (3D) study of a viscous flow in a rectangular channel, the Navier-Stokes equation must be solved. But under some simplifying assumptions, a single Poisson equation is obtained and solved to estimate the flow velocity profile as [5]:

$$v_x(y,z) = \frac{a\ h^2}{\eta}\left[1 - \left(\frac{y}{l}\right)^2 - \left(\frac{z}{h}\right)^2\right] \qquad \text{(IV.5-1)}$$

Where, η is the dynamic viscosity determined from experimental measurements (Figure IV.5-2) and α is the pressure gradient ($a = -\frac{\partial P}{\partial x}$). The parameters h and l are the mold height and width, respectively.

The simplifying assumptions used are:

- Incompressible flow: $div\ \vec{v} = \vec{0}$
- Steady flow: $\frac{\partial \vec{v}}{\partial t} = \vec{0}$
- Laminar flow : $(\vec{v}.\vec{\nabla})\vec{v} = \vec{0}$
- External volume forces are neglected with respect to the viscous force: $\vec{f}_{v\ ext} = \vec{0}$
- Pressure on the flow front: $P_{front} = P_{atmosphere}$
- Pressure at the gate: $P = P_{inj}$
- Non-isothermal flow with an imposed temperature at the mold entrance.
- Symmetry with respect to the geometry median plane.
- Flow along the x axis: $\vec{v} = \overrightarrow{v_x}(y, z)$

Our main concern in this work is the prediction of the flow induced fiber orientation in an arbitrary plane flow where the velocity components depend solely upon the plane coordinates x and y. So equation IV.5-1 is simplified to give:

$$v_x(y) = \frac{a\ h^2}{\eta}\ [1 - \left(\frac{y}{l}\right)^2] \qquad \text{(IV.5-2)}$$

On the other hand, Jeffery's model is only valid for a single ellipsoidal particle suspended in a Newtonian fluid where no fiber-wall and fiber-fiber interactions exist [75]. The model description shows that the fiber orientation evolution depends on the fiber aspect ratio (with D, the largest fiber section diameter), leading it to be based on two parameters: the fiber length L and the orientation vector P as illustrated in figure IV.5-3 [75]. Jeffery's theory takes into account others important assumptions: 1) the fibers length and diameter are uniform; 2) the number of fibers per unit volume is uniform; 3) the axis of revolution lies in the x-y plane; 4) no-slip conditions prevail at the interface between the fiber and the Newtonian fluid; 5) the velocity field is only locally perturbed by the fiber motion; 6) the state of the fiber orientation is symmetrical with respect to the x axis. Under these assumptions, the fiber motion may be predicted through the solution of [75]:

$$\dot{P} = -\frac{1}{2}(\omega\ P) + \frac{1}{2}\ \lambda(\dot{\gamma}\ P - \frac{\dot{\gamma}}{P\ P\ P}) \qquad \text{(IV.5-3)}$$

where P is the fiber orientation vector defined as P = (sinθ cosΦ, sinθ sinΦ, cosΦ) [75]; ω is the vorticity tensor with $\omega_{ij} = \frac{\partial v_j}{\partial x_i} - \frac{\partial v_i}{\partial x_j}$; $\dot{\gamma}$ is the shear rate defined as $\dot{\gamma} = \frac{\partial v_x(y)}{\partial y}$; and λ is a scalar related to the aspect ratio as:

$$\lambda = \frac{\beta^2 - 1}{\beta^2 + 1}. \quad \text{(IV.5-4)}$$

Since the fiber axis of symmetry remains in the flow plane, its orientation is fully characterized by the angle between its axis of symmetry and the x-axis called Φ (Figure IV.5-3). The fiber center of gravity moves with the local Newtonian fluid velocity.

It is well known that the injection molding filling flow is, by its nature, non-isothermal and non-Newtonian with a moving boundary (the flow front). Here, the flow motion equation (Equation IV.5-2) coupled with the fiber motion model of Jeffery (Equation IV.5-3) gives rise to a more general and concise fiber orientation description where the flow field effect is considered. Finally, the orientation angles Φ are governed by a differential equation in the form of [49], [132]:

$$\Phi = -tan^{-1}\left[\frac{1}{\beta}\, tan^{-1}\left(\frac{dv_x(y)/dy}{\beta + 1/\beta}\, t - \, tan^{-1}\left(\beta\, tan\Phi_0\right)\right)\right] \quad \text{(IV.5-5)}$$

Consequently, rewriting equation IV.5-5 using equation IV.5-2 gives (Equation IV.5-6):

$$\Phi = -tan^{-1}\left[\frac{1}{\beta}\, tan^{-1}\left(-\frac{2\, a\, h^2}{\eta}\, \frac{y/l^2}{\beta + 1/\beta}\, t - \, tan^{-1}\left(\beta\, tan\Phi_0\right)\right)\right] \quad \text{(IV.5-6)}$$

Where, Φ_0 is the initial orientation condition taken at t = 0. In our case, in the central zone where the fibers are nearly aligned transverse to the flow direction, Φ_0 is taken as 0 while near the mold wall a value of π/2 is used because of the shear induced orientation leading to flow-align fibers.

According to equation IV.5-6, the optimum average state of fiber orientation is calculated at each section for the PP/Co 2.5 composite injected into a rectangular mold, and is superimposed on the experimental results for a well comparison (Figure IV.5-4). The results indicate very good qualitative agreement with good transverse and longitudinal correlation coefficients ($0.83 \leq R^2 \leq 1$), thus obtaining an average total correlation coefficient of $R^2 = 0.96$. The first observation is

that closer to the walls or to the center line, higher correlation coefficients are obtained. Near the walls, the converging flow tends to strongly flow-align the fibers, while in the central zone the diverging flow tend to align perpendicular the fibers, thus giving a radial fiber orientation pattern through the width [2], [26]. It is expected that imposing $\Phi_0 = 0$ at the center line and $\Phi_0 = \pi/2$ at the mold wall will give precise results comparing to other positions. The slight differences observed between the experimental values and the predictions at some positions are firstly due to the initial imposed fiber orientation Φ_0. Then, probably due to imposing viscosity values which are obtained from the rheological tests, to the assumption of constant wall temperature (185°C), and also to a non-uniform fiber aspect ratio and number of fibers per unit volume [5]. With this is mind, the original derivation of most fiber orientation theories assumes a homogeneous deformation field and/or orientation field, while in real processing situations, it is not common for either the flow field nor the fiber orientation field to be uniform [125]. Globally, it can be said that the proposed approach can successfully predict the flow induced fiber orientation by considering the close interaction between the fiber orientation and the flow field for injection molding of thin geometries.

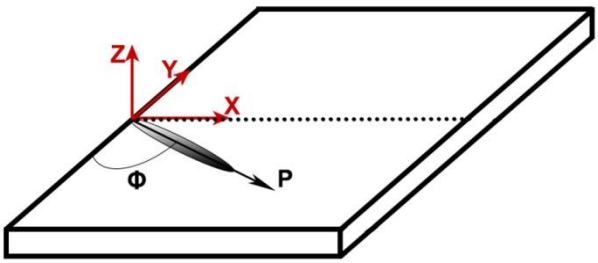

Figure IV.5-3: Definition of the fiber orientation vector.

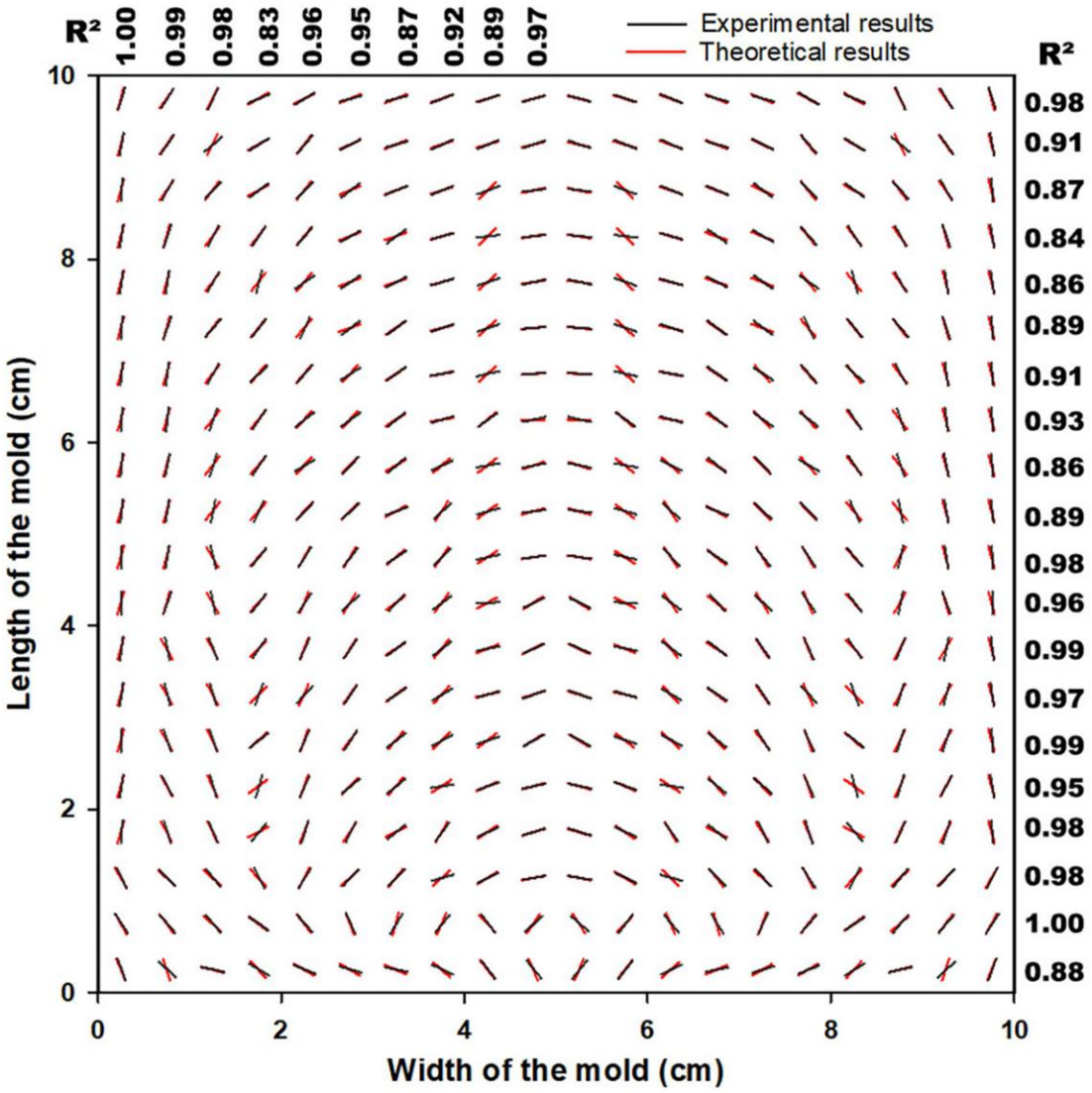

Figure IV.5-4: Experimental and predicted fiber orientation for the PP/Co 2.5 composite injected in the rectangular mold.

IV.5.3. Application

From the discussion presented above, a number of important questions related to the effectiveness of our model can be made and must be addressed by our experimental investigation. (1) Is our model also accurate in the case of more complex geometries? (2) Does the gate position has an effect on the correlation factor (R^2)? (3) Does the matrix and the fiber nature (aspect ratio) have an effect on the model accuracy? (4) Are the boundary conditions still valid?

To address these questions, an application of our model using another polymer and fibers in more complex mold geometries is presented. So a second mold was selected consisting of a rounded

rectangle plate of uniform thickness with a planar geometry. As seen in figure IV.5-5, four different combinations of cavity width (15×50×1; 10×50×1; 5×50×1 and 3×50×1 mm^3) and gate position were examined. To determine how the matrix rheological properties and the fiber aspect ratio (β=4.3 for the cactus fiber compared to 7.75 for the coir fiber) can affect orientation, the fiber orientation state of the samples with HDPE reinforced with cactus fibers at 2.5 wt.% is investigated.

Before analyzing the fiber orientation state for the rounded rectangular molds, it is important to study the flow front advancement. To establish accurate observation, pictures of the HDPE short shots were digitalized using the Plot Digitizer software (ver. 2.6.6.0), then superimposed with the fiber orientation state (Figure IV.5-5) to get a complete profile. It is important to emphasize that adding low fiber content (2.5 wt.%) does not significantly affect the flow front advancement and behavior [5]

From the fiber orientation state as a function of the flow front advancement (Figure IV.5-5), it can be seen for all the molds with a transverse gate position (Figure IV.5-5a,b,c and d) that the melt begins to progress in a radial pattern until reaching the mold length. Then the front distorts into a pronounced curved line parallel to the radial flow to be distorted again into a pronounced curved line in the opposite direction as the melt reaches the rounded part of the mold. The significant extensional flow component along the mold width leads to a strong transverse fiber orientation following the shape of the flow front advancement, while near the mold surfaces shearing tend to align the fibers along the circumferential direction. On the other hand, decreasing the length from 15 to 3 mm leads to the flow only advancing into a pronounced curved line, thus pushing all the fibers to be aligned transversely to the flow direction along the width. Conversely, for the longitudinal gate position (Figure IV.5-5a',b',c' and d'), the front starts advancing following a parabolic shape with a pronounced degree of curvature at the centerline, but this curvature decreases as the flow front progresses. This is probably due to the rounded shape of the mold side. The shearing/stretching flow components in this case results in a significant transverse orientation near a point gate and to a flow alignment for the other fibers. Decreasing the width causes a high orientation in the flow direction. For both cases (transverse and longitudinal gate position), decreasing the mold width or length substantially increases

shearing due to the fiber-wall interactions, thus leading to fast fiber reorientation along the wall direction [62].

For our model application, the fiber orientation state was predicted for the eight composites using equation IV.5-6 and some assumptions. As the melt temperature decreases once reaching the mold surface, the temperature in the middle is assumed to be the injection temperature (200°C) while decreasing near the mold wall to 195°C. For this reason, the rheological properties were studied at both temperatures as shown in figure IV.5-6. The first observation is the drop in the viscosity with increasing frequency which is an indication of a non-Newtonian pseudo-plastic behavior [5], [35]. Then, addition of 2.5 wt.% of cactus fiber increases the material viscosity due to their rigid structure and strong hydrogen interactions (higher number of interacting chains) as the fibers begin to form a network [5], [35]. Finally, it was assumed that the fiber orientation along the semi-circles of the rounded rectangular molds is considered to be tangent to the circumferential direction. From the observation made on the fiber orientation state for the rounded molds (Figure IV.5-5) and the disk (Figure IV.5-1), it can be concluded that the fibers tend to adopt an orientation along the circumferential direction independently of the matrix and fiber used.

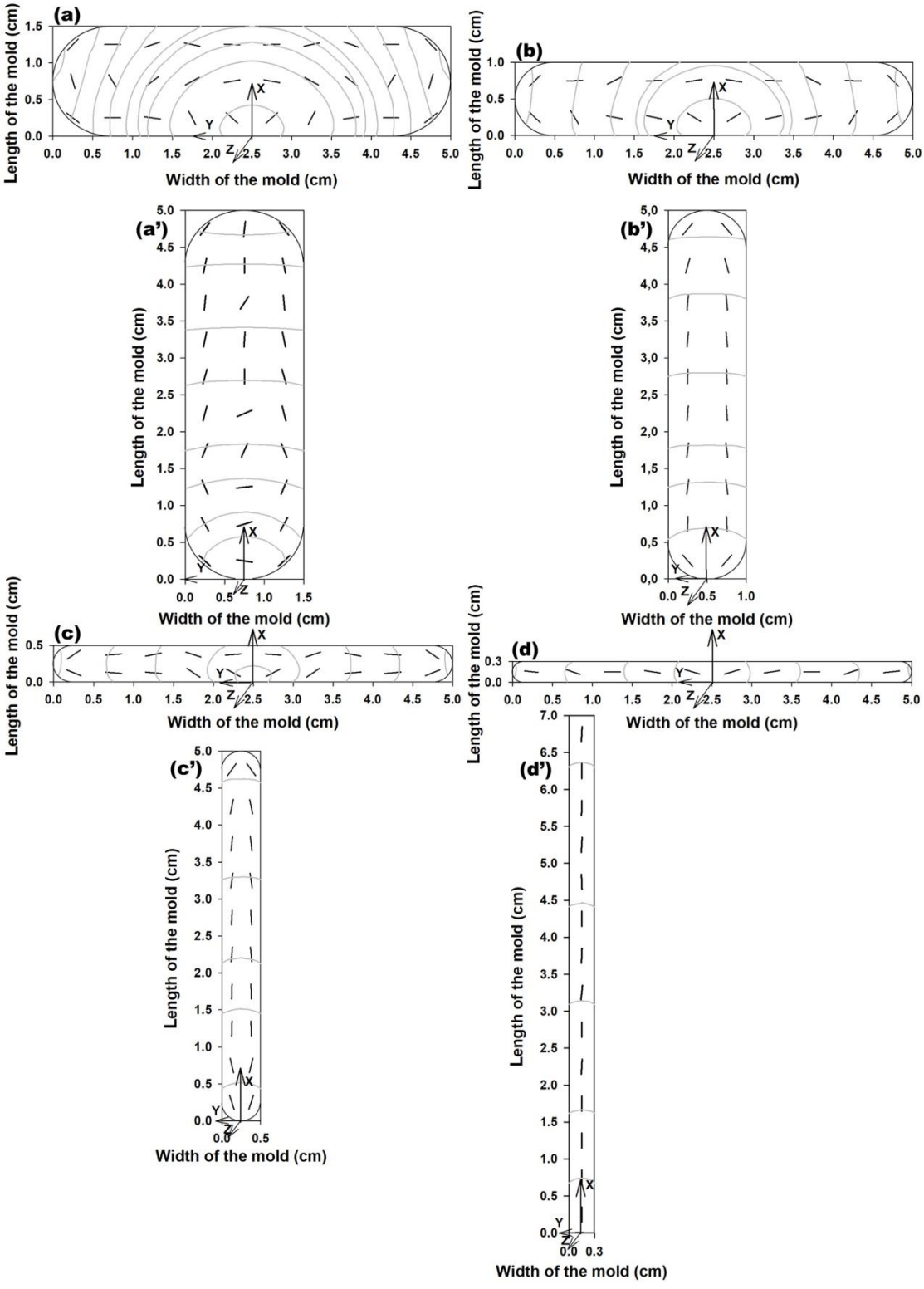

Figure IV.5-5: Average orientations state as a function of the flow front advancement for the HDPE/Ca 2.5 composite: (a, b, c and d) transverse gate position and (a', b', c' and d') longitudinal gate position.

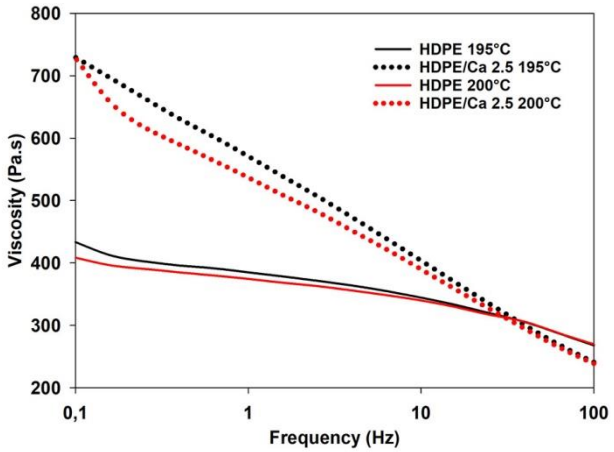

Figure IV.5-6: Viscosity curve for the HDPE and HDPE/Ca 2.5 composite at 195°C and 200°C.

So the fiber orientation from the model was superimposed on the experimental ones for the HDPE/Ca 2.5 composites in figure IV.5-7 and IV.5-8. A very good qualitative correlation was found for the eight composites ($R^2 \geq 0.73$). However, it can be seen that for molds with a longitudinal gate position (figure IV.5-7), better agreement is obtained with higher correlation factors $0.9 \leq R^2 \leq 1$ compared to $0.73 \leq R^2 \leq 0.91$ for the molds with a transverse gate position (figure IV.5-8). The reason for this difference is associated to the presence of an extensional flow along the centerline. For a similar deformation rate, the fibers in dilute suspensions have substantially higher extensional stresses than fibers in shear, thus leading to a major flow rearrangement. It is therefore clear that the theoretical model based on several assumptions (see Mathematical section) does not take into account several parameters such as surface tension and melt shrinkage, in addition of the combined effect of extensional and shear gradients. All these factors are more important in the case of extensional flow, which generally leads to error predictions [5], [130]. Globally, it can be said for all the molds that the small differences observed between the theoretical and experimental results are also due to the discussion reported in the mathematical section. To conclude, it can be said that our model can be very efficient to predict the fiber orientation, whatever the matrix, fiber and mold shape.

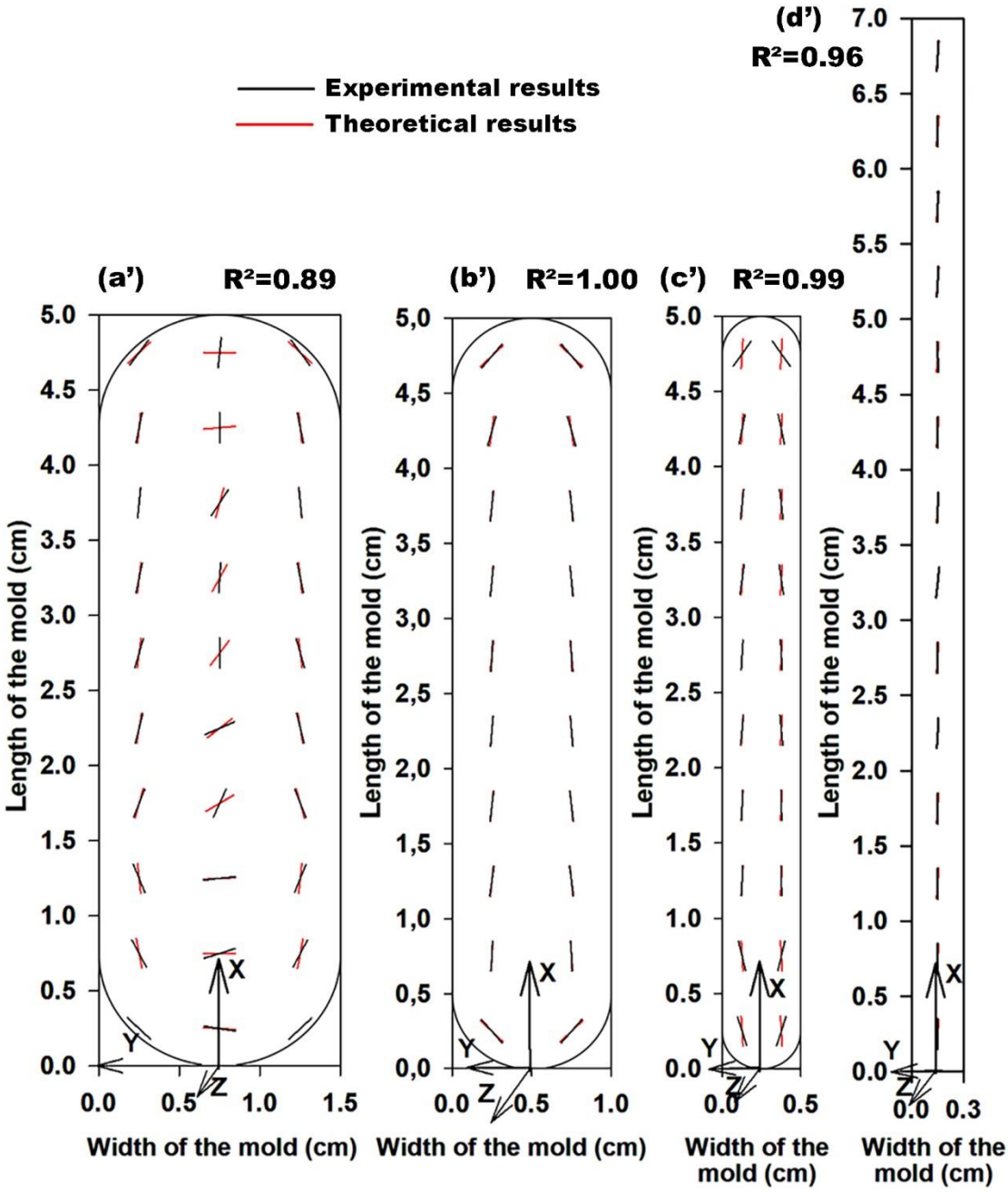

Figure IV.5-7: Experimental and predicted fiber orientation for the HDPE/Ca 2.5 composite injected in the rounded rectangular molds for the longitudinal gate position.

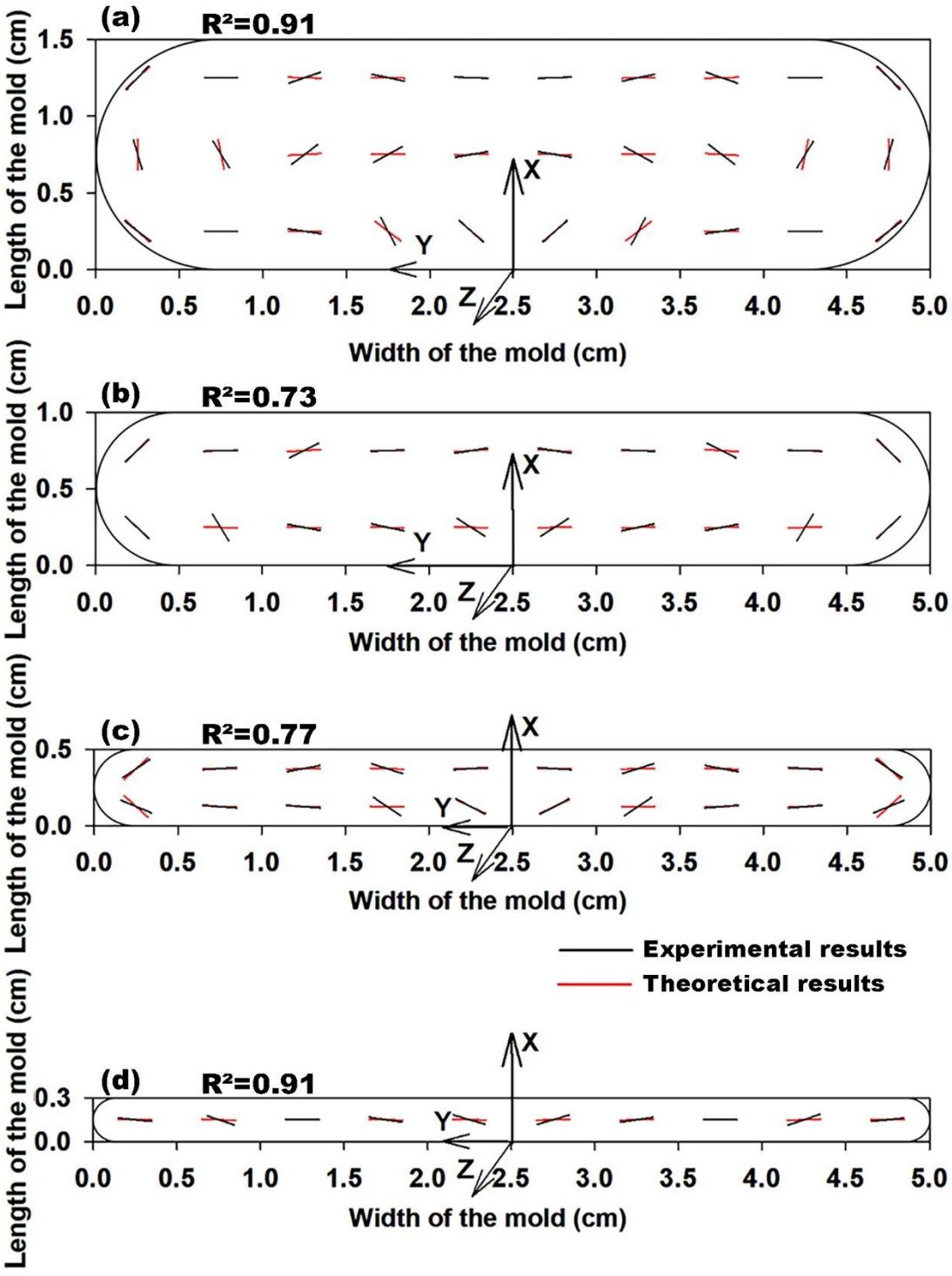

Figure IV.5-8: Experimental and predicted fiber orientation for the HDPE/Ca 2.5 composite injected in the rounded rectangular molds for the transversal gate position.

IV.6. Deduction of the whole material mechanical properties

In the chapters II, III and IV, three models aiming at the mechanical properties prediction of thermoplastic composites reinforced with short fibers before design were proposed. They are mainly intended for the prediction of the young modulus, tensile strength and torsion modulus. In order to provide physically admissible responses, it is important, even necessary; to identify the material parameters in which these constitutive laws depend, such as the properties of the matrix, fibers as well as the materials rheological behavior. With this in mind, a number of simple experiments are often used, which can activate these parameters such as the measurements of the fibers aspect ratio and the composites viscosity. Then, we look for a set of parameters which allow the models to reproduce the experimental results with a fairly good precision.

In this section, the whole material mechanical properties will be predicted by combining the three developed models: self-consisting approach, model for the flow characterization and model to predict the fiber orientation. Indeed, the predicted flow-induced fibers orientations were introduced in the developed self-consistent approach. Then, the obtained theoretical results will be validated with the experimental ones obtained in chapter II.

The choice was made on thermoplastic composites based on polypropylene reinforced with different short coir fiber content (2.5, 5 and 10 wt.%) injected in square molds cavity (100x100x1 mm^3). As mentioned before, it was assumed that the three composites have the same fiber orientations state. So, the first step of this investigation was to consider nine predicted orientation families as illustrated in figure IV.6-1. Then, the nine families were incorporate iteratively in the developed self-consistent approach according to their volume fraction in the matrix to deduce the young modulus, tensile strength and torsion modulus.

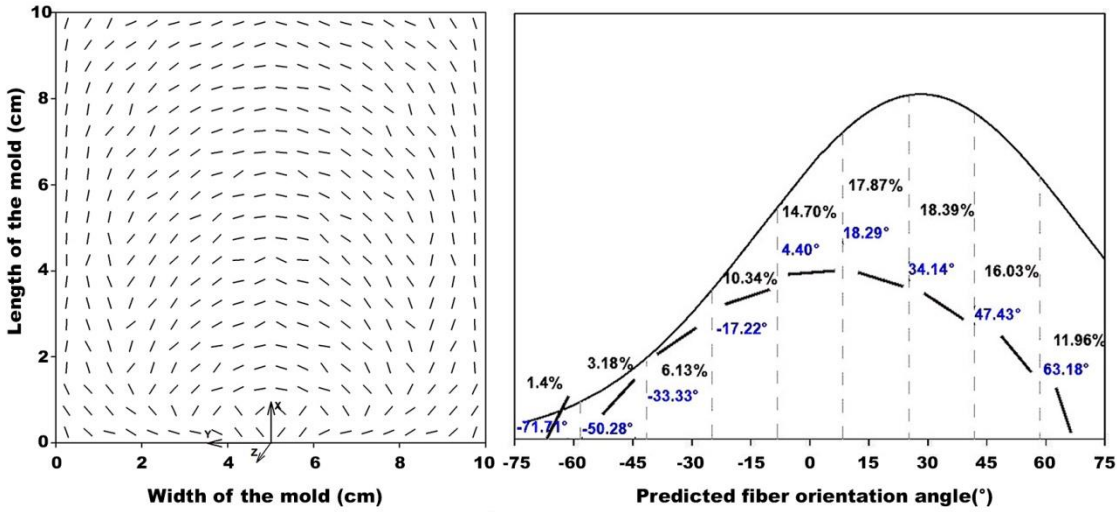

Figure IV.6-1: Predicted fiber orientation families distribution.

Figure IV.6-2 compares the experimental and predicted elastic modulus and tensile strength of the PP/coir fibers bio-composites. Overall, it was observed that our approach produced great predictions for the Young's modulus for all the composites, with a maximum deviation of 4% for PP reinforced with 10 wt.% of coir fibers. This small discrepancy is mainly due to the considered predicted fibers angles and the assumption of uniform length and aspect ratio [2], [133]. In practice, the alignment is quite good, but there is a significant distribution in length and aspect ratio produced during processing [133]. However, our model overestimates the tensile strength from a deviation of 6.21% to 27% for PP reinforced with 2.5 and 10% coir fiber content, respectively. This discrepancy is still acceptable due to the considered hypothesis. On one hand, the assumption of either uniform stress (Reuss) or uniform strain (Voigt) is an oversimplification [2]. On the other hand, no account has been taken for the stress transfer that occurs through the ends of the fibers [133]. In our case, short fibers were chosen as reinforcement for a thermoplastic matrix meaning that the stress transfer mostly depends on fiber orientation and concentration. It was also seen in all the models that at low fiber content, the predicted tensile strength is close to the experimental one, but higher deviations are observed as fiber concentration increases. This can be attributed to good fiber dispersion and distribution in the polymer matrix at low concentration, but as fiber content increases their wettability by the matrix may be more limited leading to some agglomeration [2]. This effect is also not included in our calculations.

Finally, figure IV.6-3 presents the experimental and the theoretical torsion modulus at three different frequencies (0.1, 1 and 10 Hz) for PP/coir fibers bio-composites. It was observed that the deviation increases with increasing frequency. This probably means that other factors than orientation plays a major role in the torsion behavior. It can have said that with increasing frequency, apart from the degree of orientation, simultaneous morphology and molecular mobility changes occur, both of which affect the torsion properties [2]. A second, significant source of discrepancies is due to the assumption of perfect adhesion. Poor adhesion is a particular problem in composites with hydrophilic natural fibers and hydrophobic polymer matrices, and the resultant slip at the interface will reduce the average stress in the fibers [133]. The developed model assumes perfect adhesion, and this assumption is generally acceptable for modeling the modulus at very low stresses [133].

To conclude, our results indicate that the proposed approach can be considered useful for the material mechanical properties estimation, with an acceptable deviation. While to improve the good agreement with the experimental results, we need more accurate experimental data. However, the approach adopted here is to use simple models that are capable of capturing the main experimental trends without undue complexity

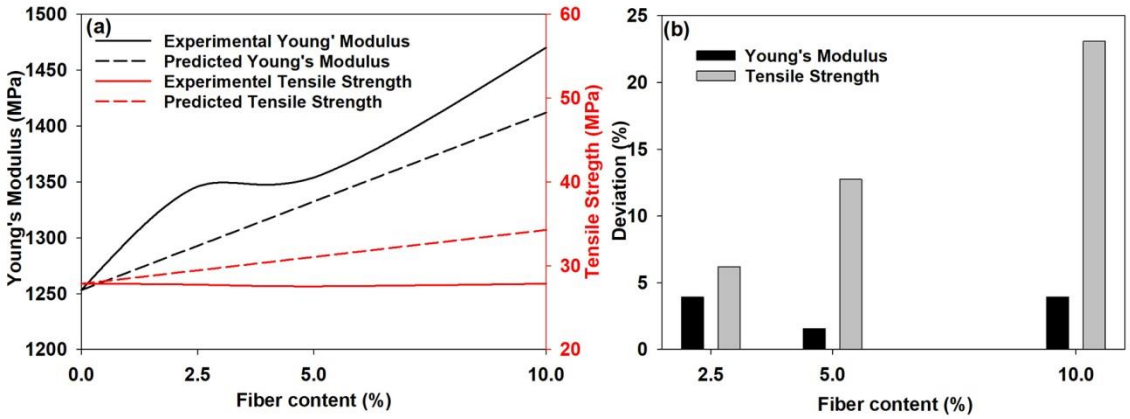

Figure IV.6-2: Comparison between the predicted and experimental Young's modulus and Tensile strength.

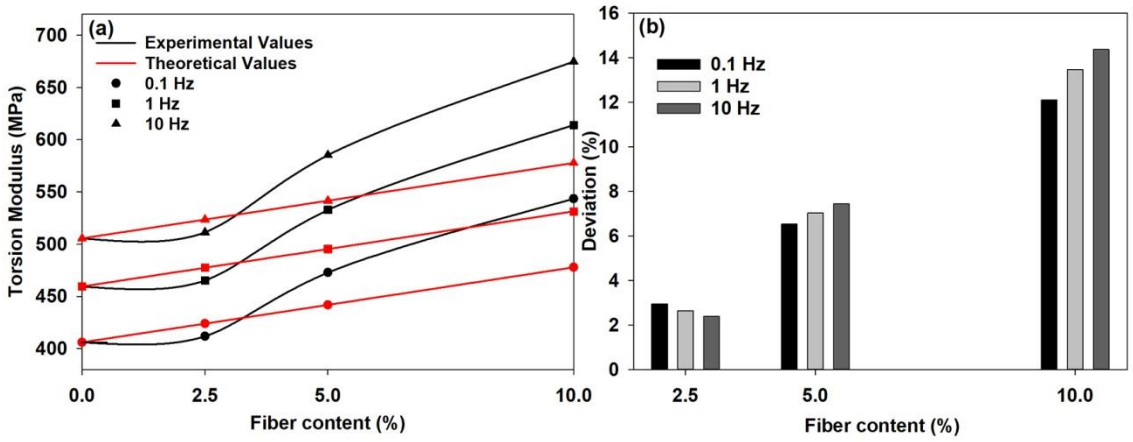

Figure IV.6-3: Comparison between the predicted and experimental Torsion modulus.

IV.7. Conclusion

A successful design requires a good estimation of the product performance before production. Considering that the final products properties are strongly affected by the fiber orientation during injection molding, several studies were done to predict the material mechanical properties where the fiber orientation are well known. Although Jeffery was the first to relate the rotation rate of a rigid ellipsoidal particle immersed in a Newtonian fluid, his investigation assumed that the fiber orientation evolution was decoupled from the flow field which can lead to important prediction errors. In this work, we proposed a theoretical approach which considers the close interaction between the flow field and the fiber orientation by using the classical Jeffery's equation. For an arbitrary plane flow where the velocity components depend solely on the plane coordinates, our model was validated with experimental results taken from a square thin-walled mold using short coir fiber reinforced polypropylene. Then, to evaluate its efficiency, the effect of rheological properties, mold geometry and fiber aspect ratio on the flow induced fiber orientation was examined using high density polyethylene reinforced with cactus fibers (2.5 wt.%). At the end of this part, the developed model was introduce in the self-consistent approach developed in the first chapter in order to deduce the whole material mechanical properties in terms of young's modulus, tensile strength and torsion modulus. To conclude, the results obtained by combining the three models were in good agreement with the experimental results.

GLOBAL CONCLUSION

As mechanical properties of short fiber reinforced thermoplastic injected components depend on flow induced fiber orientation, there is considerable interest in validating and improving models which link the flow field and fiber orientations to mechanical properties. So the ultimate goal of this thesis project was to firstly develop a model for material mechanical properties prediction using a knowing state of fiber orientation, followed by the development of a model for the flow field characterization during the injection molding process and at the end a model for the fiber orientation prediction. Combining the three models will allow a complete injection molding study by deducing the whole material mechanical performance prediction before design. To achieve these objectives:

- A self-consistent approach was developed to predict the composite properties while considering the effect of reinforcement content (2.5, 5, and 10 wt%) and a knowing state of fibers orientation. Thus, a modified Hirsch model was proposed by taking the empirical parameter (x) to depend on the fiber orientation factor (a). The new model was found to give better overall predictions of the experimental data compared with the original Hirsch and Tsai-Pagano models.
- A three-dimensional model was developed for the non-isothermal and non-Newtonian mold filling prediction. Thus, the incompressible Navier–Stokes equations are simplified into a single Poisson equation, and then solved to estimate the flow velocity, which under a constant flow rate allows the flow front shape and position prediction for the composites. The effect of fiber concentration (2.5, 5, 10, and 15 wt%), temperature, viscosity and shear rate on the flow front progression of polymer are also investigated. The results indicate very good qualitative agreement with good correlation coefficients (R^2 >0.99) for the five samples. Finally, to provide a better understanding of the effect of different processing conditions (pressure, melt, and mold temperature) on the flow front evolution; several simulations were performed using Autodesk Moldflow Insight. As expected, the filling position was found to increase by increasing all these parameters but to different extent related to fiber concentration.
- A quantitative model was developed for the flow induced fiber orientation prediction. Indeed, combining the flow field equation developed previously, with the fiber orientation equation established by Jeffery, it is feasible to begin addressing the area of mold design, the ultimate goal of this thesis. The resulted equation relates the fiber orientation angle to

the flow field, the fiber aspect ratio and the mold shape. Finally, to validate the model, experimental data were taken with different matrices, fibers and mold geometries, where good agreements (R^2 >0.8) were obtained for the fiber orientations measurements.

– At the end, a model combining the three developed equations is addressed and validated with the experimental results. Effectively, the predicted fibers orientation angles were introduced in the first equation (self-consistent approach) to deduce the material mechanical performance. Very qualitative agreements were found with a correlation factor better than 0.9.

REFERENCES

[1] M. M. Kabir, H. Wang, T. Aravinthan, F. Cardona, and K.-T. Lau, "Effects of Natural Fibre Surface on Composite Properties : a Review," *Energy, Environ. Sustain.*, pp. 94–99, 2007.

[2] F. Semlali Aouragh Hassani *et al.*, "Mechanical Properties Prediction of Polypropylene/Short Coir Fibers Composites Using a Self-Consistent Approach," *Polym. Compos.*, vol. 40, no. 5, pp. 1919–1929, 2019.

[3] W. Ouarhim, N. Zari, R. Bouhfid, and A. el kacem Qaiss, "Mechanical performance of natural fibers–based thermosetting composites," *Mech. Phys. Test. Biocomposites, Fibre-Reinforced Compos. Hybrid Compos.*, pp. 43–60, 2019.

[4] R. Sengupta *et al.*, "A Short Review on Rubber / Clay Nanocomposites With Emphasis on Mechanical Properties," *Polym. Eng. Sci.*, vol. 47, pp. 2182–2189, 2010.

[5] F. Semlali Aouragh Hassani *et al.*, "Injection Molding of Short Coir Fiber Polypropylene Biocomposites : Prediction of the Mold Filling Phase," *Polym. Compos.*, vol. 40, no. 10, pp. 4042–4055, 2019.

[6] R. Chang and W. Yang, "Numerical simulation of mold filling in injection molding using a three-dimensional finite volume approach," *Int. J. Numer. Methods Fluids*, vol. 37, no. 2, pp. 125–148, 2001.

[7] F. Semlali Aouragh Hassani, M. El Achaby, M. O. Bensalah, D. Rodrigue, R. Bouhfid, and A. Qaiss, "Injection molding of short fiber thermoplastic bio-composites: Prediction of the fiber orientation," *J. Compos. Mater.*, vol. 54, no. 30, pp. 1–11, 2020.

[8] A. Bernasconi, P. Davoli, A. Basile, and A. Filippi, "Effect of fibre orientation on the fatigue behaviour of a short glass fibre reinforced polyamide-6," *Int. J. Fatigue*, vol. 29, no. 2, pp. 199–208, 2007.

[9] B. E. Verweyst, P. H. Foss, and J. F. O. Gara, "Fiber Orientation in 3-D Injection Molded Features," *Polym. Process.*, vol. 4, pp. 409–420, 1999.

[10] M. Sepehr, G. Ausias, and P. J. Carreau, "Rheological properties of short fiber filled polypropylene in transient shear flow," *Non-Newtonian Fluid Mech*, vol. 123, pp. 19–32, 2004.

[11] P. A. Fowler, J. M. Hughes, and R. M. Elias, "Biocomposites: technology, environmental credentials and market forces," *J. Sci. Food Agric.*, vol. 86, no. 12, pp. 1781–1789, 2006.

[12] C. C. Ibeh, *Thermoplastic Materials: Properties, manufacturing methods and applications, CRC Press, 1st Edition*. 2011.

[13] S. Mouhoubi, H. Osmani, T. Bali, and S. Abdeslam, "Elaboration et etude des proprietes des composites polyester/alfa traitee et non traitee," *Verres, Céramiques Compos.*, vol. 2, no. 1, pp. 34–40, 2012.

[14] P. Taylor, A. Kici, and E. Bogacz, "Review of Natural Fibers . Part I— Vegetable Fibers," *J. Nat. Fibers*, vol. 9, no. 3, pp. 150–167, 2012.

[15] E. Bodros, I. Pillin, N. Montrelay, and C. Baley, "Could biopolymers reinforced by randomly scattered flax fibre be used in structural applications ?," *Compos. Sci. Technol.*, vol. 67, no. 3–4, pp. 462–470, 2007.

[16] P. Wambua, J. Ivens, and I. Verpoest, "Natural fibres : can they replace glass in fibre reinforced plastics ?," *Compos. Sci. Technol.*, vol. 63, no. 9, pp. 1259–1264, 2003.

[17] S. V Joshi, L. T. Drzal, A. K. Mohanty, and S. Arora, "Are natural fiber composites environmentally superior to glass fiber reinforced composites ?," *Compos. Part A*, vol. 35, no. 3, pp. 371–376, 2004.

[18] A. Ashori, "Wood – plastic composites as promising green-composites for automotive industries !," *Bioresour. Technol.*, vol. 99, no. 11, pp. 4661–4667, 2008.

[19] M. J. John and S. Thomas, "Biofibres and biocomposites," *Carbohydr. Polym.*, vol. 71, no. 3, pp. 343–364, 2008.

[20] A. Ben Mabrouk, H. Kaddami, S. Boufi, F. Erchiqui, and A. Dufresne, "Cellulosic nanoparticles from alfa fibers (Stipa tenacissima): Extraction procedures and reinforcement potential in polymer nanocomposites," *Cellulose*, vol. 19, no. 3, pp. 843–853, 2012.

[21] H. Essabir, R. Bouhfid, and A. Qaiss, *Alfa and doum fiber-based composite materials for different applications*. Elsevier Ltd., 2017.

[22] M. Cheikh Rouhou, S. Abdelmoumen, S. Thomas, H. Attia, and D. Ghorbel, "Use of green chemistry methods in the extraction of dietary fibers from cactus rackets (Opuntia ficus indica): Structural and microstructural studies," *Int. J. Biol. Macromol.*, vol. 116, pp. 901–910, 2018.

[23] F. Semlali Aouragh Hassani, M. El Achaby, R. Bouhfid, and A. E. K. Qaiss, "Modeling for the process and the prediction of the thermal and mechanical behavior for the biopolymers and bio-composites," in *Naheed Saba, Mohammad Jawaid, Mohamed Thariq. Biopolymers and Biocomposites from Agro-Waste for Packaging Applications. Elsevier, 1st edition.*, 2021, p. 271.

[24] W. Ouarhim, F. Z. Semlali Aouragh Hassani, R. Bouhfid, and A. el kacem Qaiss, "Numerical, experimental and simulation study of natural fiber-based composites on injection molding," *Polym. Compos. Manuf.*, pp. 121–134, 2020.

[25] Q. M. P. Nguyen, X. Chen, Y. C. Lam, and C. Y. Yue, "Effects of polymer melt compressibility on mold filling in micro-injection molding," *J. Micromechanics Microengineering*, vol. 21, no. 9, pp. 1–9, 2011.

[26] F. Semlali Aouragh Hassani, W. Ouarhim, N. Zari, R. Bouhfid, and A. Qaiss, "Natural fiber-based biocomposites," in *K Kumar, J Paulo Davim. Biodegradable Composites Materials, Manufacturing and Engineering. De Gruyter, 1st edition.*, 2019, pp. 49–79.

[27] F. X. E. M. Delgado-Aguilar, F. Julián, Q. Tarrés, J.A. Méndez, P. Mutjé, "Bio composite from bleached pine fibers reinforced polylactic acid as a replacement of glass fiber

reinforced polypropylene, macro and micro-mechanics of the Young's modulus," *Compos. Part B Eng.*, vol. 125, pp. 203–210, 2017.

[28] P. M. a H. Oliver-Ortega, L.A. Granda, F.X. Espinach b, M. Delgado-Aguilar a, J. Duranc and A, "Stiffness of bio-based polyamide 11 reinforced with softwood stone ground-wood fibres as an alternative to polypropylene- glass fibre composites," *Eur. Polym. J.*, vol. 84, pp. 481–489, 2016.

[29] R. Gupta, N. Sulaiman, and A. Gupta, "An improved algorithm for prediction of Young's Modulus of wood plastic composites," *Sci. Res. Essays*, vol. 8, no. 16, pp. 649–656, 2013.

[30] K. A. Krishnan, R. Anjana, and K. E. George, "Effect of Alkali-Resistant Glass Fiber on Polypropylene / Polystyrene Blends : Modeling and Characterization," *Polym. Compos.*, pp. 1–9, 2014.

[31] H. Hu, L. Onyebueke, and A. Abatan, "Characterizing and Modeling Mechanical Properties of Nanocomposites- Review and Evaluation," *J. Miner. Mater. Charact. Eng.*, vol. 9, no. 4, pp. 275–319, 2010.

[32] F. R. J. S. AHMED, "A review of particulate reinforcement theories for polymer composites," *J. Mater. Sci. 25*, vol. 25, pp. 4933–4942, 1990.

[33] J. P. López, P. Mutjé, M. À. Pèlach, N.-E. El Mansouri, S. Boufi, and F. Vilaseca, "Analysis of the tensile modulus of polypropylene composites reinforced with stone groundwood fibers," *BioResources*, vol. 7, no. 1, pp. 1310–1323, 2012.

[34] M. A. Sawpan, K. L. Pickering, and A. Fernyhough, "Hemp Fibre Reinforced Poly(Lactic Acid) Composites," *Adv. Mater. Process. IV*, vol. 29–30, pp. 337–340, 2007.

[35] W. Ouarhim, F. Semlali Aouragh Hassani, A. Qaiss, and R. Bouhfid, "Rheology of polymer nanocomposites," in *Sabu Thomas, Sarathchandran, C. Nithin Chandran. Rheology of Polymer Blends and Nanocomposites Theory, Modelling and Applications. Elsevier, 1st Edition.*, 2019, pp. 73–96.

[36] M. Ravanagh, "Rheological characterisation of polymer gels," *Rheol. CHARACTERISATION Polym. GELS*, vol. 23, no. 97, pp. 533–562, 1998.

[37] A. Bjrn, P. S. de La Monja, A. Karlsson, J. Ejlertsson, and B. H., *Rheological Characterization*. 2000.

[38] F. Ciornei and S. Alaci, "Characterization of Rheological Properties of Semisolid Materials Used As Thermal Interfaces . Part Ii : Experimental Tests," *Eng. Stud. Res.*, vol. 21, no. 2, pp. 19–25, 2015.

[39] M. M. Cross, "Rheology of non-newtonian fluids: a new flow equation for pseudoplastic systems," *COLLOID Sci.*, vol. 20, no. 5, pp. 417–437, 1965.

[40] H. Physiologique, P. Universit, P. Vii, R. April, and I. When, "Rheology of eoncentrated disperse systems II . A model for non-newtonian shear viscosity in steady flows," *Rheol. Acta*, vol. 17, no. 6, pp. 632–642, 1978.

[41] C. Baravian, D. Vantelon, and F. Thomas, "Rheological Determination of Interaction Potential Energy for Aqueous Clay Suspensions," *Langmuir*, vol. 19, no. 19, pp. 8109–8114, 2003.

[42] H. A. Barnes, "ShearThickening (Dilatancy) in Suspensions of Nonaggregating Solid Particles Dispersed in Newtonian Liquids," *Rheology*, vol. 33, pp. 329–366, 1989.

[43] R. L. Hoffman, R. L. Hoffman, and M. Company, "Discontinuous and Dilatant Viscosity Behavior in Concentrated Suspensions . I . Observation of a Flow Instability," *Rheology*, vol. 16, no. 1, pp. 155–173, 1972.

[44] A. B. Metzner and M. Whitlock, "Flow Behavior of Concentrated (Dilatant) Suspensions Flow Behavior of Concentrated (Dilatant)," *Trans. Soc. Rheol.*, vol. 2, pp. 239-254 (1958), 1958.

[45] B. J. Maranzano and N. J. Wagner, "Flow-small angle neutron scattering measurements of colloidal dispersion microstructure evolution through the shear thickening transition," *J. Chim. Phys.*, vol. 117, no. 22, pp. 10291–10302, 2002.

[46] W. Brostow, "Drag reduction in flow : Review of applications , mechanism and prediction," *J. Ind. Eng. Chem.*, vol. 14, no. 4, pp. 409–416, 2008.

[47] R. D. Moser, P. Moin, and A. Leonard, "A spectral numerical method for the Navier-Stokes equations with applications to Taylor-Couette flow," *J. Comput. Phys.*, vol. 52, no. 3, pp. 524–544, 1983.

[48] C. E. Siewert, "Poiseuille, thermal creep and Couette flow: Results based on the CES model of the linearized Boltzmann equation," *Eur. J. Mech. B/Fluids*, vol. 21, no. 5, pp. 579–597, 2002.

[49] R. C. Givler, M. J. Crochet, and R. B. Pipes, "Numerical Prediction of Fiber Orientation in Dilute Suspensions," *J. Compos. Mater.*, vol. 17, no. 4, pp. 330–343, 1983.

[50] Fransisco Folgar and Charles L. Tucker III, "Orientation Behavior of Fibers in Concentrated Suspensions," *J. Reinf. Plast. Compos.*, vol. 3, no. 2, pp. 98–119, 1984.

[51] Y. Gao *et al.*, "Flow-induced Crystallization of Long Chain Aliphatic Polyamides under a Complex Flow Field : Inverted Anisotropic Structure and Formation Mechanism," *Polymer (Guildf).*, vol. 73, pp. 91–101, 2015.

[52] R. S. Bay and C. L. Tucker, "Fiber Orientation in Simple Injection Moldings. Part II: Experimental Results," *Polym. Compos.*, vol. 13, no. 4, pp. 317–331, 1992.

[53] B. R. Whiteside, P. D. Coates, P. J. Hine, and R. A. Duckett, "Glass fibre orientation within injection moulded automotive pedal - Simulation and experimental studies," *Plast. Rubber Compos.*, vol. 29, no. 1, pp. 38–45, 2000.

[54] A. Özdemir, O. Uluer, and A. Güldaş, "Flow front advancement of molten thermoplastic materials during filling stage of a mold cavity," *Polym. Test.*, vol. 23, no. 8, pp. 957–966, 2004.

[55] A. Megally and A. M. Etude, “Etude et modélisation de l’orientation de fibres dans des thermoplastiques renforcés,” 2005.

[56] P. Shokri and N. Bhatnagar, “Effect of the Post-Filling Stage on Fiber Orientation at the Mid-Plane in Injection Molding of Reinforced Thermoplastics,” *Phys. Procedia*, vol. 25, pp. 79–85, 2012.

[57] A. Redjeb, “Simulation numérique de l’orientation de fibres en injection de thermoplastique renforcé,” Ecole Nationale supérieure des mines de Paris, 2007.

[58] S. T. Chung and T. H. Kwon, “Numerical simulation of fiber orientation in injection molding of short-fiber-reinforced thermoplastics,” *Polym. Eng. Sci.*, vol. 35, no. 7, pp. 604–618, 1995.

[59] A. Coulon, “Injection des polyamides renforcés de fibres de verre longues : Relations mise en oeuvre/comportement thermomécanique,” 2008.

[60] A. J. Pontes, N. M. Neves, and A. S. Pouzada, “The role of the interaction coefficient in the prediction of the fiber orientation in planar injection moldings,” *Polym. Compos.*, vol. 24, no. 3, pp. 358–366, 2003.

[61] P. Caton-Rose, P. J. Hine, and B. Parveen, “Prediction of Fibre Orientation in Short Glass Fibre Reinforced Composite Injection Moulding,” *19Th Int. Conf. Compos. Mater.*, pp. 1706–1713, 2013.

[62] M. Vincent, T. Giroud, A. Clarke, and C. Eberhardt, “Description and modeling of fiber orientation in injection molding of fiber reinforced thermoplastics,” *Polymer (Guildf).*, vol. 46, no. 17, pp. 6719–6725, 2005.

[63] M. Gupta and K. K. Wang, “Fiber orientation and mechanical properties of short-fiber-reinforced injection-molded composites: Simulated and experimental results,” *Polym. Compos.*, vol. 14, no. 5, pp. 367–382, 1993.

[64] K. Han, Y. Im, K. Han, and Y. Im, “Modified hybrid closure approximation for prediction of flow-induced fiber orientation,” *Rheology*, vol. 43, no. 3, pp. 569–589, 1999.

[65] D. H. Chung and T. H. Kwon, “Fiber orientation in the processing of polymer composites,” *Korea-Australia Rheol.*, vol. 14, no. 4, pp. 175–188, 2002.

[66] R. S. Bay and C. L. Tucker, “Fiber orientation in simple injection moldings. Part I: Theory and numerical methods,” *Polym. Compos.*, vol. 13, no. 4, pp. 317–331, 1992.

[67] S. G. Advani, “The Use of Tensors to Describe and Predict Fiber Orientation in Short Fiber Composites,” *J. Rheol. (N. Y. N. Y).*, vol. 31, no. 8, p. 751, 1987.

[68] W. C. Jackson, S. G. Advani, and C. L. Tucker, “Predicting the Orientation of Short Fibers in Thin Compression Moldings,” *J. Compos. Mater.*, vol. 20, no. 6, pp. 539–557, 1986.

[69] Ihsane MODHAFFAR, “Modélisation numérique et simulation de l’orientation des fibres courtes dans une matrice thermoplastique,” 2016.

[70] H. Miled, "Modélisation de l'orientation de fibres induite par l'écoulement et comportement élastique anisotrope à l'état solide," Ecole Nationale Supérieure des Mines de Paris, 2010.

[71] G. L. Hand, "A theory of anisotropic fluids," *J. Fluid Mech.*, vol. 13, no. 1, pp. 33–46, 1961.

[72] Florian Ghering, "Etude du comportement mécanique et de l'endommagement de composites thermoplastiques renforcés de fibres courtes de chanvre : Approche expérimentale et modélisation," Université de Lorraine, 2013.

[73] G. Crevecoeur, "Morphology and Mechanical Properties of Thermoplastic Composites Containing a Thermotropic Liquid Crystalline Polymer," *Polym. Eng. Sci.*, vol. 30, no. 9, pp. 532–542, 1990.

[74] A. Pedicini and R. J. Farris, "Mechanical behavior of electrospun polyurethane," *Polymer (Guildf).*, vol. 44, pp. 6857–6862, 2003.

[75] G. B. Jeffery, "The Motion of Ellipsoidal Particles Immersed in a Viscous Fluid," *Proc. R. Soc. A Math. Phys. Eng. Sci.*, vol. 102, no. 715, pp. 161–179, 1922.

[76] P. W. Aaron P. R. Eberle , Gregorio M. Vélez-García , Donald G. Baird, "Fiber orientation kinetics of a concentrated short glass fiber suspension in startup of simple shear flow," *J. Nonnewton. Fluid Mech.*, vol. 165, no. 3–4, pp. 110–119, 2010.

[77] A. Redjeb, L. Silva, P. Laure, M. Vincent, and T. Coupez, "Three dimensional numerical simulations of fiber orientation in injection molding."

[78] G. G. Lipscomb, R. Keunings, G. Marrucci, and and M. M. Denn, "A Continum theory for fiber suspensions," *Adv. Mater.*, pp. 497–499, 1984.

[79] P. Caton-Rose, P. Hine, F. Costa, X. Jin, J. Wang, and B. Parveen, "Fibre Orientation and Mechanical Property Predictions for Short Glass Fibre Reinforced Injection Moulding," *Polym. Process.*, pp. 1–5, 2011.

[80] H. Essabir, M. Raji, E. M. Essassi, D. Rodrigue, R. Bouhfid, and A. el kacem Qaiss, "Morphological, thermal, mechanical, electrical and magnetic properties of ABS/PA6/SBR blends with Fe3O4 nano-particles," *J. Mater. Sci. Mater. Electron.*, vol. 28, no. 22, pp. 17120–17130, 2017.

[81] R. Boujmal, H. Essabir, S. Nekhlaoui, M. O. Bensalah, R. Bouhfid, and A. Qaiss, "Composite from polypropylene and henna fiber: Structural, mechanical and thermal properties," *J. Biobased Mater. Bioenergy*, vol. 8, no. 2, pp. 246–252, 2014.

[82] M. M. Haque, M. Hasan, M. S. Islam, and M. E. Ali, "Physico-mechanical properties of chemically treated palm and coir fiber reinforced polypropylene composites," *Bioresour. Technol.*, vol. 100, no. 20, pp. 4903–4906, 2009.

[83] F. Gehring, V. Bouchart, P. Dinzart, and P. Chevrier, "Etude expérimentale du comportement de polymères thermoplastiques renforcés : Polypropylène chargé de fibres

de chanvre," *20ième Congrès Français de Mécanique*, pp. 1–6, 2011.

[84] P. Shokri and N. Bhatnagar, "Fiber orientation at the mid-plane in injection molding of reinforced thermoplastics," *Phys. Procedia*, vol. 25, pp. 79–85, 2012.

[85] S. T. Chung and T. H. Kwon, "Coupled analysis of injection molding filling and fiber orientation, including in-plane velocity gradient effect," *Polym. Compos.*, vol. 17, no. 6, pp. 859–872, 1996.

[86] M. Kumaresan, S. Sathish, and N. Karthi, "Effect of Fiber Orientation on Mechanical Properties of Sisal Fiber Reinforced Epoxy Composites," *Appl. Sci. Eng.*, vol. 18, no. 3, pp. 289–294, 2015.

[87] A. P. Jackson, J. F. V Vincent, and R. M. Turner, "Comparison of nacre with other ceramic composites," *J. Mater. Sci.*, vol. 25, no. 7, pp. 3173–3178, 1990.

[88] C. P. Jiang, Z. H. Tong, and Y. K. Cheung, "A generalized self-consistent method for piezoelectric fiber reinforced composites under antiplane shear," *Mech. Mater.*, vol. 33, no. 5, pp. 295–308, 2001.

[89] A. Qaiss and M. Bousmina, "Biaxial Stretching of Polymers Using a Novel and Versatile Stretching System," *Polym. Eng. Sci.*, vol. 51, no. 7, pp. 1347–1353, 2011.

[90] B. Standard and B. Iso, "Plastics — Determination of tensile properties," *Part*, vol. 1, no. 1, pp. 527–1, 2009.

[91] S. Mortazavian and A. Fatemi, "Effects of fiber orientation and anisotropy on tensile strength and elastic modulus of short fiber reinforced polymer composites," *Compos. Part B Eng.*, vol. 72, pp. 116–129, 2015.

[92] R. J. Crowson, M. J. Folkes, and P. F. Bright, "Rheology of short glass fiber-reinforced thermoplastics and its application to injection molding I. Fiber motion and viscosity measurement," *Polym. Eng. Sci.*, vol. 20, no. 14, pp. 925–933, 1980.

[93] P. Singh and M. R. Kamal, "The effect of processing variables on microstructure of injection molded short fiber reinforced polypropylene composites," *Polym. Compos.*, vol. 10, no. 5, pp. 344–351, 1989.

[94] H. Essabir *et al.*, "Bio-composites based on polypropylene reinforced with Almond Shells particles: Mechanical and thermal properties," *Mater. Des.*, vol. 51, pp. 225–230, 2013.

[95] T. H. Nam, S. Ogihara, N. H. Tung, and S. Kobayashi, "Effect of alkali treatment on interfacial and mechanical properties of coir fiber reinforced poly(butylene succinate) biodegradable composites," *Compos. Part B Eng.*, vol. 42, no. 6, pp. 1648–1656, 2011.

[96] H. Bensalah, K. Gueraoui, H. Essabir, D. Rodrigue, R. Bouhfid, and A. el kacem Qaiss, "Mechanical, thermal, and rheological properties of polypropylene hybrid composites based clay and graphite," *J. Compos. Mater.*, vol. 51, no. 25, pp. 1–14, 2017.

[97] F. Z. Arrakhiz, M. Malha, R. Bouhfid, K. Benmoussa, and A. Qaiss, "Tensile, flexural and

torsional properties of chemically treated alfa, coir and bagasse reinforced polypropylene," *Compos. Part B Eng.*, vol. 47, pp. 35–41, 2013.

[98] I. O. Yaman, H. M. Aktan, and N. Hearn, "Active and Non-active Porosity in Concrete Part II: Evaluation of Existing Models," *Mater. Struct.*, vol. 35, no. 2, pp. 110–116, 2002.

[99] H. Essabir, M. O. Bensalah, D. Rodrigue, R. Bouhfid, and A. Qaiss, "Mechanics of Materials Structural , mechanical and thermal properties of bio-based hybrid composites from waste coir residues : Fibers and shell particles," *Mech. Mater.*, vol. 93, pp. 134–144, 2016.

[100] H. Essabir, A. Elkhaoulani, K. Benmoussa, R. Bouhfid, F. Z. Arrakhiz, and A. Qaiss, "Dynamic mechanical thermal behavior analysis of doum fibers reinforced polypropylene composites," *Mater. Des.*, vol. 51, pp. 780–788, 2013.

[101] F. R. Cichocki and J. L. Thomason, "Thermoelastic anisotropy of a natural fiber," *Compos. Sci. Technol.*, vol. 62, no. 5, pp. 669–678, 2002.

[102] H. Ku, H. Wang, N. Pattarachaiyakoop, and M. Trada, "A review on the tensile properties of natural fiber reinforced polymer composites," *Compos. Part B Eng.*, vol. 42, no. 4, pp. 856–873, 2011.

[103] G. Kalaprasad, K. Joseph, S. Thomas, and C. Pavithran, "Theoretical modelling of tensile properties of short sisal fibre-reinforced low-density polyethylene composites," *J. Mater. Sci.*, vol. 32, no. 16, pp. 4261–4267, 1997.

[104] D. W. Hadley, P. R. Pinnock, and I. M. Ward, "Anisotropy in oriented fibres from synthetic polymers," *J. Mater. Sci.*, vol. 4, no. 2, pp. 152–165, 1969.

[105] C. H. W. Shih-Min, "Flow analysis of micro-channel in injection molding," *J. Polym. Eng.*, vol. 27, no. 2, pp. 107–127, 2007.

[106] C. Guo, L. Zhou, and J. Lv, "Effects of expandable graphite and modified ammonium polyphosphate on the flame-retardant and mechanical properties of wood flour-polypropylene composites," *Polym. Compos.*, vol. 21, no. 7, pp. 449–456, 2013.

[107] H. Shin and E. of I. F. D. Park, "Analysis of Incomplete Filling Defect for Injection-Molded Air Cleaner Cover Using Moldflow Simulation," *Polymers (Basel).*, vol. 2013, pp. 1–13, 2013.

[108] C. Y. Khor *et al.*, "Three-dimensional numerical and experimental investigations on polymer rheology in meso-scale injection molding," *Int. Commun. Heat Mass Transf.*, vol. 37, no. 2, pp. 131–139, 2010.

[109] H. Shin and E. Park, "Analysis of Crack Phenomenon for Injection-Molded Screw Using Moldflow Simulation," *AppliedPolymer Sci.*, vol. 113, pp. 2702–2708, 2009.

[110] W. Young, "Three-Dimensional Nonisothermal Mold Filling Simulations in Resin Transfer Molding," *Polym. Compos.*, vol. 15, no. 2, pp. 118–127, 1994.

[111] M. R. Kamal and S. Kenig, "The injection molding of thermoplastics part I: Theoretical model," *Polym. Eng. Sci.*, vol. 12, no. 4, pp. 294–301, 1972.

[112] J. L. White and H. B. Dee, "Flow visualization for injection molding of polyethylene and polystyrene melts," *Polym. Eng. Sci.*, vol. 14, no. 3, pp. 212–222, 1974.

[113] J. L. White, "Fluid mechanical analysis of injection mold filling," *Polym. Eng. Sci.*, vol. 15, no. 1, pp. 44–50, 1975.

[114] L. . Seow and Y. . Lam, "Optimizing flow in plastic injection molding," *J. Mater. Process. Technol.*, vol. 72, no. 3, pp. 333–341, 1997.

[115] J. M. Castro and C. W. Macosko, "Studies of mold filling and curing in the reaction injection molding process," *AIChE J.*, vol. 28, no. 2, pp. 250–260, 1982.

[116] A. Tallarico and M. Dragoni, "Viscous Newtonian laminar flow in a rectangular channel: Application to Etna lava flows," *Bull. Volcanol.*, vol. 61, no. 1–2, pp. 40–47, 1999.

[117] S. Arulanandam and D. Li, "Liquid transport in rectangular microchannels by electroosmotic pumping," *Colloids Surfaces A Physicochem. Eng. Asp.*, vol. 161, no. 1, pp. 89–102, 2000.

[118] J. M. Castro and C. W. Macosko, "Studies of mold filling and curing in the reaction injection molding process," *AIChE J.*, vol. 28, no. 2, pp. 250–260, 1982.

[119] K. M.R. and K. S., "The injection molding of thermoplastics. Part II: Experimental test of the model," *Polym. Eng. Sci.*, vol. 12, no. 4, pp. 302–308, 1972.

[120] X. Lei, Z. Gerhard, and J. Bing-yan, "Numerical simulation method for weld line development in micro injection molding process," *Huagong Xuebao/CIESC J.*, vol. 60, no. 2, pp. 444–449, 2009.

[121] H. Y. Lin and W. Bin Young, "Analysis of the filling capability to the microstructures in micro-injection molding," *Appl. Math. Model.*, vol. 33, no. 9, pp. 3746–3755, 2009.

[122] D. H. Chung and T. H. Kwon, "Invariant-based optimal fitting closure approximation for the numerical prediction of flow-induced fiber orientation Invariant-based optimal fitting closure approximation for the numerical prediction of flow-induced fiber," *J. Rheol. (N. Y. N. Y).*, vol. 46, no. 1, pp. 169–193, 2002.

[123] A. S. G. M. A. Okagawa, R. G. Cox, "The Kinetics of Flowing Dispersions VI. Transient Orientation and Rheological Phenomena of Rods and Discs in Shear Flow," *J. Colloid Interface Sci.*, vol. 45, no. 2, pp. 303–329, 1973.

[124] M. C. Altan, "A Review of Fiber-Reinforced Injection Molding: Flow Kinematics and Particle Orientation," *J. Thermoplast. Compos. Mater.*, vol. 3, no. 4, pp. 275–313, 1990.

[125] M. C. Altan, S. Subbiah, S. I. Guceri, and R. B. Pipes, "Numerical Prediction of Three-Dimensional Fiber Orientation in Hele-Shaw Flows," *Polym. Eng. Sci.*, vol. 30, no. 14, pp. 848–859, 1990.

[126] J. Rosenberg and M. Denn, "Simulation of non-recirculating fiber suspensions flows of dilute fiber suspensions," *J. Non-Newtonian Fluid Mech.*, vol. 37, no. 2–3, pp. 317–345, 1990.

[127] F. D. V. Verleye, A. Couniot, "Numerical prediction of fibre orientation in complex injection-moulded parts," *Trans. Eng. Sci.*, vol. 4, pp. 303–312, 1994.

[128] H. Kikuchi, "The Relation Between Thickness and Warpage in a Disk Injection Molded From Fiber Reinforced PA66," *Polym. Eng. Sci.*, vol. 36, no. 10, pp. 1317–1325, 1996.

[129] R. J. Crowson, "Rheology of Short Glass Fiber-Reinforced Thermoplastics and its Application to Injection Molding. II. The Effect of Material Parameters," *Polym. Eng. Sci.*, vol. 20, no. 14, pp. 934–940, 1980.

[130] G. G. Lipscomb, M. M. Denn, D. U. Hur, and D. V. Boger, "The flow of fiber suspensions in complex geometries," *J. Nonnewton. Fluid Mech.*, vol. 26, no. 3, pp. 297–325, 1988.

[131] S. G. Advani, "Flow and Rheology in Polymer Composites Manufacturing, Volume 10," in *Composite Materials Series. Elsevier, 1st Edition.*, 1994, pp. 147–202.

[132] M. S. Ingber and L. M. A, "A numerical study of threedimensional Jeffery orbits in shear flow," *J. Rheol. (N. Y. N. Y).*, vol. 38, no. 6, pp. 1829–1843, 1994.

[133] A. G. Facca, M. T. Kortschot, and N. Yan, "Predicting the elastic modulus of natural fibre reinforced thermoplastics," *Compos. Part A Appl. Sci. Manuf.*, vol. 37, no. 10, pp. 1660–1671, 2006.

RECOMMENDATION FOR FUTURE WORKS

This thesis project is presented as a first step towards improving thermoplastics reinforced short natural fiber mechanical properties, in order to produce high performance materials more suitable for structural and exterior applications. In fact, in this thesis project, it was shown that the combination of the three developed models make it possible to anticipate the molded part performances and thus optimizing the injection molding process. However, some aspects were not studied in this project by choice (time limitation), but are of scientific interest for future work. Thus, the following recommendations are suggested:

- Optimizing the self-consistent approach by considering the specific fiber morphology and higher fiber content.
- Optimizing the three-dimensional model for the flow front prediction by considering higher fiber content.
- Deep study of the flow behavior at the cavity entrance (phase 1) to have the possibility to predict the flow front shape and position before reaching the mold corners.
- Characterization of the flow front behavior for more complex mold geometry.
- Study the effect of fiber-fiber interactions on the fiber orientation.
- Development of a more concise model for 3D fiber orientation prediction.
- Development of software based on the three developed models.

SCIENTIFIC PRODUCTIONS

PAPERS IN SCOPUS INDEXED JOURNALS

1. **Fatima-Zahra Semlali Aouragh Hassani**, Wafa Ouarhim, Mohammed Ouadi Bensalah, Hamid Essabir, Denis Rodrigue , Rachid Bouhfid, Abou el Kacem Qaiss. Mechanical Properties Prediction of Polypropylene/Short Coir Fibers Composites Using a Self-Consistent Approach. *Journal of Polymer Composites*. vol. 40, no. 5, 2019. **(PUBLISHED)**

2. **Fatima-Zahra Semlali Aouragh Hassani**, Wafa Ouarhim, Nadia Zari, Mohammed Ouadi Bensalah, Denis Rodrigue, Rachid Bouhfid , Abou el kacem Qaiss. Injection molding of short coir fiber polypropylene biocomposites: Prediction of the mold filling phase. *Journal of Polymer Composites*. vol. 40, no. 10, 2019. **(PUBLISHED)**

3. **Fatima-Zahra Semlali Aouragh Hassani**, Wafa Ouarhim, Marya Raji, Mohamed El Mehdi Mekhzoum, Mohammed Ouadi Bensalah, Hamid Essabir, Denis Rodrigue, Rachid Bouhfid, Abou el kacem Qaiss. N-silylated benzothiazolium dye as a coupling agent for polylactic acid/date palm fiber bio-composites. *Journal of Polymers and the environment*. vol. 27, no. 12, 2019. **(PUBLISHED)**

4. **Fatima-Zahra Semlali Aouragh Hassani**, Wafa Ouarhima, Mounir El Achaby, Youssef Tamraoui, Mohammed-Ouadi Bensalah, Denis Rodrigue, Rachid Bouhfid, Abou el kacem Qaiss. Recycled tires shreds based polyurethane binder: Production and characterization. *Journal of mechanics of materials*. vol. 144, 2020. **(PUBLISHED)**

5. **Fatima-Zahra Semlali Aouragh Hassani**, Khadija El Bourakadi, Nawal Merghoubd, Abou el kacem Qaiss, Rachid Bouhfid. Effect of chitosan/modified montmorillonite on the antibacterial and mechanical properties of Date Palm fiber trays. *International Journal of Biological Macromolecules*. vol. 148, 2020. **(PUBLISHED)**

6. **Fatima-Zahra Semlali Aouragh Hassani**, Mounir El Achaby, Mohammed-Ouadi Bensalah, Denis Rodrigue, Rachid Bouhfid, Abou El Kacem Qaiss. Injection molding of short fiber thermoplastic bio-composites: Prediction of the fiber orientation. *Journal of Composite Materials*. vol. 54, no. 30, 2020. **(PUBLISHED)**

7. Oumayma M''ghari, **Fatima-Zahra Semlali Aouragh Hassani**, Mohamed El Mehdi Mekhzoum, Nadia Zari, Rachid Bouhfid, Abou el Kacem Qaiss. Elaboration of a composite material based on plaster reinforced with phase change material/Oakum Fiber: physical, thermal and mechanical properties. *Journal of Energy Storage*. **(PUBLISHED)**

8. Hanane Chakhtouna, **Fatima-Zahra Semlali Aouragh Hassani**, Nadia Zari, Rachid Bouhfid, Abou el Kacem Qaiss. Potential applications of poly(cis-1,4-isoprene)/titanium dioxide composite in wastewater treatment. **(SUBMITTED)**

REVIEWS

1. Hamid Essabir, Marya Raji, **Fatima-Zahra Semlali Aouragh Hassani**, Khadija El Bourakadi, Mohamed El Mehdi Mekhzoum, Rachid Bouhfid, Abou el kacem Qaiss. Recent Advances in Materials for 3D Printing: From Design to Application and Processing. (**SUBMITTED**)

2. Marya Raji, Hamid Essabir, **Fatima-Zahra Semlali Aouragh Hassani**, Rachid Bouhfid, Abou el kacem Qaiss. Recent advances in thermosetting laminated and sandwich structure based nanofiller (**SUBMITTED**).

BOOK CHAPTERS

1. **Fatima-Zahra Semlali Aouragh Hassani**, Wafa Ouarhim, Nadia Zari, Rachid Bouhfid, Abou el kacem Qaiss. Natural fiber-based biocomposites. K Kumar, J Paulo Davim. *Biodegradable Composites Materials, Manufacturing and Engineering*. De Gruyter, 1st Edition. **(PUBLISHED)**

2. Wafa Ouarhim, **Fatima-Zahra Semlali Aouragh Hassani**, Abou el kacem Qaiss, Rachid Bouhfid. Rheology of polymer nanocomposites. Sabu Thomas, Sarathchandran, C. Nithin Chandran. *Rheology of Polymer Blends and Nanocomposites Theory, Modelling and Applications*. Elsevier, 1st Edition. **(PUBLISHED)**

3. Wafa Ouarhim, **Fatima-Zahra Semlali Aouragh Hassani**, Rachid Bouhfid, Abou el kacem Qaiss. Numerical, Experimental, and Simulation study of natural fibers based

composites on injection Molding. Kaushik Kumar and J. Paulo Davim. *Polymers and Composites Manufacturing*. De Gruyter, 1st Edition. **(PUBLISHED)**

4. **Fatima-Zahra Semlali Aouragh Hassani**, Wafa Ouarhim, Rachid Bouhfid, Abou el kacem Qaiss. Effect of mold design on the fiber orientation in the case of injection molding: experiment and simulation. Kaushik Kumar and J. Paulo Davim. *Polymers and Composites Manufacturing*. De Gruyter, 1st Edition. **(PUBLISHED)**

5. **Fatima-Zahra Semlali Aouragh Hassani**, Rachid Bouhfid, Abou el kacem Qaiss. Modelling for the process and the prediction of the thermal and mechanical behaviour for the biopolymers and biocomposites. Naheed Saba, Mohammad Jawaid, Mohamed Thariq. *Biopolymers and Biocomposites from Agro-Waste for Packaging Applications*. Elsevier, 1st Edition. **(PUBLISHED)**

6. Khadija El Bourakadi, **Fatima-Zahra Semlali Aouragh Hassani**, Abou el kacem Qaiss, Rachid Bouhfid. Antimicrobial coated food packaging paper from agricultural biomass. Naheed Saba, Mohammad Jawaid, Mohamed Thariq. *Biopolymers and Biocomposites from Agro-Waste for Packaging Applications*. Elsevier, 1st edition. **(PUBLISHED)**

7. **Fatima-Zahra Semlali Aouragh Hassani**, Rachid Bouhfid, Abou el kacem Qaiss. Date palm fiber extraction and treatment. Mohamad Midani, Naheed Saba; Othman Y. Alothman. *Date Palm Fiber Composites: Processing, Properties and Applications*. Springer, 1st Edition. **(PUBLISHED)**

8. **Fatima-Zahra Semlali Aouragh Hassani**, Rachid Bouhfid, Abou el kacem Qaiss. Recent advances in fabrication of hybrid natural fiber composites. Hybrid Natural Fiber Composites. (**ACCEPTED**)

9. **Fatima-Zahra Semlali Aouragh Hassani**, Rachid Bouhfid, Abou el kacem Qaiss. Rheological properties of hybrid nanocomposites based on graphene and other nanoparticles (**ACCEPTED**).

10. **Fatima-Zahra Semlali Aouragh Hassani**, Rachid Bouhfid, Abou el kacem Qaiss. Modeling of damage evaluation and failure of laminated composite materials. Mohammad

Jawaid Ahmad Hamdan Mohamed Thariq Hameed Sultan. *Structural Health Monitoring System for Synthetic , Hybrid and Natural Fiber Composites*. Springer. 1st Edition. **(PUBLISHED)**

11. **Fatima-Zahra Semlali Aouragh Hassani**, Rachid Bouhfid, Abou el kacem Qaiss. Mechanical characterization of cellulose nanoparticle based advanced materials (**ACCEPTED**).

12. **Fatima-Zahra Semlali Aouragh Hassani**, Rachid Bouhfid, Abou el kacem Qaiss. Mechanical modeling of hybrid nanocomposites based on cellulose nanocrystals/nanofibrils and nanoparticles (**ACCEPTED**).

13. **Fatima-Zahra Semlali Aouragh Hassani**, Rachid Bouhfid, Abou el kacem Qaiss. Modeling of vibration damping for a viscoelastic sandwich structure (**SUBMITTED**).

14. **Fatima-Zahra Semlali Aouragh Hassani**, Rachid Bouhfid, Abou el kacem Qaiss. Improvement of Fibre-Matrix-Adhesion of vegetable Natural Fibres by Chemical Treatment. (**SUBMITTED**)

15. Khadija El Bourakadi, **Fatima-Zahra Semlali Aouragh Hassani**, Abou el kacem Qaiss, Rachid Bouhfid. Packaging and biocomposites. (**SUBMITTED**)

PATENT

1. Rachid Bouhfid, Wafa Ouarhim, Abou el kacem Qaiss, **Fatima-Zahra Semlali Aouragh Hassani**. Préparation d'un matériau composite à partir des granulés de pneus recyclés. MA44364A1.

ORAL COMMUNICATION

1. **Work shop:** Participation with oral presentation in "1ST Workshop Composite and Nanocomposite Materials", held at Mohamed VI Polytechnic University, Ben Guerir, Morocco.

2. **Work shop:** Participation with oral presentation in "2ND Workshop Composite and Nanocomposite Materials", held at the training center, Marrakesh, Morocco.

3. **Symposium:** Participation with oral presentation in "1ST International Symposium on Composite and Nanocomposite Materials (ISymposite I) ", held at the Moroccan foundation for advanced science innovation and reasearch (MASCIR), Rabat, Morocco.

4. **Symposium:** Participation with a Poster in "1ST International Symposium on Composite and Nanocomposite Materials (ISymposite I) ", held at the Moroccan foundation for advanced science innovation and reasearch (MASCIR), Rabat, Morocco.

5. **Conference:** Participation with oral presentation in "2ND Wood and Biofibre International Conference (WOBIC2019) ", held in Kota Kinabalu, Sabah, Malaysia.

Résumé

Le but de ce projet de thèse est de développer des méthodes et des techniques pour prédire avec précision les propriétés mécaniques d'un matériau composite avant sa conception. Cela permettra d'améliorer la qualité des pièces ainsi que de réduire les coûts et le temps de production, conduisant ainsi à réduire / éliminer les longs essais expérimentaux.

Tout d'abord, une approche auto-cohérente a été développée sur la base d'une version modifiée du modèle de Hirsch pour prédire les propriétés mécaniques du composite tout en tenant compte de l'effet de la concentration et de l'orientation des fibres. Considérant que l'orientation des fibres dépend étroitement du champ d'écoulement, un modèle tridimensionnel pour la prédiction du remplissage de moule non isotherme et non newtonien a été développé pour étudier le comportement de l'écoulement. En effet, les équations incompressibles de Navier – Stokes sont simplifiées en une seule équation de Poisson, puis résolues afin d'estimer la vitesse d'écoulement, ce qui sous un débit constant permet la prédiction de la forme et de la position du front d'écoulement des composites. Enfin, un modèle quantitatif permettant la prédiction de l'orientation des fibres induites par l'écoulement pour différents cas d'écoulement rencontrés est présenté. L'équation résultante relie l'angle d'orientation de la fibre au champ d'écoulement, le facteur de forme de la fibre et la forme du moule.

Pour conclure, en combinant les trois modèles développés, il est possible de commencer à prédire les propriétés mécaniques des matériaux avant la conception, indépendamment des matériaux utilisés, objectif ultime de cette thèse.

***Mots-clefs (8)** : Moulage par injection - Thermoplastiques - Fibres naturelles - Composites - Modélisation - Performances mécaniques - Front d'écoulement - Orientation des fibres.*

Abstract

The aim of this thesis project is to develop methods and techniques to accurately predict the whole material mechanical properties before design. This will enable to improve parts quality as well as reducing production cost and time, thus leading to reduce/eliminate lengthy experimental testing.

Firstly, a self-consistent approach was developed based on a modified version of Hirsch model to predict the composite mechanical properties while considering the effect of reinforcement content and orientation. Considering that, the fiber orientation depends closely on the flow field, a three-dimensional model for the non-isothermal and non-Newtonian mold filling prediction model was developed to study the flow behavior. Indeed, the incompressible Navier–Stokes equations are simplified into a single Poisson equation, and then solved to estimate the flow velocity, which under a constant flow rate allows the flow front shape and position prediction for the composites. Finally, a quantitative model allowing the flow induced fiber orientation prediction for different flow cases encountered is presented. The resulted equation relates the fiber orientation angle to the flow field, the fiber aspect ratio and the mold shape.

To conclude, by combining the three developed models, it is feasible to begin predicting the materials mechanical properties before design, independently of the used materials, the ultimate goal of this thesis.

***Mots-clefs (8):** Injection molding – Thermoplastics – Natural fibers – Composites – Modeling – Mechanical performance – Flow front – Fiber orientation.*